D.J.G. Burggraaf

Design of a motion compensating tool to improve the installation of offshore wind turbines

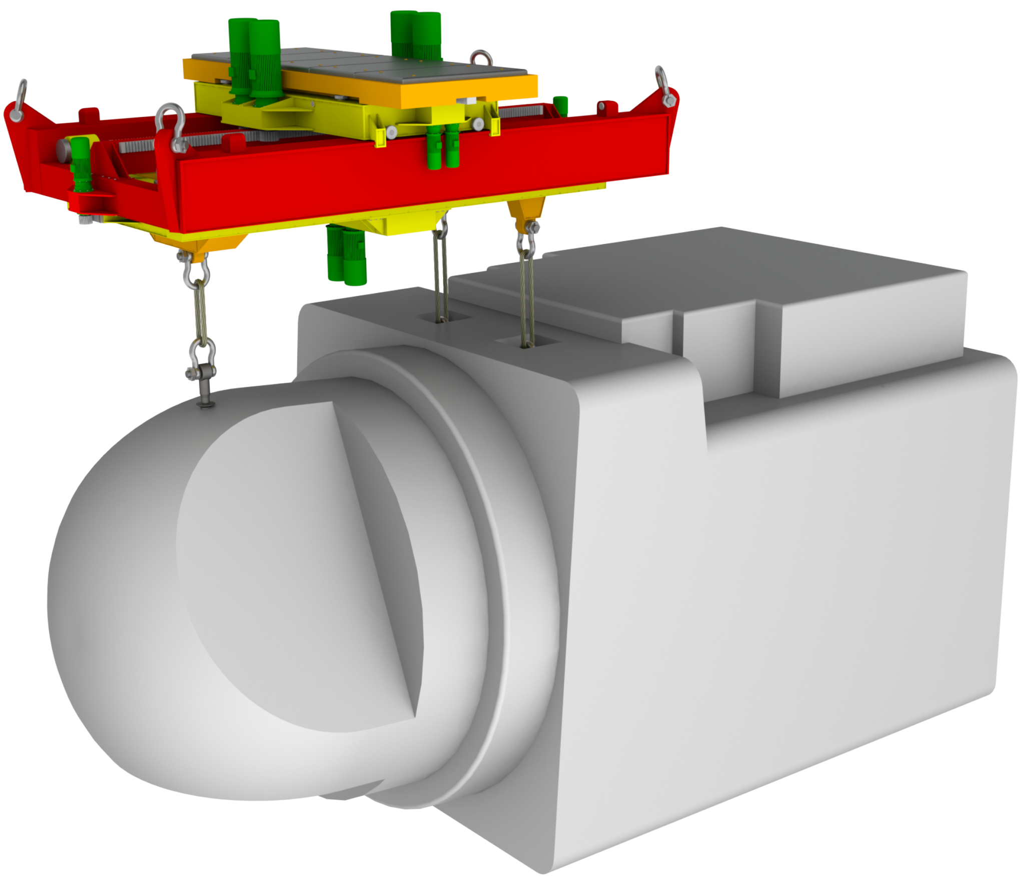

TU Delft

Design of a motion compensating tool to improve the installation of offshore wind turbines

A novel method for the installation of the nacelle

By

D.J.G. Burggraaf

Master Thesis

in partial fulfilment of the requirements for the degree of

Master of Science
in Mechanical Engineering

at the Department Maritime and Transport Technology of Faculty Mechanical, Maritime and Materials Engineering of Delft University of Technology
to be defended publicly on 06-07-2022

Student number:	4591135
MSc Track:	Multi-Machine Engineering
Report number:	2022.MME.8678
Supervisors:	Dr. ir. H. Polinder
	Dr. J. Jovanova
	ir. O.F. van der Meij
Thesis committee:	Dr. ir. H. Polinder
	Dr. J. Jovanova
	Dr. ing. S. Schreier
	ir. O.F. van der Meij
Date:	22-06-2022

Preface

This work is the last piece to complete my master of science in Multi-Machine Engineering at the TU Delft. Completing this research would not have been possible without the help of certain people and I would like to express my gratitude for their support.

First of all, I would like to thank my supervisors from the university, dr. ir. H. Polinder and dr. J. Jovanova for their guidance during this project. I'm also very grateful for the opportunity to do my master thesis in cooperation with Huisman Equipment. I would like to express my gratitude to Olaf van der Meij, my company supervisor, for all the help during my thesis. Furthermore, I would like to give many thanks to Terence Vehmeijer, for his critical view and advice. I would also like to thank Jan Los for helping me solve problems concerning the control theory.

Moreover, I would like to thank my family, girlfriend and friends for supporting me during the complete duration of my master of science.

Diego Burggraaf
Stampersgat, June 22, 2022

Summary

New trends in the offshore wind industry show that wind farms are being built further onto sea. This trend also means that the wind turbines have to be installed in deeper water resulting in new challenges. Currently, offshore wind turbines are commonly installed using jack-up vessels that use long support legs to position themselves on the seabed. However, the maximum operating depth of these vessels is limited which increases the interest in good alternatives for this vessel. Since a floating installation vessel is not limited by the depth of the sea it is a promising alternative for the jack-up vessel. But unlike a jack-up vessel the floating installation vessel has no support legs to protect itself against the negative effects of the weather and sea conditions. This master thesis is therefore interested in a tool to improve the installation of offshore wind turbines by decreasing the unwanted additional motions of a floating installation vessel. The goal of this study is reduced to the following research question:

What hook mounted motion compensation tool can be developed for turbine installation from a floating vessel, and how does its performance compare to the conventional installation process?

The initial step of the research was to understand the installation process of an offshore wind turbine. The installation of a wind turbine is highly dependent on the location and sea conditions, this is why there is no standardized procedure for the installation. Contrary to the overall installation procedure, the order in which the components of a wind turbine are installed is similar for every installation. First the foundation is installed which is followed by a transition piece. The transition piece is then followed by the tower, nacelle and turbine blades in that specific order. From the literature it is clear that the installation of a wind turbine requires a lot of precision which can easily be compromised by bad weather conditions leading to too much motion. The offshore industry is not the only one that faces problems due to unwanted motion and therefore a lot of existing solutions can be found inside the offshore industry, but also in other industries.

The research scope was bounded by a case study. Improving the installation process of an offshore wind turbine includes a broad range of possibilities. To decrease the number of possibilities, the installation of each component was studied and it was found that the installation of the nacelle was the most innovative and improvable installation step. The other parts of a wind turbine either had existing proper working solutions or were already heavily studied. The Haliade X wind turbine from GE was selected as reference turbine, because it is representative for the current and future generations of wind turbines. Besides the turbine an installation vessel was selected for its dimensions. The Les Alizés from Jan de Nul is a floating installation vessel that is capable of installing the Haliade X. The assumption was made that the vessel is equipped with a 3D-motion compensated crane so that data was available on the dynamics of the lifting hook during the installation of the nacelle.

The design methodology applied in this master thesis was comprised of an analysis, synthesis and evaluation phase introduced by John Christopher Jones. Using this methodology seven concepts were created that could possibly compensate for unwanted motion during the installation of the nacelle. The concepts were then evaluated using an analytic hierarchy process which compares each aspect of a concept against another. The concept comprised of two XY-tables was selected for the final design phase. This concept allows the nacelle to be moved below the main frame from which it is suspended. A counterweight is moved in the

opposite direction to maintain the moment equilibrium about the center of gravity of the tool.

The final concept design was built up from five main parts: nacelle carrier, lower x-table, main frame, upper y-table and counterweight carrier. Basic structural design was performed to develop the concept. The primary structure of each part was designed from hollow rectangular steel sections. The calculations were done with the standards for marine operations and marine warranty (DNVGL-ST-N001). A 3D-model of the tool was created in SolidWorks to give a clear view on the overall design of the tool which can be seen in Fig. 1. The tool, including the counterweight of 130 tonnes is estimated to weigh 170.9 tonnes.

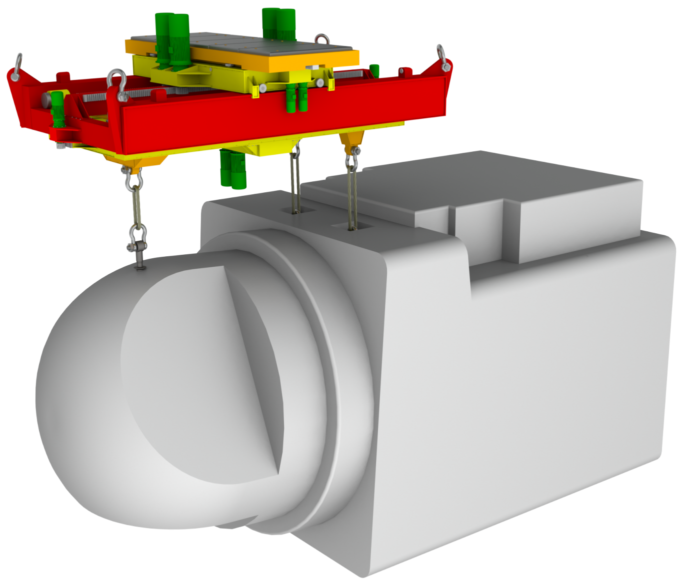

Figure 1: 3D-model of the concept

A dynamic analysis was performed to study whether the dynamic behaviour of the concept. A mathematical model was developed to represent the dynamics of the system. The model was then analysed using MATLAB with Simulink. In this thesis a proportional-integral-derivative (PID) controller was used to control the position of the nacelle. Since an extensive control study did not fit inside the scope of this thesis an automatic PID Tuner from MATLAB was used to linearize the system and calibrate the controller. The tests with the first working principle and model showed unexpected results. To identify the cause of these results, two adaptations of the original model were made together with different control errors. These experiments showed that a damping effect can be achieved when only the counterweight is moved and the nacelle remains fixed. However, the dynamical analysis was therefore inconclusive about the performance of the initial working principle, where the position of the nacelle and counterweight were coupled to maintain the moment equilibrium.

Summary in Dutch

Nieuwe trends in de offshore-industrie tonen aan dat offshore wind farms steeds verder op zee worden gebouwd. Dit betekent ook dat deze windturbines in diepere wateren moeten worden geïnstalleerd wat leidt tot nieuwe uitdagingen. Momenteel worden offshore windturbines vaak geïnstalleerd door een jack-up schip. Deze schepen gebruiken een systeem waarmee ze zichzelf vast kunnen zetten op de bodem, maar dit betekent ook dat deze schepen een maximale werkdiepte hebben. Dit wekt interesse om op zoek te gaan naar andere alternatieven voor dit schip. Een drijvend installatieschip heeft geen maximale werkdiepte en is daarom een veelbelovend alternatief. Maar omdat dit schip zichzelf juist niet op de bodem kan positioneren hebben de zee- en weersomstandigheden meer invloed. Dit afstudeerrapport focust zich daarom op het ontwerpen van een tool die de installatie van offshore windturbines kan verbeteren vanaf een drijvend installatieschip om zo de extra ongewenste bewegingen te verminderen. Het doel van deze studie is samengevat in de volgende onderzoeksvraag:

Wat voor beweging compenserende tool kan ontwikkeld worden voor de installatie van offshore windturbines vanaf een drijvend installatieschip, en hoe presteert deze vergeleken met het huidige installatieproces?

De eerste stap van het onderzoek was het analyseren van het huidige installatieproces. De manier waarop een offshore wind farm geïnstalleerd wordt hangt heel erg af van de locatie en zeecondities. Dit is waarom er geen standaardprocedure vast te stellen is voor het installeren van een offshore wind farm. In tegenstelling tot het overkoepelende installatieproces worden de onderdelen van een turbine wel altijd in dezelfde volgorde geïnstalleerd. Als eerst wordt de fundatie geïnstalleerd gevolgd door het transitiestuk. Dan worden de toren, nacelle en bladen opeenvolgend geïnstalleerd. Uit de literatuur blijkt dat het installeren van de onderdelen erg veel precisie vereist wat vervolgens snel in gevaar kan worden gebracht door ongewenste bewegingen. De offshore-industrie is niet de enige die kampt met problemen door ongewenste bewegingen en daarom zijn er ook al veel bestaande oplossingen binnen en buiten de offshore industrie te vinden.

De studie is afgebakend door middel van het opstellen van een case study. Het verbeteren van het installatieproces kan op vele manieren gedaan worden. Om het aantal mogelijkheden te verminderen is de installatie van elk onderdeel bestudeerd en uit onderzoek is gebleken dat de installatie van de nacelle het meest innovatief was en potentie had tot verbetering. De andere onderdelen hebben al goed werkende oplossingen of zijn al hevig bestudeerd. De Haliade X van GE is gekozen als referentie, omdat deze turbine representatief is voor de huidige generatie turbines en die van de toekomst. Naast de turbine is ook een installatieschip gekozen voor referentie, de Les Alizés die behoort tot de vloot van Jan de Nul. Tevens is er aangenomen dat de kraan van het schip uitgerust is met een 3D-bewegingscompensator. Op deze manier kon er gebruik worden gemaakt van beschikbare data over de dynamica van de kraanhaak tijdens de installatie.

De ontwerpmethode die is toegepast in deze thesis bestond uit een analyse, synthese en evaluatie welke is bedacht door John Cristopher Jones. Met deze methode zijn zeven concepten bedacht die mogelijk kunnen compenseren voor de ongewenste bewegingen tijdens de installatie van de nacelle. De concepten zijn vervolgens geëvalueerd met een analytische hiërarchie methode. Het concept bestaande uit twee XY-tafels werd geselecteerd voor het uiteindelijke ontwerp. Dit concept maakt het mogelijk dat de nacelle onder het hoofdframe waar het aan hangt, bewogen kan worden. Een contragewicht wordt dan in de tegenovergestelde

richting verplaatst om het momentevenwicht te bewaren.

Het concept is in het uiteindelijke ontwerp opgebouwd uit vijf onderdelen: nacelle carrier, onderste x-tafel, hoofdframe, bovenste y-tafel en contragewicht. Een fundamenteel structureel ontwerp is gemaakt waarbij elk onderdeel werd opgebouwd uit stalen balken met een rechthoekig koker profiel. De berekeningen maken gebruik van de norm DNVGL-ST-N001 voor marine operaties en waarborging. Een 3D-model van het ontwerp is gemaakt in SolidWorks om een duidelijk beeld te geven en is te zien in Fig. 2. De tool, inclusief het contragewicht van 130 ton heeft een geschat gewicht van 170.9 ton.

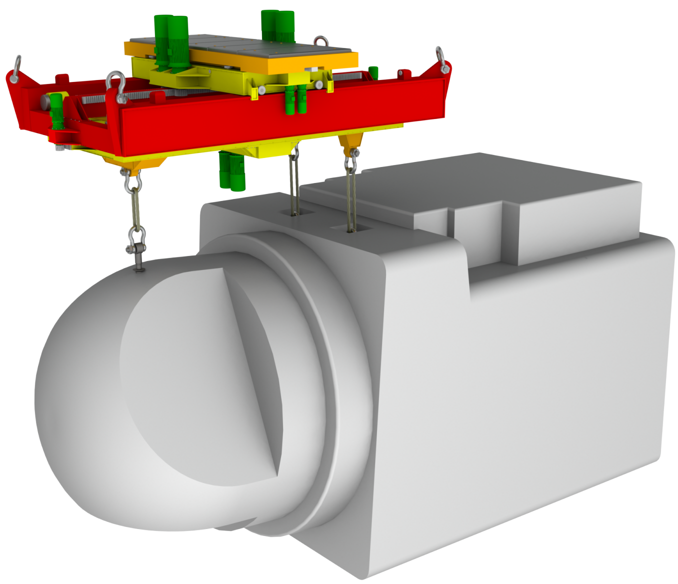

Figure 2: 3D-model van het ontwerp

Een dynamische analyse is vervolgens uitgevoerd om te onderzoeken of het concept ook daadwerkelijk werkt. Een wiskundig model is ontwikkeld dat het concept representeert. Dit model is vervolgens geanalyseerd met behulp van MATLAB en Simulink. Voor deze thesis is gebruik gemaakt van een proportionele-integrerende-differentiërende (PID) regelaar om de positie van de nacelle te regelen. Omdat een uitgebreidere studie op het gebied van regelsystemen niet binnen dit onderzoek valt is er gekozen om MATLAB het model te laten linearizeren en de regelaar af te stellen. De resultaten van de simulaties met het eerste model leiden tot onverwachte resultaten. Om de oorzaak van deze resultaten te onderzoeken zijn twee variaties op het originele concept bedacht samen met verschillende foutregelingen voor de regelaar. De daaropvolgende simulaties lieten zien dat er wel degelijk een dempingseffect gecreëerd kan worden, maar alleen wanneer slechts het contragewicht werd aangestuurd en de nacelle op dezelfde positie werd gehouden.

Acronyms

AHP	analytic hierarchy process	1, 38, 39
CoG	Centre of Gravity	1, 41–43, 47, 49, 61, 67, 71, 73, 95
DAF	Dynamic amplification factor	1, 49, 50
DOF	degrees of freedom	1, 16, 25, 28, 36, 38
DP	dynamic positioning	1, 16, 25
EoM	equations of motion	1, 71
FIV	floating installation vessel	1, 15, 16, 23, 31
HMC	Hook Mounted Compensator	1, 16, 30, 38, 49, 52
MP	monopile	1, 22
OWF	offshore wind farm	1, 15, 19, 21, 24
OWT	offshore wind turbine	1, 15, 16, 19, 26, 28, 30, 38
PID	proportional-integral-derivative	1, 65, 68, 70, 72, 74, 76, 77
SHL	Static Hook Load	1, 49
SKL	Skew load factor	1, 49, 50
TP	transition piece	1, 20, 25

Contents

1 Introduction

The increasing energy demand, the fact we are running out of fossil fuels and the acceptance of global warming has led to an increase in the demand for renewable energy sources. Wind energy is one of the most promising renewable energy sources currently available. It's very clean and is the first to generate a similar amount of electricity when compared to fossil-based energy sources (1) and a large portion of comes from offshore wind turbines (OWT). Since 2009 Europe has increased its offshore wind capacity tremendously. Where the cumulative installed capacity was roughly 2.5 GW in 2009 it reached 22 GW at the end of 2019 (2).

The first offshore wind farms (OWF) were built relatively close to the shore, but recent trends show that new farms are being built further off the coast. When building an offshore wind farm further of the coast it also means that the installation depth increases simultaneously. These trends can be seen in Fig. 3 and Fig. 4 where the increasing average water depth and distance to shore of recently installed OWFs are presented.

The increasing depth and distance to shore introduces new challenges in the offshore wind industry. A jack-up vessel is a common installation vessel for offshore wind turbines, this vessel can lift itself out of the water with the help of long support legs. This ability makes the vessel highly suitable for offshore operations as it is less affected by the weather conditions. However, a consequence of this jack-up system is a maximum operating depth, and due to the increasing the water depths of OWFs the usability of the current jack-up vessels therefore becomes limited.

A promising alternative for a jack-up vessel is a floating installation vessel (FIV), since this vessel is not limited by a maximum operating depth since it has no jack-up system. Unlike a jack-up vessel, a floating vessel is more susceptible to wind and waves, resulting in more unwanted motions. The increase in motion decreases the workability of the floating installation vessel (3). And since the installation of a wind farm can be heavily delayed when a vessel is not able to operate due to bad weather conditions it is relevant to find a solution.

Huisman is a company that designs, manufactures and services heavy construction equipment for the world's leading companies in the renewable energy, oil and gas, civil, naval and entertainment markets. They are investigating options for a tool that increases the workability of a floating vessel for the installation of offshore wind turbines. Such a tool could reduce the weather downtime and increase the installation rate for OWTs
.

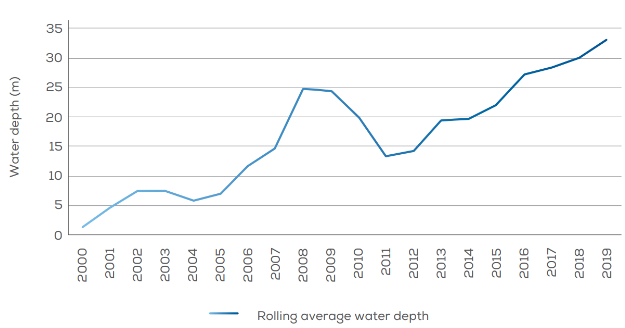

Figure 3: The average water depth of recently installed wind farms

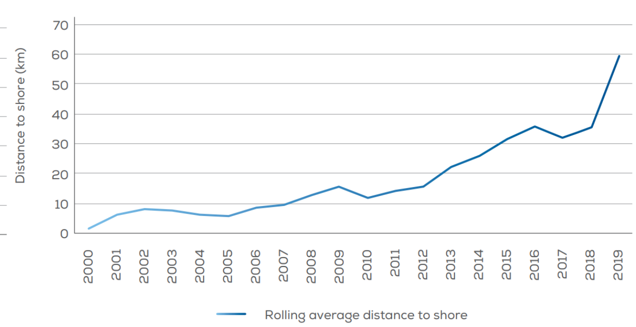

Figure 4: The average distance to shore of recently installed wind farms

1.1 Aim and objective

As stated in the previous paragraph the energy generated by offshore wind farms has to increase in the coming decades. Technological developments in the field of wind energy show that newer wind turbines with a higher capacity and efficiency characteristics will help meeting this demand. Despite their high output it is still necessary to install a large number of wind turbines in the near future. Therefore, improvements in the installation process are crucial to help reaching the increasing sustainable energy demand.

The recent trends of building wind farms further of the shore, in deeper seas and the use of larger wind turbines, mean that floating installation vessels are becoming more viable for offshore turbine installations. Because a FIV has no supports on the seabed it is very susceptible to wind- and wave-induced motions. The introduction of more unwanted motions has gained interest to look into solutions that can reduce the effects during offshore operations. This is why Huisman is interested in developing a tool which can compensate or dampen unwanted motions.

This study aims to develop a solution that can compensate for increasing motions during the installation of an offshore wind turbine. Motion compensation during the installation of an OWT can be done on the vessel, the crane, the load or somewhere in between. Completely compensating the vessels motion is very difficult to achieve due to its size and mass, but it is partially done using dynamic positioning (DP). DP enables a vessel to automatically maintain its position using only thrusters (4). The second option is to decouple the crane's motions from the vessel. Placing a motion compensating solution between the crane and the vessel is possible, but for cranes lifting heavy loads this is not very efficient since the whole crane structure has to be compensated then as well. The third option aims to uncouple the load from the crane. This results in what in this thesis will called a 'Hook Mounted Compensator (HMC)' and it is a solution located between the crane and the load. The HMC's location has significant potential since it can include the motions of both the vessel and the crane. This is not a completely new idea, however existing solutions like (5) and (6) often only compensate for heave motion. This study aims to expand the idea to a motion compensator that can compensate in one or more different degrees of freedom (DOF). Therefore, the following research question is formulated to achieve the goal of this study:

What hook mounted motion compensation tool can be developed for turbine installation from a floating vessel, and how does its performance compare to the conventional installation process?

Logically the main research question can't be answered directly, so several sub-questions are formulated:

Q1. How is the current installation process for offshore wind turbines defined and how can the relevant installation steps be described?

Q2. What are common problems that arise during the installation of an offshore wind turbine as a result of unwanted motion and how do these problems affect the installation process?

Q3. The installation of which turbine component is the most innovative and has the most potential to improve the installation of an offshore wind turbine?

Q4. What methods can be adopted to generate and evaluate different concepts for hook mounted compensators?

Q5. What is the technological feasibility of the developed concept?

1.2 Research Scope

The scope of the study is set by the following points:

- To narrow down the size of the study and have a solid base to develop motion compensating solutions a case study will be defined. This will be done after the required background information has been studied. In this case study one part of the turbine will be selected where the concept will be designed for. Additionally, an existing offshore wind turbine and installation vessel will be selected to function as reference for the final concept design.
- The concept will be developed on a theoretical level where the technological feasibility can be explored. The conclusions that will be made in this thesis are therefore based on a theoretical concept and no experiments are conducted.

1.3 Thesis approach

In this master thesis a concept will be designed that can compensate for motion during the installation of an offshore wind turbine from a floating installation vessel. The approach that will be taken in this study is shown in the flowchart in Fig. 5.

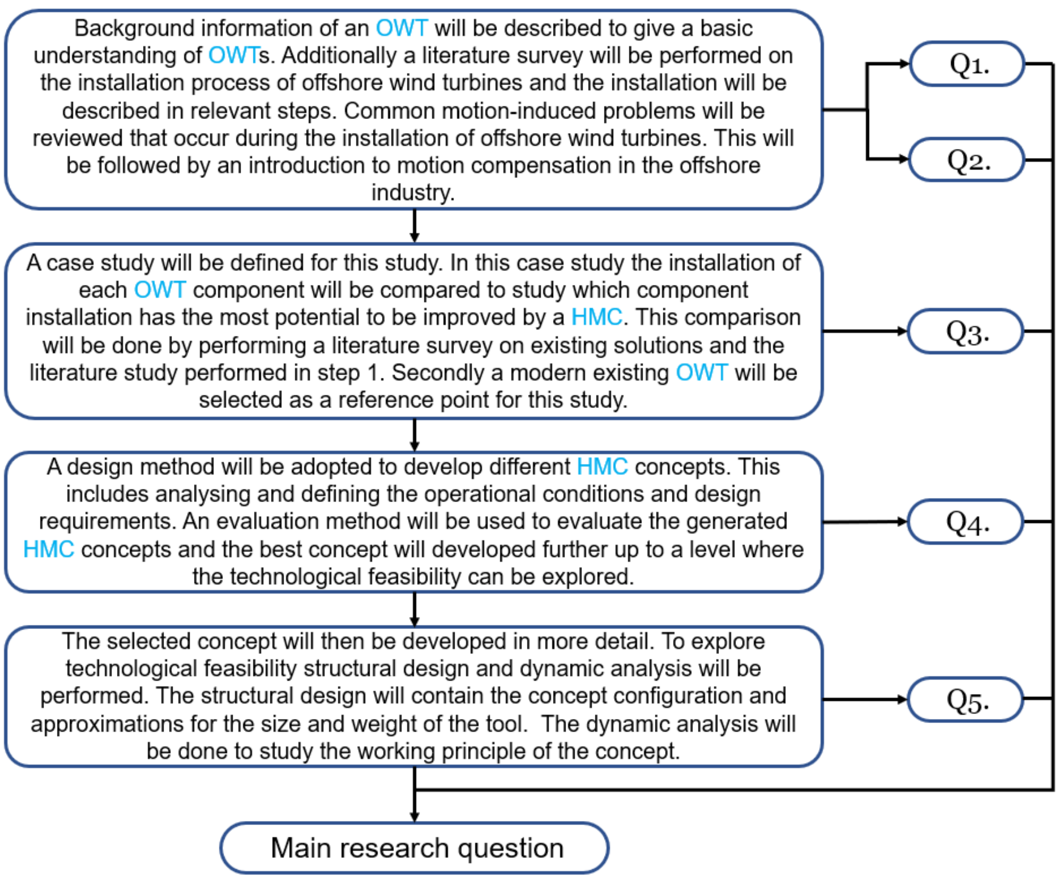

Figure 5: Thesis approach

2 Background Information

This chapter contains the basic knowledge required to do a study about improving the installation of offshore wind turbines. Firstly, it is important to be familiar with the anatomy of an OWT to understand these large-scale structures. The conventional installation process of an OWT and an OWF will also be described. This will also include common motion-related problems to confirm the relevance of this study. The third section will introduce existing types of motion compensating solutions and examples of where these solutions are applied.

2.1 Offshore wind turbines

2.1.1 Parts of an offshore wind turbine

The first wind turbine that was used to convert wind to electricity was created in 1888 (7). Since then, the development of wind turbines has come a long way, and especially the development of offshore wind turbines. A wind turbine is a huge machine and is made from many mechanical as well as electrical parts. For the scope of this study, the offshore wind turbine will be discussed by its five main parts. Every part can be found in Fig. 6.

Turbine foundation
Undoubtedly one of the most important parts of a wind turbine is its foundation. It is the part of the wind turbine which interacts directly with the bottom of the sea. Foundations can be divided into two main categories: bottom-fixed or floating foundations. The different types of bottom-fixed and floating foundations can be seen in Fig. 7. Here the foundations A to E are bottom-fixed foundations and F and G are floating foundations. For each foundation the approximate water depth of where it can be constructed is also given.

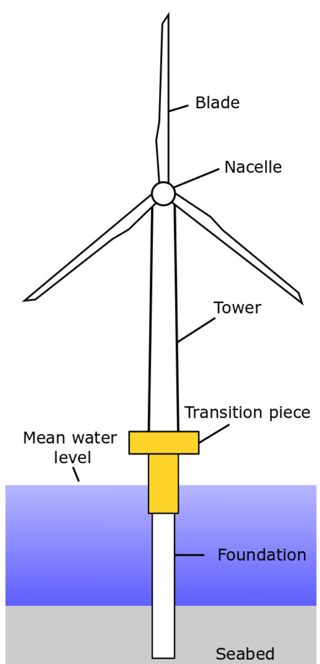

Figure 6: Offshore wind turbine parts

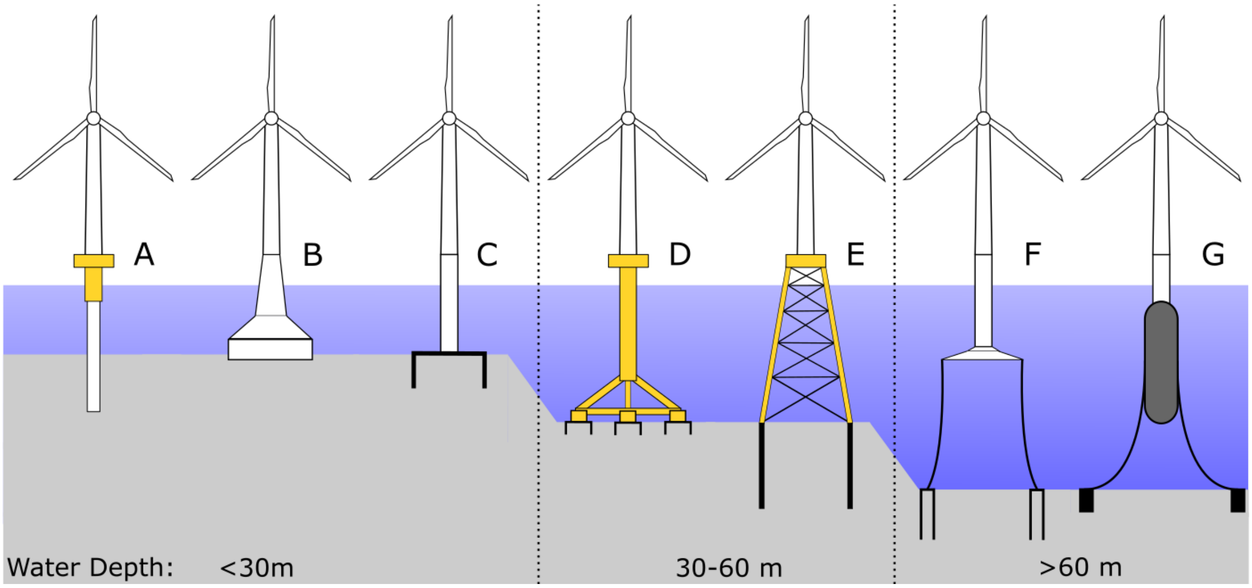

Figure 7: Types of foundations adapted from (9)

The trend of building offshore wind farms in deeper areas has caused an increase in interest for floating foundations. However bottom fixed foundations are still dominating the market as is apparent from recently built wind farms or farms which are still under construction. In Table 2 the new offshore wind installations in Europe with grid connection in 2020 are presented and floating foundations were only used in the Windfloat Atlantic wind farm, for the other eight new wind farms bottom-fixed foundations were used (8). Taking another look at Table 2 it can be seen that the choice for the type of bottom-fixed foundation is not very diverse. The monopile foundation has been dominating the market for years and still continues to do so. The monopile is a relatively simple design as it is a large steel tube pile which is driven into the seabed. Although it is possible that floating foundations will become more popular in the coming decades as offshore wind farms are being built further onto sea, the decision was made to choose the monopile foundation as reference point for this study.

Transition piece

The second component is the transition piece (TP) and is located between the foundation and the tower of the wind turbine. This part enables levelling of the structure when the foundation is installed with a minor inclination (9). The transition piece also contains a construction, inspection platform and access ways to support operation and maintenance activities.

Tower

The third component, the tower is the main body of the turbine and consists of a large, tapered steel tube that is placed on the transition piece. For larger wind turbines it often contains an elevator to reach the nacelle in the top of the tower. The tower also houses the transformer which is used to increase the voltage of the power before it is send to the substation of the wind farm.

Table 2: Offshore wind farms with grid connection in 2020

Country	Wind farm	Foundation type
Netherlands	Borssele 1&2	Monopile
	Borssele 3&4	Monopile
	Borssele 5	Monopile
Belgium	Seamade	Monopile
	Northwester 2	Monopile
United Kingdom	East Anglia One	3-Legs Jacket
Germany	EnBW Albatros	Monopile
	Trianel Windpark Borkum 2	Monopile
Portugal	Windfloat Atlantic	Semi-sub

Nacelle
The nacelle is the fourth component and can be found on top of the tower. This structure includes the rotor and contains a lot of electrical components and especially one of the most important parts of the wind turbine, the generator. The nacelle is connected to the tower by a bearing which enables rotation along the axis of the tower. This way the wind turbine can position itself in such a way that it can optimally use the wind.

Blades
The last component is the turbine blade. The blades of the turbine cause the rotor of the generator to rotate and this way energy can be generated. Each blade is relatively large for its weight and this is why they are able to transform the energy efficiently.

2.1.2 Installation process

Constructing an offshore wind farm can be done in many different ways and there is no standard process when it comes to installing an OWF (10). However, the installation order of an offshore wind turbine is always the same. This section will summarise the installation process and consider what types of vessels are commonly used when installing an offshore wind turbine.

Step 1: Transport
The first step in installing an offshore wind turbine is to transport the turbine components to the installation site. Because the installation process can be different for each installation it is difficult to define this step. This mostly depends on the type of turbine, location and the vessels available for use. We assume that the foundation and transport piece will be transported together. After these are installed the tower, nacelle and blades will be transported to the installation site on the installation vessel.

Step 2: Foundation installation
The foundation of the offshore wind turbine is the first component that gets installed. When the monopile has reached the site the first step is to upend the monopile using a gripper and place it vertically on the seabed. The next part of the installation is clearly described in (11). After the placement of the monopile a

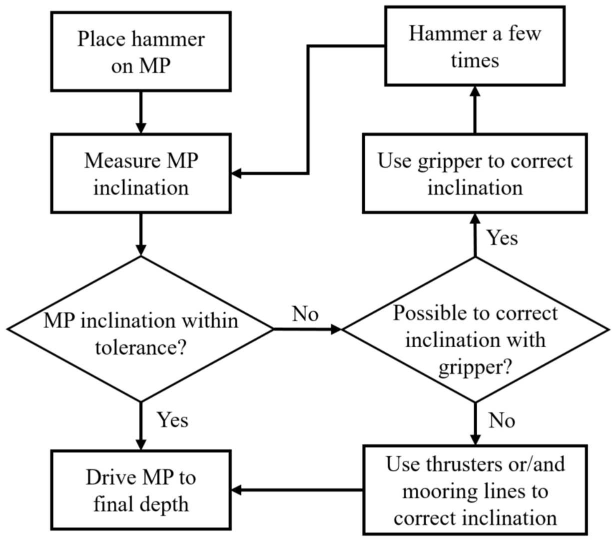

Figure 8: Flowchart of hammering a monopile adapted from (11)

hydraulic hammer is placed on top of the monopile. The next step is to drive the monopile into the seabed to the desired depth. During this operation it is mandatory to measure the inclination of the monopile which can be a result of the current and waves. If there is indeed an inclination and it can be corrected using the gripper this is done. After a number of blows the gripper is no longer able to correct the inclination of the MP and if the inclination is within the tolerance boundaries it is driven to the final penetration depth. If the inclination exceeds the tolerance boundaries it can still be corrected using thrusters and/or mooring lines. The whole process is given in the flowchart in Fig. 8. The installation of the monopile can be assisted by a drill that can be placed inside the steel structure of the foundation. Drilling is often required when the foundations are being installed on a rocky seabed.

Step 3: Transition piece and tower installation

When the monopile is in place the transition piece can be installed on the monopile. The first step to install the transition piece is to align it with the monopile. Then the transition piece is lowered to initiate the mating phase. If the mating points remain inside the set boundaries the transition piece can lowered further onto the monopile and finally reaching the support brackets. Hereafter the inclination of the transition piece is checked and when it falls outside the tolerance it needs to be done over and lifted up again (12). After the transition piece is successfully installed on the foundation it is time to place the tower on top of it. The installation of the tower is merges with the installation of the transition piece, because the installation of the tower is very similar to the installation of the transition piece (13).

Step 4: Nacelle installation

The next component to be installed is the nacelle of the wind turbine. The nacelle will be lifted from the installation vessel and will then be mated to the turbine tower. The alignment and installation of the nacelle is commonly assisted by an installation crew in the top of the tower.

Step 5: Blade installation

There are several methods to mount the blades to the nacelle. In this study a method will be considered where three blades are installed separately. To install the blades the rotor hub of the nacelle is rotated to a horizontal position. Then the blade is lifted to the same level as the rotor by a crane. The blade has a large guiding pin that goes into a flange hole to align the blade with the rotor. During this operation the guiding pin is well monitored to make sure that the installation goes smoothly. When the guiding pin is inserted it is followed by multiple shorter bolts. If one blade is installed the rotor is turned in order to install the next blade until all three blades are installed (14). The blade installation process is given in the flowchart of Fig. 9. If the generic installation process is summarized it is possible to create the flowchart in Fig. 10.

Installation vessels

The complete installation process cannot be executed without the help of installation vessels. The dominant installation vessel is the jack-up vessel as previously mentioned in the introduction. This vessel uses long support legs to enable jacking up above the water until the desired operating height is reached. The first jack-up vessels were originally intended for the oil and gas industry and had not enough capacity to handle larger turbines. For this reason, special vessels were built which were designed to handle the installation of the larger wind turbines which are currently being built. One of the main advantages of the jack-up vessel is its ability to completely negate the effects of waves during the installation. However, the support legs result in a maximum operating depth. One of the largest jack-up installation vessels which is currently under construction has a maximum operating depth of 80 meters (15) and can be seen in Fig. 11. Soil conditions are also an important factor to consider as a jack-up vessel cannot be used on every type of soil. An example is the currently planned wind park Arcadis Ost 1 located 20 kilometres northeast of the island of Rugen in the Baltic Sea (16).

An alternative for the jack-up vessel is a floating installation vessel. This vessel has the advantage that it avoids every bit of interaction with the soil, which makes it possible to install wind turbines on locations where the soil conditions are not optimal. The second advantage is that a floating vessel has no maximum operating depth as a result of support legs. This is what makes the FIV vessel very interesting for future wind farms which are being built further onto sea. The company that is building the Voltaire is also building a new floating installation vessel, the Les Alizés. This vessel can be seen in Fig. 12.

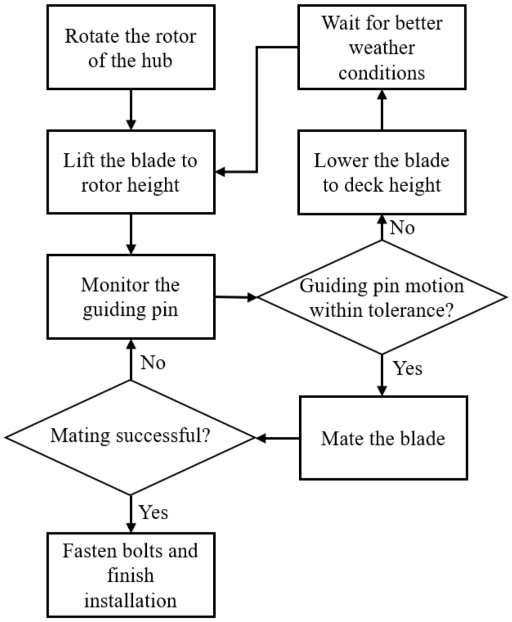

Figure 9: Flowchart of the blade installation process adapted from (14)

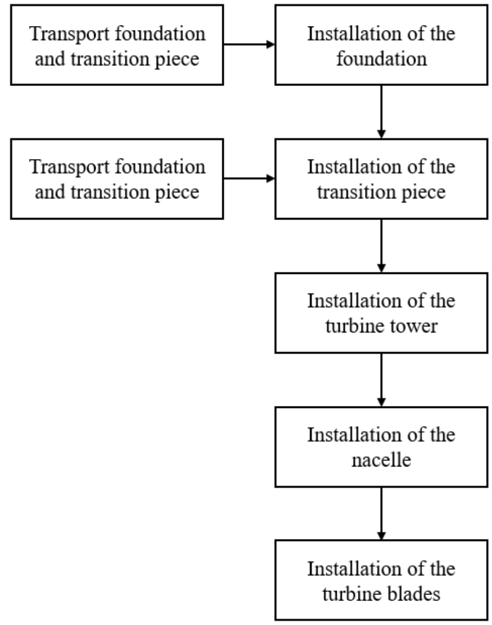

Figure 10: Flowchart of the general installation process

Figure 11: Jack-up vessel the Voltaire (15)

Figure 12: Floating installation vessel the Les Alizés (17)

2.2 Challenges

Due to the complexity and scale of the construction of an offshore wind farm it is not surprising that challenges are present during the process. For example, finding a suitable installation location is often one of the first challenges for the installation of an OWF (18). The planning and logistics of the complete operation also prove to be challenging because it is highly dependent on the weather and sea conditions (19). This study will focus on the challenges caused by unwanted motions during the installation of the parts of the wind turbine. These motions affect various systems in the offshore industry as parameters like wind speed, wave height and current have a large impact. In this section commonly used terms for the position of a vessel will first be discussed. Then multiple motion-induced problems will be presented that can be found in the literature to confirm that relative motion is an issue.

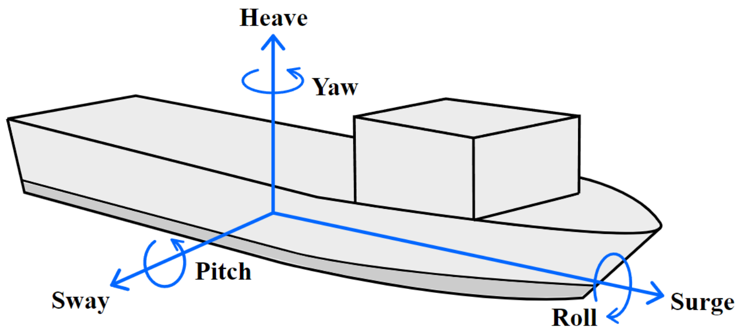

Figure 13: The degrees of freedom of a ship

First the vessel is analysed to understand the sources and behaviour of the motions. The main source for motion is the wave influence on the installation vessel. These motions are then transferred through the ship via the crane to the load. To get a better understanding of the dynamics, the vessel, the crane and the load will be discussed separately. The first system is the installation vessel which is heavily affected by the conditions of the sea. The installation vessel has six degrees of freedom to describe its position and orientation. The DOF can be described as three translations (surge, sway and heave) and three rotations (roll, pitch and yaw) and are shown in Fig. 13. Most ships are currently equipped with a dynamic positioning system which was already mentioned in section 1.1. This means that the sway, surge and yaw are relatively well controlled. The previously mentioned installation vessel Les Alizés is for example equipped with a DP class 2 system. The class 2 system ensures that whenever a passive component fails the vessel still is kept in position for a long enough time to safely terminate the operation (4).

The motions of the installation vessel that are not compensated are transferred to the load via the ship mounted crane. In addition to the vessel's motions, the crane is also prone to motions induced by the wind at sea. The summation of all these motion sources eventually has an effect on the movement of the load.

In (11) several problems are presented during the installation of the monopile. It is very important that the monopile remains within the inclination boundaries during the hammering. The sea state, wind and current are the limiting parameters for the efficiency and success of this operation. Each parameter plays an important role in the dynamic motion of the monopile and floating installation vessel. Each time the step of measuring and correcting the inclination of the monopile has to be performed it adds a significant delay to the installation.

In (12) the possible critical and restrictive events are described during the installation of the transition piece. A critical event is defined as an event which is irreversible and has an enormous impact on the installation process. A restrictive event is an event which could be reversible or the operation could be tried again. The first restrictive event that can occur is the misalignment of the monopile and the transition piece due to horizontal motions of the bottom of the TP. If the bottom of the TP is not inside the mating boundaries and the process is continued it can lead to structural damage. Another consequence could be structural failure of the hoist wires or slings due to the impact. This event is critical as these consequences can cause a significant delay in OWT construction planning. The mating process of the tower on top of the transition piece faces similar problems. This also applied to the installation of the nacelle on top of the tower, because all of them are vertical installations hindered by horizontal differences. However, it is worth mentioning that the installation gets more sensitive to motion with each extra component installed. When the transition piece was installed only the dynamic behaviour of the foundation has to be taken into account. Whereas when the nacelle gets installed the dynamic behaviour from the foundation, transition piece and tower have to be considered.

The turbine blades are the last pieces that need to be installed to complete the structure of the wind turbine. The blades are relatively large for their weight which makes them very susceptible to wind forces. As said in the previous paragraph the blade has to be carefully mated to the rotor hub of the wind turbine. When the relative motion of the guiding pin of the blade is too large the blade will be kept in position next to the hub for a maximum of 30 minutes. If during this period the relative motion is sufficient the process will continue, if not the blade will be lowered back to deck level until the weather conditions have improved.

Although the floating installation vessel is very promising, a challenge arises when this type of vessel is to be deployed for offshore wind turbine installation. As the vessel has no fixation on the seabed it is heavily affected by the motion of the waves. This causes motion-induced problems during the precise installation of a turbine. Another issue arises during the transport of components to the installation site. As said earlier in this paragraph, this can be done in different ways. Depending on the method, it is possible that components have to be transferred from one floating vessel to the floating installation vessel. This interaction will face more relative motion than when the parts had to be transferred to a jack-up vessel.

All in all, it can be concluded that relative motion can delay the installation of an OWT drastically. The weather conditions are the main reason for relative motion between the installation vessel and the installation surface. The next section will discuss the basics of motion compensation and also presents some interesting examples of solutions deployed in and outside the offshore industry to handle these problems.

2.3 Types of motion compensation

Since unwanted motion is a well-known problem in the offshore industry it is not surprising that a lot of research has been done on this topic. Additionally, there are already a lot of motion compensating solutions on the market. This section will explain the differences between three types of motion compensation techniques. A few interesting examples of already existing motion compensating solutions are also included.

Passive motion compensation

A passive compensation system is an open-loop system without any feedback. One of the simplest passive compensators is a parallel spring-damper combination (3). This simple compensator is given schematically in Fig. 14. With technological advancements the spring was replaced by newer technologies like hydraulic pistons and eventually pneumatic systems. The advantage of a passive compensator is that it is load driven and no additional input is required. A perfect example of a passive motion compensating system outside the offshore industry is the suspension in a car. It dampens the motions caused by bumps in the road without any extra input.

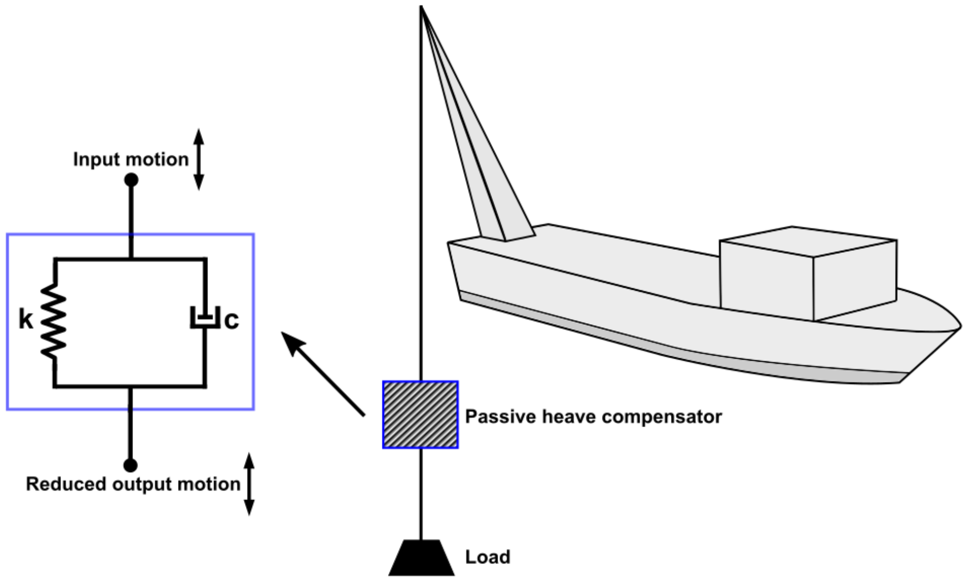

Figure 14: Schematic design of a parallel spring-damper combination for passive motion compensation. Adapted from (3).

Active motion compensation

Contrary to passive systems, active motion compensation systems use feedback in a closed-loop to effectively dampen the motion. Active motion compensation requires an input that is often in the form of measurements. For heave compensation it means that the heave movement of the vessel is measured and is relayed back to the closed-loop system. The system contains a controller which translates the measurements to adequate actions to counter the movement. A widely used example of an active motion compensation solution is a so called 'motion compensation platform'. The platform is able to compensate for motion in one or more degrees of freedom. Cruise ships make extensive use of this technique as it can be applied to pool tables, bowling lanes, medical beds and much more (20). In Fig. 15 and Fig. 16 examples of motion compensated platforms are given.

Figure 15: Motion compensation platform from Huisman (25).

Figure 16: A motion compensated pool table from Stable (20).

Active motion compensation can also be found in many other industries besides the offshore industry. To gain inspiration for possible solutions it may be valuable to also explore other industries. The first example is the technology called 'inertially stabilized platforms' which can be found in a wide range of applications. According to (33) it has purposes in the military, scientific and even in commercial fields. An accessible commercial product is the stabilization systems for cameras or phones. The system consists of a set of driven gyroscopes and the amount depends on how much degrees of freedom it can stabilize. An example of a camera stabilizer is given in Fig. 17. A second interesting technology that could provide a possible solution can be found in specific type of simulator that falls under the category 'cable robot'. In Fig. 18 a vehicle simulation system is considered that is controlled by six cables giving full control over 6 DOF of a platform. Vehicle simulators are not new, but this type of simulators replaces the previous hydraulic control system with cables. The main advantages are that this type of robot weighs much less while still providing the same external loads. An image of a similar simulator is given in Fig. 18.

Figure 17: Example of a camera stabilizer from (34).

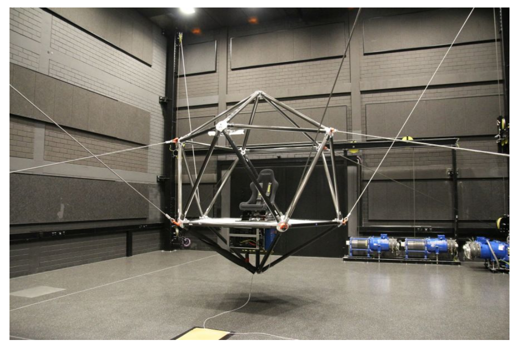

Figure 18: A cable-controlled simulator from (36).

Hybrid motion compensation

A third option is to use a combination of active and passive components in a compensation system. A hybrid system is used when it is not necessary to use a full active system. The advantage of a hybrid system is that it can still achieve a relative high level of precision with a lower energy consumption rate. Additionally, a hybrid system is often cheaper, because it requires less expensive sensors and controllers.

2.4 Case study

In section 1.2 it was mentioned that a case study would be used to set the boundaries for this study and to lay a foundation for the concept design. Since a tool is to be designed that improves the installation of an OWT it is mandatory to choose for which part the tool will be designed. Additionally, an existing offshore wind turbine and installation vessel are selected for reference for the design.

2.4.1 Selected turbine component

Previously the installation process of an OWT was analysed and it was clear that although some component installations are somewhat similar, they mostly are different. This is the reason why it is important to choose the installation of one component instead of a general approach that works for every component. The selection will be done by using the method of elimination. The first option is to compensate motion during

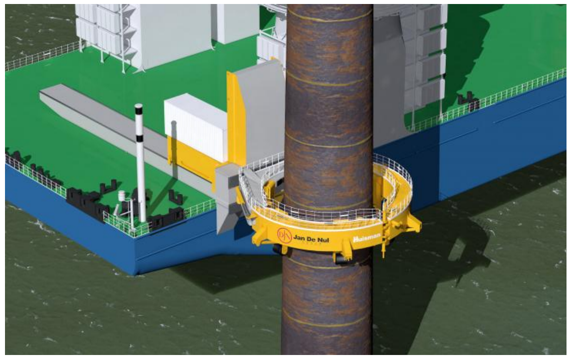

Figure 19: A monopile gripper developed by Huisman for Jan de Nul Group (39)

the installation of the foundation. When the monopile has to be placed on the seabed it is mostly important to keep the monopile within the set inclination boundaries. In some weather conditions this task can be difficult, but an efficient and good working tool already exists. This tool is called a 'monopile gripper' and can be seen in Fig. 19. The gripper holds the monopile and is able to adjust the foundation to keep it within the inclination boundaries. Because a good working solution already exists the installation of the monopile is eliminated for this study.

The installation of the transition piece and tower are very similar to the installation of the foundation as they also heavily depend on the motions perpendicular to the monopile's length. However, a solution like the monopile gripper is not developed for these steps. This makes these steps more suitable for a new motion compensating concept.

The nacelle is the next component which is installed and as the installation height gets bigger the installation also becomes more difficult. Especially as the operating space of the crane gets smaller as the component needs to be installed at greater heights. The installation of the nacelle requires a high level of precision and is assisted by an installation crew. This makes safety an additional important factor in determining under which weather conditions the installation can proceed. So, the nacelle installation is a potential candidate for the development of a motion compensating tool.

The last piece to consider is the installation of the turbine blades. As this is probably the most difficult installation step it could also be a good step to develop a motion compensating solution for. However, the installation of a turbine blade is heavily studied and many approaches and tools are developed (21). For example, the boom based manipulator and the boom lock are used for blade installations from a jack-up vessel. This equipment is used to adjust the movement of the blade during lifting operations as is shown in Fig. 20. The blade dragon, shown in Fig. 21 has the same function, but is already used in combination with a floating installation vessel.

Figure 20: Boom lock (38)

Figure 21: Blade dragon (37)

The installation of the foundation, transition piece and tower are relatively simple as these installations are performed around sea level. These components have parts which guide them to achieve mating. The remaining problem is when a component hits another component at a high speed due to heave motion. Heave compensation solutions are well studies and developed up to level that a HMC has not much additional value. As mentioned previously the installation gets more difficult as the installation height gets bigger and this is why it is interesting to select a component which is installed at a greater height, thus the nacelle or the blades. It can be concluded that the installation of the turbine blades is also well studied and that installation tools exist in abundance. For this reason, a motion compensating tool will developed with the goal to improve the installation of the nacelle.

2.4.2 Selected wind turbine

Because the concept will be developed for a OWTs that are currently being built and for future large OWTs it is important to select one that is representative for these turbines. The Haliade X created by GE is one of the most powerful offshore turbines in existence and has a capacity factor that is 60-64% above the standard (22). This turbine also has a monopile foundation which was the dominant foundation. For this study the specifications of the 12 MW version will be used for design requirements and the modelling stage. The general specifications and a photo of the Haliade X are given in Table 3. Since the tool will be developed for the installation of the nacelle the general dimensions of the nacelle are given in Table 4.

Table 3: General specifications of the Haliade X, 12MW

Characteristic	**Specification value**
Rated output [MW]	12
Hub height [m]	138
Rotor diameter [m]	220
Number of blades	3
Blade length [m]	107
Cut-in wind speed [m/s]	3
Rated wind speed [m/s]	12
Cut-out wind speed [m/s]	28
Design life [years]	25

Table 4: Mass and dimensions of the nacelle

Characteristic	Specification value
Nacelle mass [t]	650
Length [m]	21,8
Width [m]	9,7
Height [m]	11,7

2.4.3 Selected Installation vessel

Because the jack-up vessel has it limits the scope of the study was set to develop a motion compensating tool for offshore turbine installation from a floating installation vessel. For this study not only the dimensions of the turbine are important, but also the dimensions of the vessel containing the installation crane. A suitable vessel was already mentioned in section 2.1.2, the Les Alizés. With this information the distance between every component is known and the available space for designing a tool can be determined. The dynamic behaviour of the vessel and especially the nacelle during installation is also important for the simulation phase of this study. Since the dynamic behaviour heavily depends on the sea and weather conditions it is different for each operation. An additional factor that plays a role is the type of crane that is used for the installation of the turbine. For these reasons it is difficult to obtain concrete information on the dynamical behaviour of the nacelle.

This issue can be solved by selecting a vessel with a crane for which data is available. An interesting option is to assume that in the future turbine will be installed by a crane that is equipped with some sort of motion compensation. This motion compensated crane will reduce the increased level of motion that comes with the use of a FIV. This assumption can be supported by the argument that is highly likely that future floating installation vessels will use motion compensating systems that are available to them to decrease unwanted motions as much as possible. Huisman already has developed a 3D-motion compensated crane that reduces the unwanted motions induced by the vessel. Simulation data from this crane can be used to approximate the motion of the nacelle during installation.

So, for the remainder of this thesis the Les Alizés will be considered as the floating installation vessel and it is assumed that its crane is equipped with the 3D-motion compensated system from Huisman. With the selection of the turbine, component and the vessel it is possible to sketch the installation setting with these systems. This sketch contains the significant distances and is presented in Fig. 22.

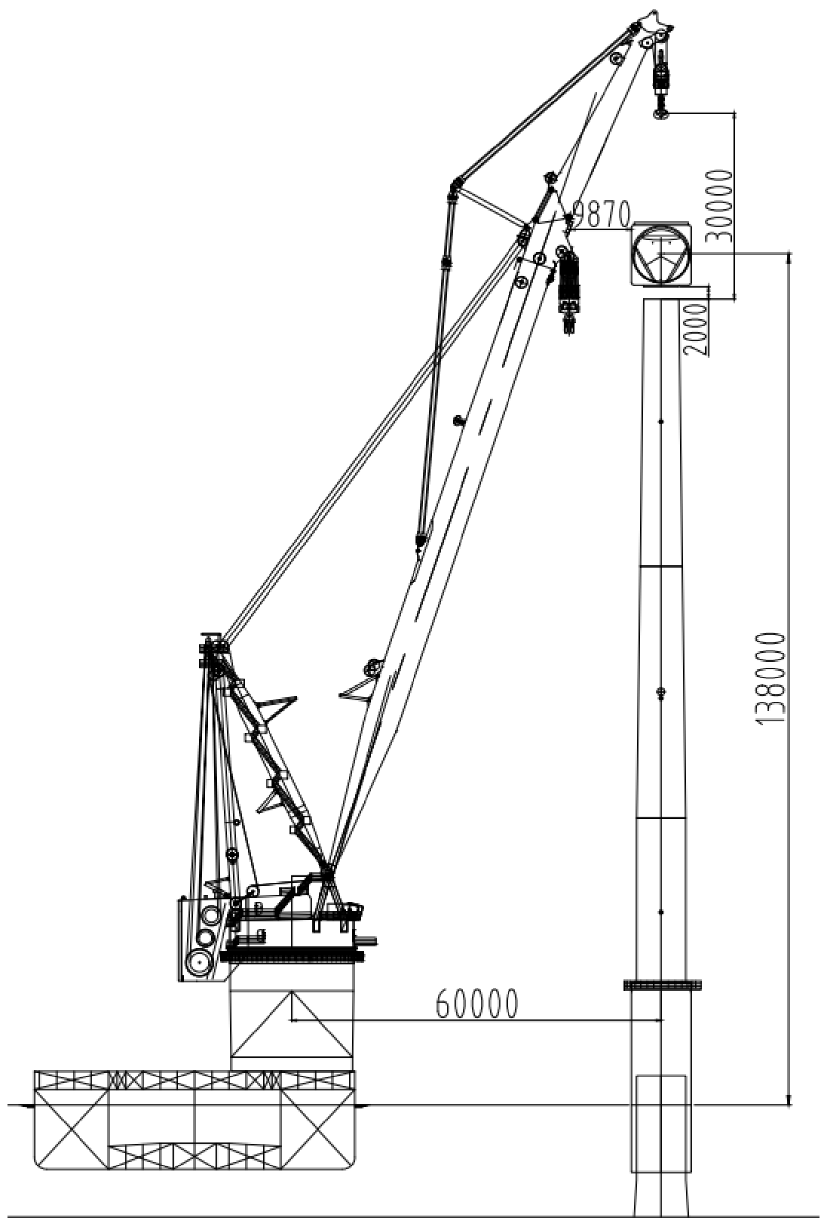

Figure 22: Dimensions of the vessel and crane

3 Developing motion compensating concepts

In this chapter a solution will be sought that can help in reducing unwanted motions during the installation. This will be done via a systematic design methodology to analyze the problem, come up with interesting concepts and select one for a final concept design.

3.1 Design Methodology

Developing concepts for a new technology can be efficiently done when a systematic design methodology is applied. Back in 1963 John Christopher Jones was the first to acknowledge this (23). He divided the design process in three distinct phases: analysis, synthesis and evaluation. The first stage, design analysis, consists of describing the design requirements and performance specifications. Design synthesis is the second phase and this is where the solutions to the requirements and specifications are produced. These solutions are then used to generate multiple concepts. The third and last stage is evaluating the different generated concepts and selecting one to work out in more detail. The selection will be done by a applying the so called 'analytical hierarchy method' which will be explained in section section 3.4. A complete overview of the design methodology is schematically given in Fig. 23.

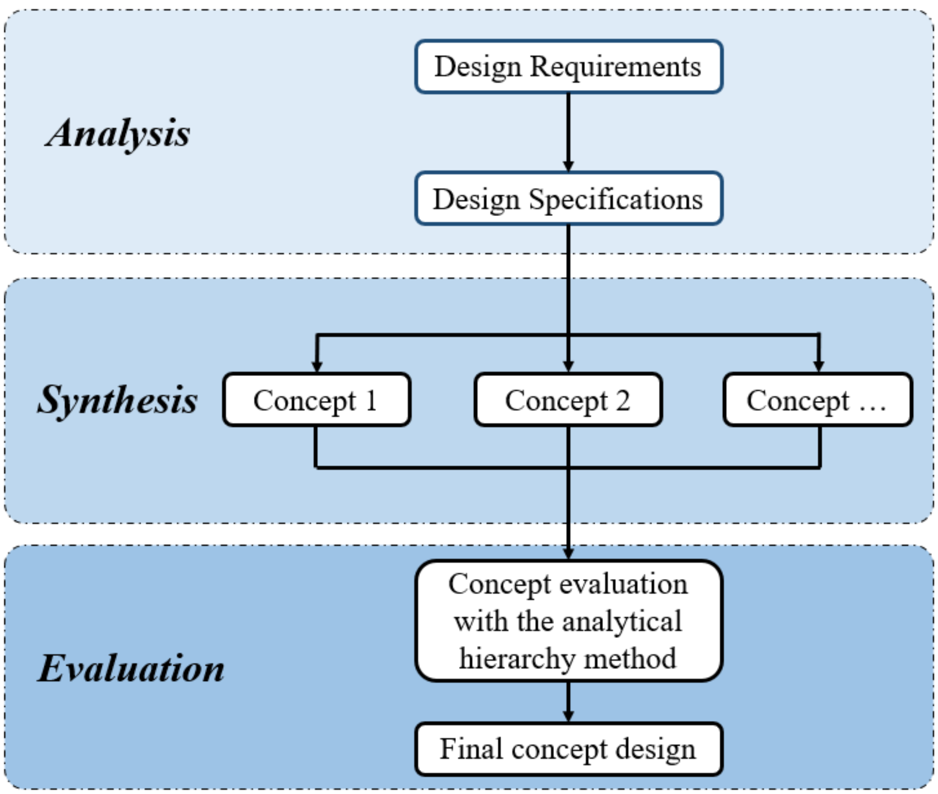

Figure 23: Overview of the design methodology

3.2 Design Analysis

The first step in the design analysis as described by Jones is to determine the design requirements. The design requirements describe the aspects of the tool which are necessary to achieve its goal. In this thesis the design requirements will be described as concrete as the case study allows. The following design requirements are considered in this research:

R1. Motion compensating technology
The core idea for the tool is that is has to improve the installation process of the turbine nacelle by reducing the motion of the nacelle. With the information provided from Huisman on the 3D-motion compensated crane a displacement of $\pm$0,3 m at the crane hook is expected when installing a nacelle. This gives a good indication of the order of movement that can be expected.

R2. Position and orientation measurements
A tool can compensate for motion in different ways, however for most cases the position and orientation of the nacelle is valuable. To enhance the installation process even further the position of the tower might also be required.

R3. Connection between the crane and the load
The tool is the connection between the crane and the nacelle. That's why the tool also required the ability to carry the nacelle

R4. Minimize impact on lifting capacity
A crane has a limited lifting capacity. The installation vessel Les Alizés has a maximum loading capacity of 5000t on its main hoist and 1500t on its auxiliary hoist. Since the nacelle has a mass of 650t the tool cannot exceed a mass of 850t.

R5. Minimize the impact on lifting height
A crane also has a limited lifting height and the nacelle has to be installed at relative large heights. The nacelle of the Haliade X has an installation height of 138m and with the Les Alizés this leaves roughly 20 meters between the nacelle and the crane hook.

R6. Maintain or improve safety
A common aspect when designing is the safety aspect of a product. Because people are present during the installation of the nacelle the safety aspect of the tool can't be neglected.

R7. Technological feasibility
Another important aspect is technological feasibility. The tool will be created for a purpose which is relatively new, meaning that there are not a lot of already existing solutions for this specific problem. This is why technological feasibility has to be kept in mind.

R8. Economic feasibility
A trivial aspect in every list of design requirements. Although this thesis does not focus on the minimization of the costs, it is taken into account to avoid very expensive materials and components.

The next step is to transform the design requirements to performance specifications. The performance specifications are a set of functions which the concept has to perform and are a direct result from the design requirements. This is done because not every design requirement can be translated to an explicit task for the concept generation phase. Looking at the requirements that are valuable for the generation of concepts two design specifications can be described:

S1. Compensate for unwanted motion of the nacelle relative to the tower
Being the core principle of the tool, this is the most important function. The tool has to reduce or compensate the motion of the nacelle using a motion compensating technology. This may also lead to a combination of multiple technologies when one is not sufficient.

S2. Measure position and orientation of the nacelle
If the tool has to compensate the motion of the nacelle is important to know the position and orientation of the nacelle during installation. This way the motion compensating system can function properly and safe and precise installation is made available.

3.3 Design synthesis

In this section solutions will be created for the design specifications. Since the main goal of the concept is to compensate motion during the installation of a turbine nacelle this function is the most important. A technology to measure the required inputs for a system is also necessary, but this is the case for every concept that is generated. Which measuring system can be applied and what needs to be measured depends on the exact concept, but will be relatively similar for each solution. So, for this thesis solutions will be developed for the core problem, the compensation of unwanted motion. Using a brainstorming session, different concepts were created and their core working principles were briefly discussed. It resulted in seven motion compensating concepts which core working principles are explained below. Each concept also comes with a drawn sketch to give a rough visual presentation.

Concept 1: Inverted quadropod
This concept aims to counter the movement of the crane tip by keeping the nacelle in the same position using its moment of inertia. The concept is comprised of four hydraulic cylinders which connect to one vertical beam that is connected to the hook and to the body of the HMC via a spherical joint. When the tip of the crane moves the upper tip of the vertical beam will follow its movement by adjusting the length of the four hydraulic cylinders. This concept is expected to work well for motion with a high frequency, because the nacelle has a very large mass. The system could reduce the motion that is transferred from the hook to the nacelle.

Concept 2: Tower gripper
The second concept uses a gripper to make a direct connection to the tower. Based on the existing idea of the monopile gripper used for monopile installation a similar gripper could be used to create a mechanical connection to the tower. The goal of the gripper is to stabilize the system and reduce the overall motion of the lifted component. Inside the ring of the gripper a spring system can be used to dampen dynamic impact of the tower on the gripper. The arm of the gripper will be able to be adjusted to place the nacelle in the correct position above the tower.

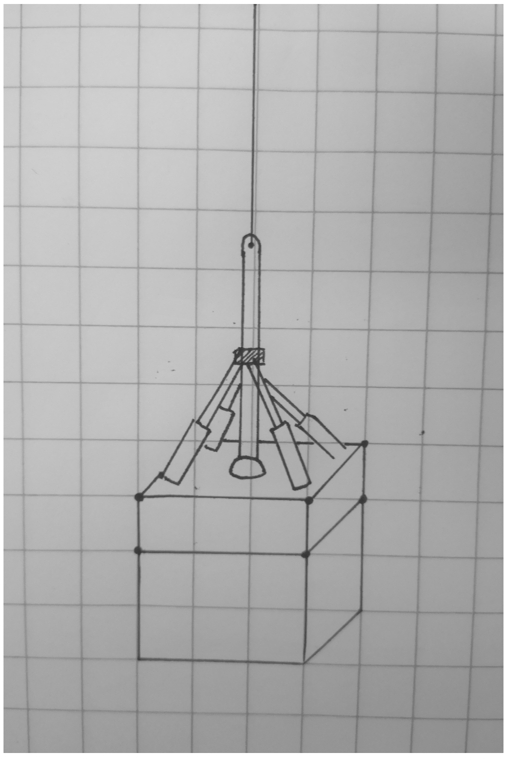

Figure 24: sketch of concept 1

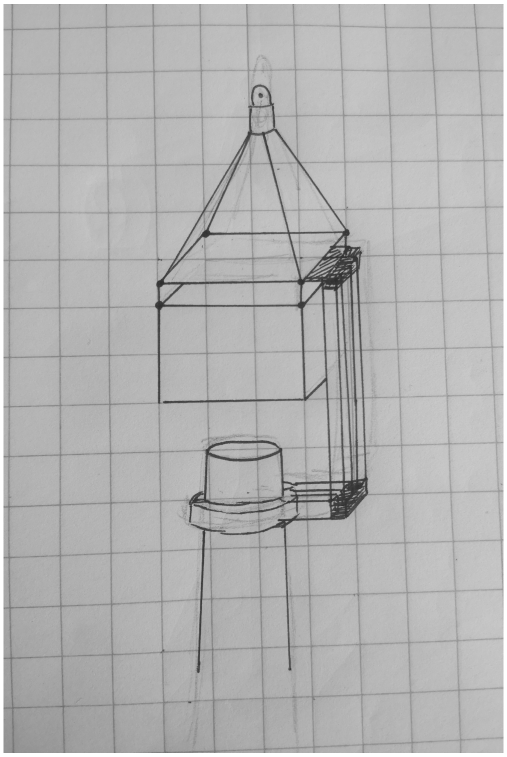

Figure 25: Sketch of concept 2

Concept 3: Guiding line

The use of guiding components during the installation of offshore wind turbines is not uncommon. The turbine blade has a guiding pin that enters the hub first ensuring that the following bolts are position in the right way preventing structural damage. This concept enlarges this principle and proposes a large guiding cable starting from the crane passing through the carrier and nacelle and is then anchored inside the tower. The cable has the goal to dampen the overall motions of the nacelle relative to the tower. The nacelle can then slowly be lowered onto the tower until the mating phase can be initiated.

Concept 4: Inverted hexapod

The hexapod system is a well-developed system and can be found in many industries. It can be used to simulate motions and dampen vibrations. It is quite similar to the quadropod idea, but it is more complicated and is also connected to the boom of the crane. When this system is used for other purposes is has an excellent control over the six DOF of the nacelle by adjust six different hydraulic actuators. The concept does require a foundation to work, for this instance this was imagined as a set of hydraulic actuators or even a more rigid structure connected to the crane.

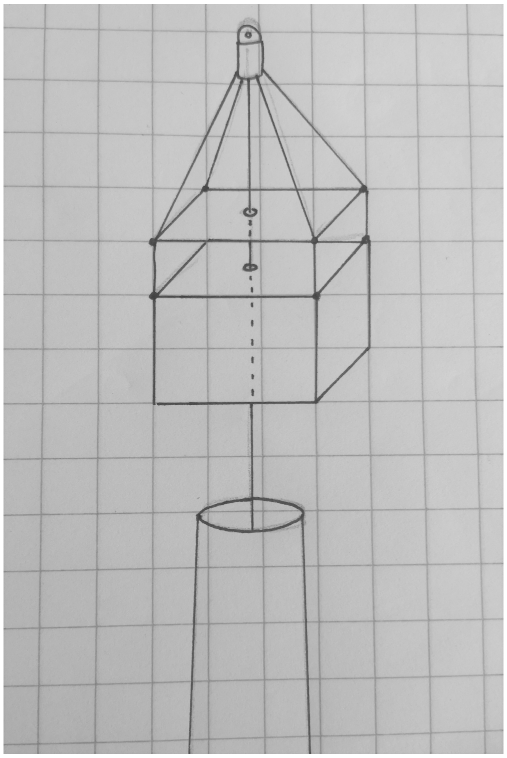

Figure 26: sketch of concept 3

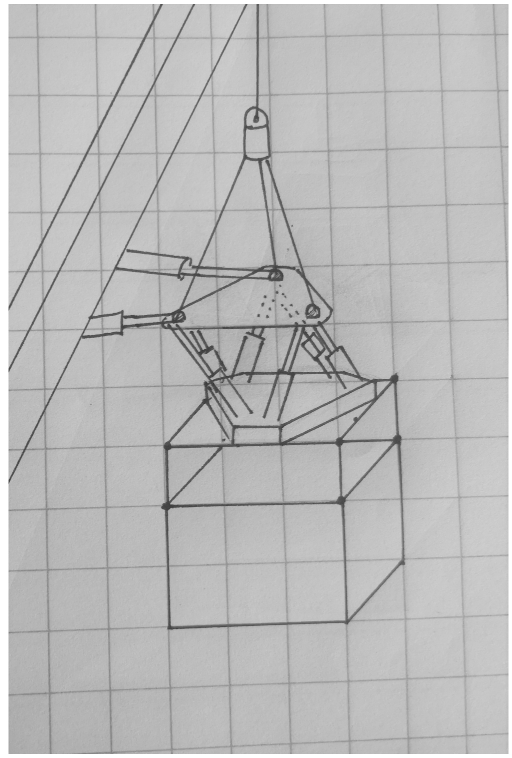

Figure 27: Sketch of concept 4

Concept 5: X-Y counterweight table

The fifth concept is comprised of a main frame that contains two x-y tables. One is used to move the nacelle in the horizontal plane and the other table is used to move a counterweight in the opposite direction on the horizontal plane. The goal is to keep the nacelle in the same position above the tower and this can be done by moving the counterweight so that the system remains stable. The distance that the counterweight has to be moved depends on its mass and on the displacement of the nacelle.

Concept 6: Intelligent tugger system

By using a system of cables, it is possible to control the position and orientation of the nacelle. The cables are connected to the crane and can use the existing cable equipment. The system is only able to pull the nacelle towards the crane and therefore has an operating range between the crane and the crane tip. This means that the crane has to be positioned is in such a way that when the crane reaches its maximum displacement outwards the crane tip is above the tower.

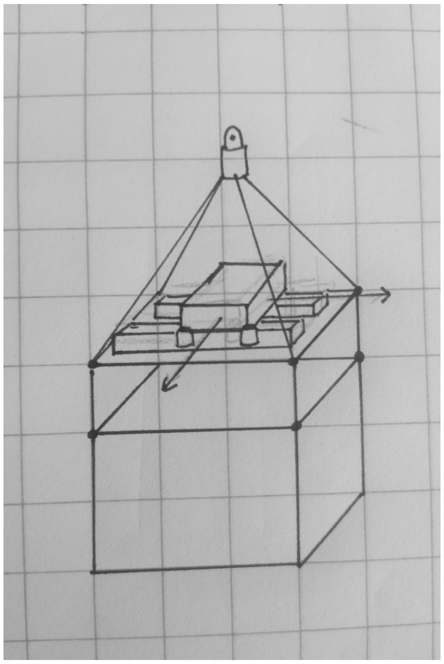

Figure 28: sketch of concept 5

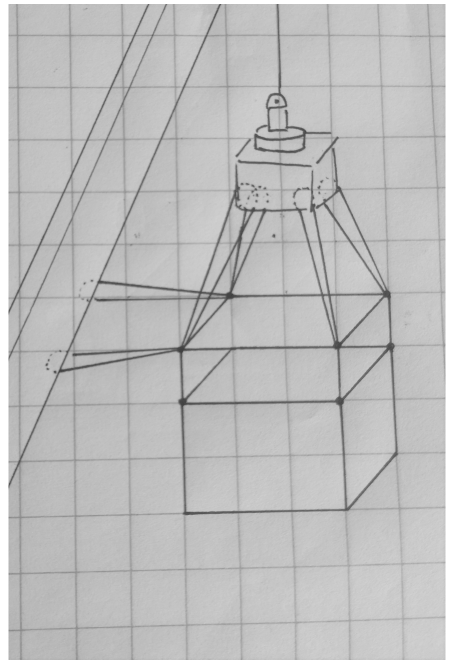

Figure 29: Sketch of concept 6

Concept 7: Propulsion system

The last concept uses thrust to control the position and orientation of the nacelle. Thrust can be created by expelling mass in one direction. This can be done by air or using some kind of liquid. The sketched concept has four propulsion components on each corner of the nacelle carrier. These components can be rotated around their vertical axis increasing their operating range. By creating a thrust in the opposite direction of the nacelle's motion it can be compensated. The thrusters can also compensate for the relative motion of the tower to decrease it.

3.4 Design evaluation

It is often difficult to evaluate non-existing concepts on a quantitative base. Therefore, the analytic hierarchy process (AHP) is selected for the evaluation of the seven defined concepts (24). This process compares each concept against the others for each evaluation criterion.

The first step is to create a set of criteria that are relevant for the evaluation of HMC concepts. The first criterion to be considered is the ability of a concept to compensate motion. This criterion comprises the number of DOF that can be compensated and to which extent. The expected weight and size of the motion compensating tool are also important aspects to consider. If a tool is very heavy it will decrease the crane's loading capacity. Secondly the possible lifting height will decrease as the motion compensating tool takes up more space. Both aspects decrease the chances of using the tool for the larger turbines of the future. Probably the most important factor to consider is the technical feasibility, because the installation of OWTs from a floating vessel is a relatively new and unexplored area. For some concepts it might be difficult to quickly determine if the concept is feasible, so from a scientific perspective it might still be interesting to look further into these concepts. Economic feasibility is always important, but is not the main focus of the study and is therefore lightly taken into account. Since the goal is to improve the weather window of the

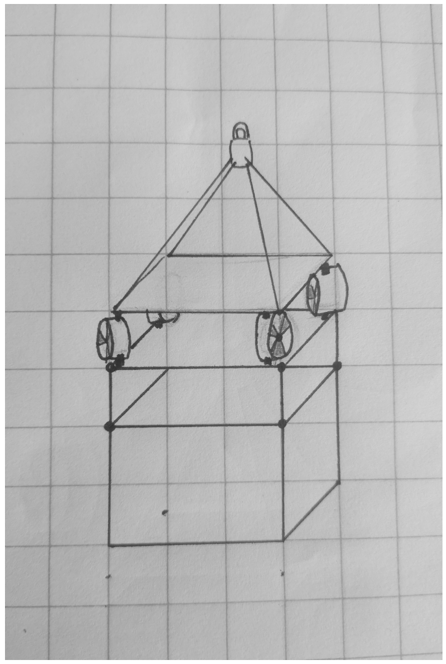

Figure 30: Sketch of concept 7

installation process it is also important to make sure that the tool does not have a large impact on the existing equipment. To summarize these points the following criteria are used to evaluate the concepts:

C1. Motion compensating capability

C2. Impact on lifting height

C3. Impact on lifting capacity

C4. Technical feasibility

C5. Economic feasibility

C6. Impact on equipment

Since not all criteria are equally important, weight factors are introduced. These factors are determined in the same way the concepts will be evaluated, only now each criteria's importance is compared to the other criteria. This results in the weight factors presented in Table 5.

With the weight factors for each criterion defined the concepts can be evaluated. When the AHP is performed it leads to the results presented in Table 6. The values used in the matrices of the AHP are for some concepts supported by basic calculations when possible. These calculations are included in Appendix B and include an explanation. The normalized score was multiplied with a factor of 100 to get better presentable numbers. The guiding line, propulsion system and tower gripper have a low score due to their low expected technical feasibility. The guiding line and tower gripper require a physical connection to the turbine tower which is a time consuming and complex interaction. When a propulsion system is to be applied to a nacelle that weighs 650 tonnes it requires an incredible amount of power from the system which is deemed not feasible. The inverted hexapod is very expensive, large and requires additional connections to the mast of the crane. This makes this concept not ideal for a hook mounted compensator. The tugger system has a relative low

Table 5: Overview of weightfactors

Criterion	Weight factor
Motion compensating capability	0,22
Impact on lifting height	0,09
Impact on lifting capacity	0,06
Technical feasibility	0,39
Economic feasibility	0,04
Impact on equipment	0,20

mass and size, but a system that is solely comprised of tuggers has some critical limits. The load can only be pulled in the direction of the crane mast and the acceleration of the load is dependent on the maximum acceleration of the cable. Another point is that pushing the load away from the crane can only be done by using gravity. The second-best concept is the inverted quadropod, whereas it is a relative simple concept it fits the goal of a hook mounted compensator tool very well. It also has a relative low mass, but whether it will work is difficult to predict. This is why this concept is still taken into consideration and scored slightly lower than the X-Y table which is in first place. The X-Y table has very good motion compensating capabilities by keeping the centre of gravity beneath the hook of the crane. Secondly this concept is also able to compensate for the motion of the turbine tower. The only disadvantage is that if no ratio is applied, then it will require a large counter mass.

Table 6: Results of the AHP

Concept	Score	Rank
Inverted Quadropod	18,64	3
Tower Gripper	9,76	5
Guiding Line	7,31	7
Inverted Hexapod	12,86	4
X-Y Table	**23,16**	**1**
Intelligent tugger system	20,33	2
Propulsion system	7,94	6

In Table 6 it can be seen that X-Y table has a score of 23,16 which is the highest score in the list. The second concept is the intelligent tugger system with a score of 20,33. Because the analytic hierarchy method can be prone to human bias it is important to consider concepts with scores that are close to the best ranking concept. However, it can be seen that the difference between the first and the second concept is a significant 2,83 points. With this difference it can be said that the X-Y table will always remain the best ranking concept even if the comparisons are changes slightly. As a result, the X-Y table concept is chosen for the final concept design.

4 Final concept design

In the previous chapter several concepts were evaluated and the concept that had the best score was selected for a final concept design. In this chapter the concept will be further developed to get a better understanding of the working principle and design of the tool. A 3D-model of the tool will be made to estimate the size and weight.

4.1 Working principle

The core idea of the tool was briefly explained before, but for the final concept design an improved description of the tool is essential. The core working principle can be explained from a simplified static perspective. The goal of the tool is to position the nacelle above the tower at any time as precise as possible. Normally the nacelle carrier, including the nacelle is slinging beneath the crane which makes installing the nacelle on the tower more difficult. If the nacelle could be independently moved from the nacelle carrier to keep it above the tower it could make the installation much easier. This can be done by implementing a system that can position the nacelle beneath the nacelle carrier. In this concept a so called 'x-y table' will be used which can move an object in two dimensions. This results in the scenario depicted in Fig. 31, in this example only pure horizontal displacement is considered. In drawing (a) the nacelle is first in equilibrium above the tower, but when the whole system moves to the right the nacelle will be displaced to the left to remain above the tower (drawing (b)). The system in drawing (b) is in contrary to the first situation no longer in equilibrium, but a moment is created due to the position of the nacelle which could result in additional unwanted motion.

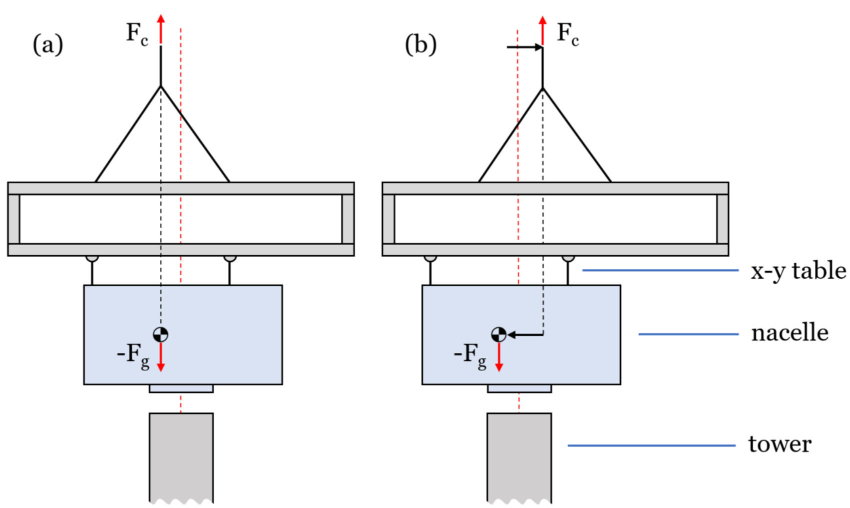

Figure 31: System in equilibrium (a) and the system in imbalance after the nacelle has moved (b)

To avoid unwanted motion caused by the displaced nacelle a counterweight can be used to counteract the resulting moment. The counterweight will move in the opposite direction of the nacelle to keep the CoG of the whole system in the same location. This new situation is drawn in Fig. 32.

Since the nacelle has a very large mass of 650 tonnes it could be better to implement a mass ratio between the nacelle and the counterweight. For counterweights with a mass lower than that of the nacelle the

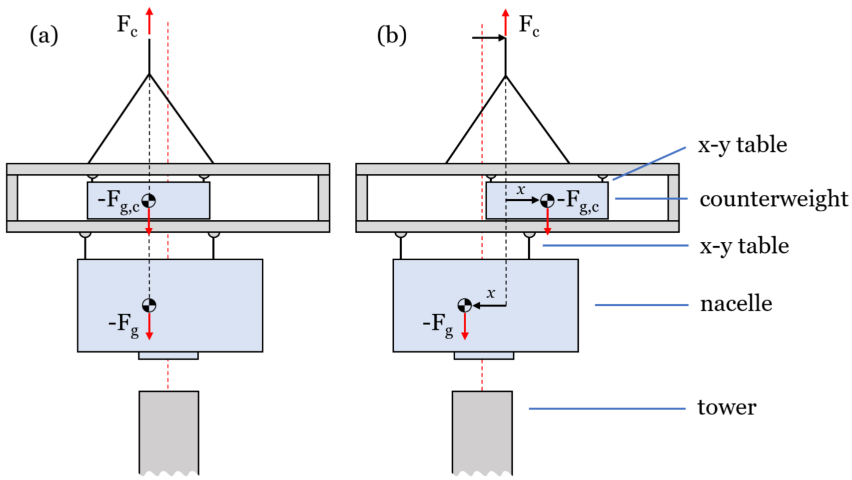

Figure 32: The system in equilibrium (a) and the system in equilibrium after the nacelle has moved (b)

displacement will have to be bigger. The different ratios can be determined by setting the moment sum about the lifting hook to zero which results in Eq. 1. The forces F_g and $F_{g,c}$ are the gravitational forces of the nacelle and counterweight respectively, x_1 and x_2 represent the displacement of each mass. A suitable mass ratio for the 3D-design will be selected in section 4.2.

$$F_g x_1 = F_{g,c} x_2 \tag{1}$$

In the concept synthesis phase an important remark was made concerning the measurement equipment necessary for the tool. Now a concept is selected it is possible to give more thought to which parameters need to be known for the tool to function. The following quantities have to be measured during operation to achieve a working tool:

- **Position and orientation of the nacelle**
  Since the tool has the main function to improve the installation of the nacelle it is important to measure its location and orientation. Firstly, the position of the nacelle within the tool has to be known, because with this information the required displacement of the counterweight can be determined. Secondly it is important to know the position and orientation of the nacelle relative to the tower. This information is important since the nacelle has to be correctly aligned to proceed with the installation.

- **Position of the counterweight**
  The position of the counterweight is also critical for the tool in the same way that the position of the nacelle within the tool is critical. Since the CoG of the tool is to be kept in the same location the counterweight has to be adequately positioned in the opposite direction of the nacelle.

4.2 Concept configuration

In this section preparatory steps of the tool design will be taken. This means that the maximum design space has to be determined alongside the expected dynamics of the tool. With this information it is then possible to create a detailed configuration for the different parts the tool consists of.

4.2.1 Wireframe design

Since the nacelle of the Haliade X is one of the few specified parts involved in the design of the tool its dimensions are used as starting point. For the design of the tool the complex shape of the nacelle is not essential so for now the nacelle is assumed to be a rectangular box where its size and position of the CoG correspond with the actual nacelle and the values are rounded of the the nearest 100mm. This will only lead to small deviations compared to the real distances, but will simplify future calculations. The size and position of the CoG can be seen from a front and side view in Fig. 33 and Fig. 34 respectively. The red dots in the drawings indicate three existing interface points where the nacelle carrier can be connected to the nacelle with special lunges designed by GE. These interface points will be used when designing the tool so that no adjustments are needed on the side of the nacelle.

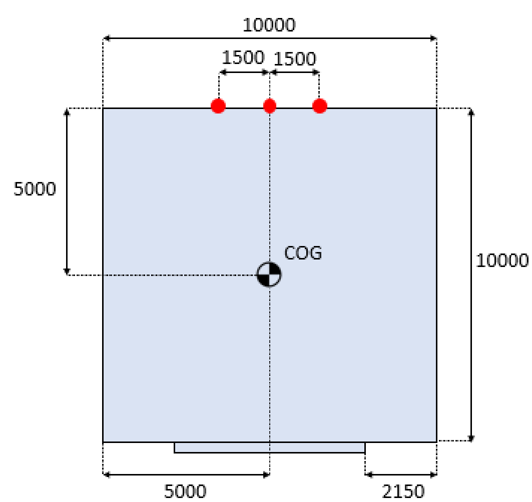

Figure 33: Simplified dimensions of the nacelle (front view)

To limit the impact of the tool on the maximum lifting height of the installation crane the dimensions of the nacelle are used as boundaries for the design. This is done because the load of the crane has to be a safe distance away from the mast during lifting operations. Therefore, the upper surface of the nacelle will be used which is 10 by 22 meters. This means that the tool cannot be longer than 22 meters and no wider than 10 meters.

The tool can be divided into three main parts: lower x-y table, main frame, upper x-y table. The lower x-y table can be separated into two frames: a carrier for the nacelle that moves in one direction and a second frame that moves in the other direction. This is also the case for the upper x-y table, which consists of two frames that can both move in a different direction. The subsystem will allow the nacelle and counterweight to be moved in two directions so that the nacelle can theoretically be kept above the turbine tower.

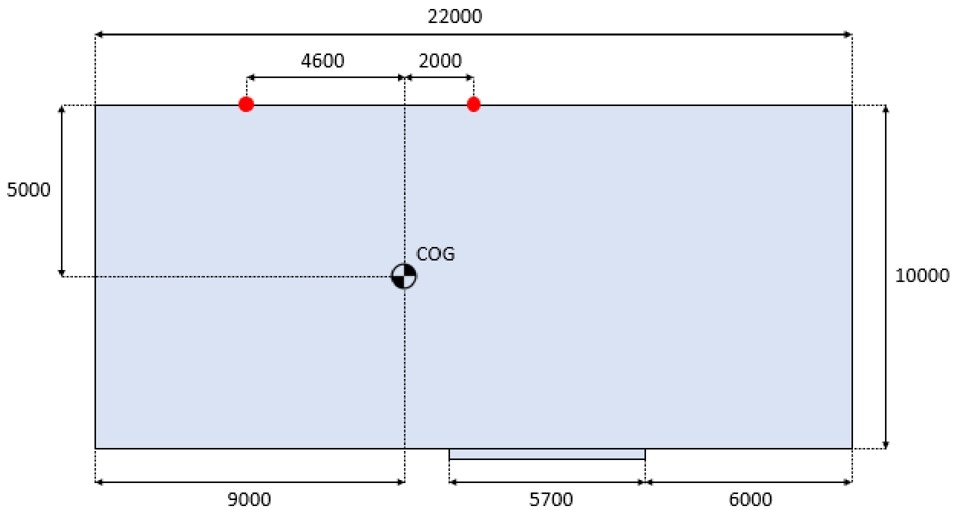

Figure 34: Simplified dimensions of the nacelle (side view)

Since the nacelle is a given, the tool will be designed from top to bottom and changes will be made to previously designed parts when necessary. The configuration of the tool will be presented using a wireframe design. The wireframe design will be a good indication for the minimum size of each part of the tool. The best direction for each part to move in can then be determined. The downside of the wireframe design is that it doesn't take the actual structural beams into account. Therefore, it is likely that the final model will be larger than predicted by the wireframe design. However, the goal of designing the tool was to check if the tool is technological feasible. This method can be used to estimate the size and weight of the tool which can help in answering this research question.

The interface points that were already mentioned can be used to determine the minimum size of the nacelle carrier. With the dimensions from Fig. 33 and Fig. 34 the wireframe has to be 3 meters by 6,6 meters. During installation the nacelle is commonly kept parallel to the installation vessel. The nacelle carrier will then move the nacelle in the y-direction.

Since the nacelle carrier will move the nacelle in the y-direction the frame above the nacelle carrier will have to move in the x-direction. This way the nacelle can be moved in both directions. This frame will from now on be referred to as the 'lower x-table'. Before the dimensions of the lower x-table can be determined the maximum displacement of the nacelle has to be determined. The dynamics of the nacelle during installation are difficult to determine, because it is different for every installation. The dynamics are highly dependent on the type of turbine, installation vessel, installation crane and weather conditions. In the case study the installation crane was assumed to be equipped with a 3D motion compensating system which allows for the use of information on such a system designed by Huisman. In Fig. 35 and Fig. 36 the dynamic behaviour of the lifting hook during the installation of the nacelle can be seen. This information is gathered from simulations of the 3D-motion compensated crane. These graphs do not provide direct information on the dynamics of the nacelle, but they can be used for an estimation. The graphs show that the lifting hook oscillates during the installation with a varying amplitude. It can be seen that the amplitude is larger in the y-direction than in the x-direction. This can be explained by cables that have better control over the movement towards and away from the crane, the x-direction, than perpendicular to the crane, the y-direction. During some installations the nacelle carrier is also controlled with cables, an example can be found in Fig. 37 and other examples can also be found in (30)(31).

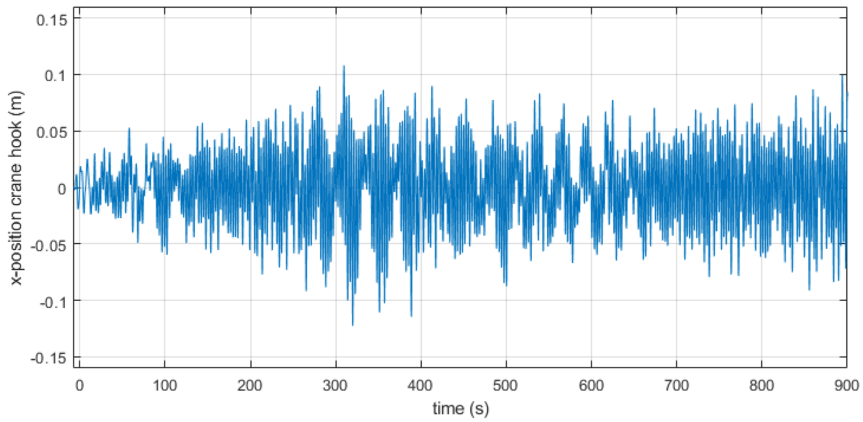

Figure 35: Hook dynamics in the x-direction

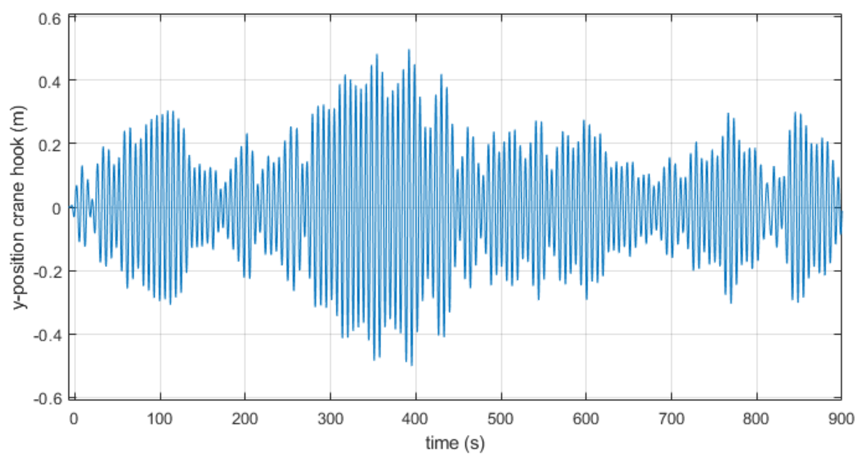

Figure 36: Hook dynamics in the y-direction

In this study it will be assumed that instead of the nacelle carrier, the tool will be connected to the crane with similar cables. With this assumption in mind the results from the simulations can be used to select a maximum displacement for the xy-tables of the tool. Since the maximum displacement of the hook is roughly 0.5 meters in the y-direction and 0.1 meters in the x-direction it can be assumed that the displacement of the nacelle will be of the same level. The tool will therefore be designed for the same amplitude and periods as the lifting hook. The results from the dynamical analysis later on in this thesis may prove this assumption to be wrong, but this has no critical consequences for the tool. This due to that the goal is to study the working principle and the design can be adjusted for different amplitudes and periods.

Figure 37: Additional cables controlling the position and orientation of the nacelle carrier (29)

As said before the lower x-table will enable the nacelle carrier to move in the y-direction. Since the amplitude of the tool is estimated to be 0.5 meters in this direction the lower x-table has to be one meter longer. This results in a wireframe of 3 meters and a width of 7,6 meters. The lower x-table then has to move ±0.1 meters in the x-direction and this results in a main frame with a width of 3,2 meters and a length of 7,6 meters.

Before continuing to determine the wireframes of the upper x-y table a mass ratio between the counterweight and then nacelle must be selected. Eq. 1 was formulated in the previous section and states that it has to hold to achieve static equilibrium. Since the maximum displacement of the nacelle is now assumed to be ±0.5 m it can be used to plot the graph in Fig. 38. Here the required amplitude of the counterweight is given for different masses and for each combination the moment equilibrium from Eq. 1 holds. To minimize the impact on the lifting capacity of the crane a counterweight will be selected that has a significant lower mass than the nacelle. A second condition to consider is the required distance to move the counterweight during operation, due to this condition it is not viable to choose a counterweight with a very low mass.

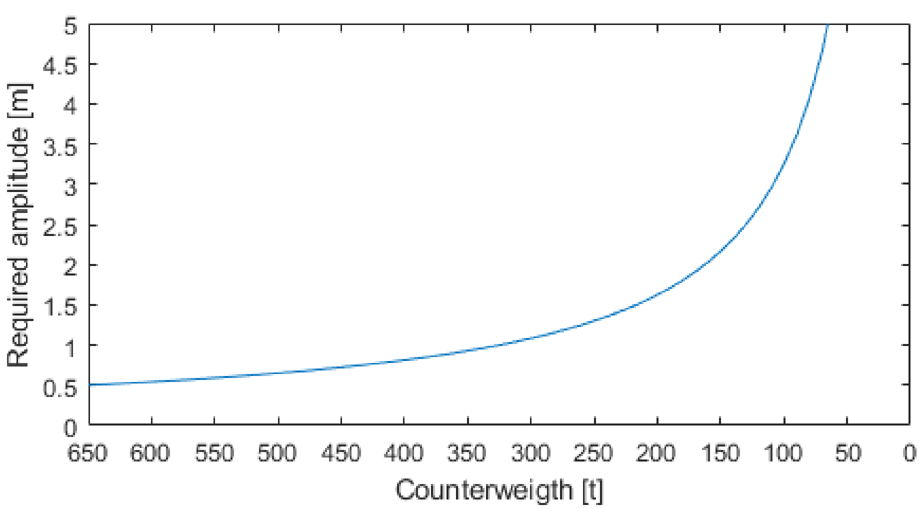

Figure 38: Mass vs. amplitude for the counterweight

In the graph it can be seen that for masses less than 100 tons the displacement increases rapidly. A suitable ratio will be a mass of 130 tonnes with a required amplitude of 2.5 meters. However, this maximum amplitude is only for the y-direction, this ratio results in a maximum displacement of ±0.5 meters in the x-direction.

The upper x-y table consists of a counterweight carrier and second frame with the same goal as the lower x-y table. The second frame will be referred to as the 'upper y-table'. As the name suggests this frame will enable the counterweight to move in the y-direction. The direction differs from the lower x-table because the main frame is relatively long in the y-direction which makes it easier to achieve the displacement of ±2,5 meters. Using the current size of the main frame it results in an upper y-table of 3,2 by 2,6 meters. Since the counterweight also has to move ±0,5 meters in the x-direction the counterweight carrier will be 2,2 by 2,6 meters.

An important note to be made is that the CoG of the nacelle is not in the center of the nacelle carrier but 1,3 meters off center. This means that the counterweight must also be positioned 1,3 meters off the center in the y-direction. To implement this in the wireframe of the main frame the distance of 1,3 meters is added to the main frame. Resulting in a main frame with a length of 8,9 meters and a width of 3,2 meters. A complete overview of the estimated dimensions for each part is given in Fig. 39.

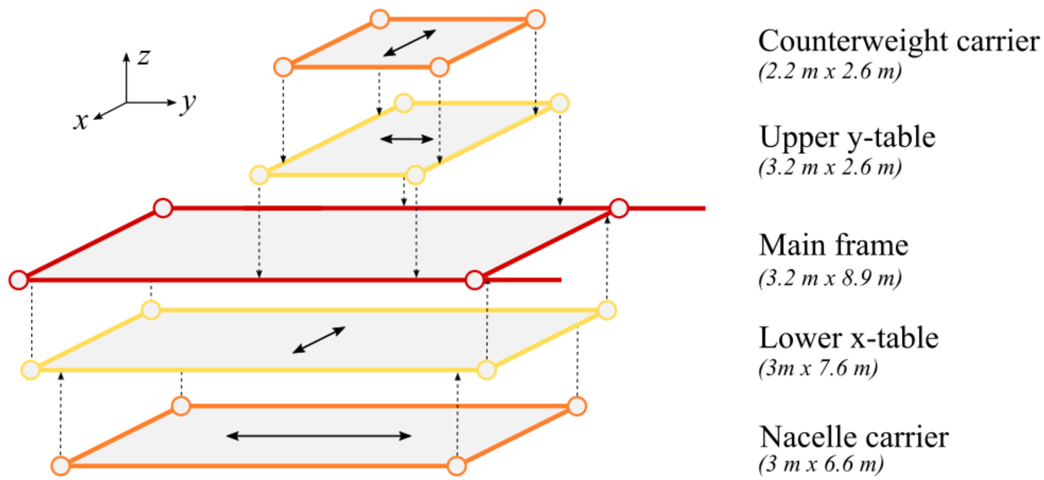

Figure 39: An overview of the wireframes with their respective dimensions and moving direction

4.2.2 Drive system

For the tool to function a form of linear actuation is needed to move the counterweight and the nacelle in the xy-plane. The goal of including the drive system in the design phase is to take the required space and configuration into account when designing the tool. A rack and pinion drive is highly suitable for the linear actuation of the tool. The system is comprised of a linear gear (rack) and a circular gear (pinion) that converts rotational motion into linear motion. The advantage of this drive system is that it can be driven by electric motors that can use available power from the installation vessel. The power required for the actuation of the counterweight and the nacelle is calculated using Eq. 2.

$$P = (F_a + F_f)v_{max} \tag{2}$$

Here is F_a the force for the estimated maximum acceleration, F_f the friction force and v_{max} the maximum velocity. In both equations the maximum values are used to account for the estimation of the expected nacelle dynamics. Looking back at Fig. 36 a period of 6.41 seconds can be read and this value can be used to simplify the dynamics to a sinusoidal function. For the amplitude of the function the expected amplitudes for the nacelle and counterweight are used. F_a and v_{max} can be calculated by Eq. 3 and Eq. 4. The friction force is calculated by multiplying the weights with a resistance factor of 0.002 to account for possible steel on steel friction between the wheels and the rails. Finally, the required power is the calculated in Table 7. The values of P_{net} are the values of P divided by 1.6 because the electric motors are allowed to work at 160% for short periods of time.

$$F_a = ma_{max} = mA\omega^2 \text{ where } \omega = \frac{2\pi}{T} \text{ with T being the period in seconds} \tag{3}$$

$$v_{max} = A\omega \tag{4}$$

Table 7: Power calculations for the rack and pinion drive system

	Nacelle y-direction	Nacelle x-direction	Counterweight y-direction	Counterweight x-direction	
A	0.5	0.1	2.5	0.5	m
T	6.41	6.41	6.41	6.41	s
ω	0.980	0.980	0.980	0.980	rad/s
m	650000	650000	130000	130000	kg
g	9.81	9.81	9.81	9.81	m/s2
μ_r	0.002	0.002	0.002	0.002	-
v_{max}	0.490	0.098	2.451	0.490	m/s
a_{max}	0.480	0.096	2.402	0.480	m/s2
F_f	12.8	12.8	2.6	2.6	kN
F_a	312.3	62.5	312.3	62.5	kN
P	159.3	7.4	771.5	31.9	kW
P_{net}	99.6	4.6	482.2	19.9	kW

4.3 Tool design

In this section the structural design of the motion compensating tool will be presented. The scope of the study allows for a basic structural approach that can be used to determine the dimensions and weight of the tool. Moreover, a structural design will help in answering the question if the tool is technological feasible. Each part of the tool will be designed with their respective dimensions determined in section 4.2. The tool will be designed for the worst load cases and with conservative safety factors, since physical tests will not be performed.

4.3.1 Load amplification factor

Before starting to design the 3D-model of the tool, the forces acting on every part have to be calculated. For the force calculations the offshore standard (DNVGL-ST-N001) for marine operations and marine warranty will be apply (32). This standard proposes a clear guideline for the design of lifting equipment.

The weight contingency factor is the first factor that has to be determined when designing offshore lifting equipment. This contingency factor also takes the accuracy of the CoG into account. Since the working principle of the concept is based on the precise position of the CoG a large safety factor would not be correct. However, in this stage of the design the performance of the system can't be evaluated so a conservative contingency factor of 1.05 is taken. This standard also suggests that for calculations purposes a conservative factor should be taken.

The Dynamic amplification factor (DAF) is the second amplification factor that will be taken into account. This factor is important since it accounts for the global dynamic effects of the vessel, crane and weather conditions. According to the standard the DAF can be selected based on the static hook load which is divided in several categories. The Static Hook Load (SHL) is the weight of the nacelle and the weight of the tool combined. The weight of the nacelle is known and is 650 tonnes, but the weight of the tool is still unknown. However, the standard suggests when the SHL is larger than 300 tonnes and less than 1000 tonnes a DAF of 1.2 can be taken. It can be assumed that the total static hook load will fall in this category since the counterweight is 130 tonnes it would mean that the tool itself could weigh 220 tonnes.

The Skew load factor (SKL) is the third factor that has to be accounted for. The main frame will be suspended from the crane hook with four cables and may also be secondarily connected to the crane as was suggested for the maximum amplitude for the nacelle. For this reason, a conservative SKL of 1.05 is taken.

The last factor is the safety factor for structural elements. The formula for the design factor is given in Eq. 5 and is taken from the DNVGL-ST-N001 standards. Here γ_h stands for the lifting factor and γ_c for the consequence factor. A lifting factor of 1.3 and a contingency factor of 1.3 should normally be taken for the design of lifting tools. This is applicable for the HMC and with these values a design factor of 1.69 can be calculated.

$$\gamma_{safety} = \gamma_h * \gamma_c \tag{5}$$

Each load amplification factor is given in Table 8. If the different amplification factors are multiplied it results in a total load amplification factor of 2.24.

4.3.2 Beam calculations

Now the total load amplification factor is calculated it can be applied in beam calculations for the tool. Each link in the previously designed wireframes will be designed as a steel beam with a rectangular hollow shape. This shape is easy to use in a basic structural design and also offers good resistance against torsion and buckling. S690 steel is selected as the material for the beams due to its high yield strength. Since the

Table 8: Overview of the load amplification factors

Factor	**Value**
Contingency factor	1.05
DAF	1.20
SKL	1.05
γ_{safety}	1.69
Load amplification factor	2.24

scope of the study only allows a basic structural design the calculations will be limited to the maximum bending and shear stress. The dimensions of a hollow rectangular beam will be indicated with the variables depicted in Fig. 40, where H is the outer beam height, h the inner beam height, W the outer beam width, w the inner beam width and t the beam thickness. The moment of inertia of a rectangular hollow beam is given in Eq. 6.

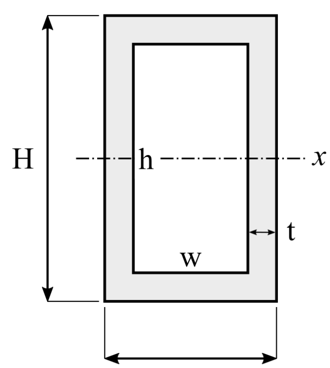

Figure 40: Dimensions of a rectangular hollow beam

$$I_x = \frac{1}{12}(WH^3 - wh^3) \tag{6}$$

The steps taken to design each beam are the same for each part of the tool. In this section the calculations for the nacelle carrier will be presented as an example. The calculation for the other parts can be found in Appendix D.

The forces acting on the wireframe of the nacelle carrier are given in Fig. 41. The nacelle carrier transfers the weight of the nacelle to the lower x-table via a set of wheels. For the corner points where $F_{z1,1}$ and $F_{z1,2}$ are applied it means that these loads can be transferred directly through the corner structures. Because F_{z2} does not act directly on the corner points of the frame beam A has to transfer this force to the corner points. Beams B and C mostly have to account for the compression and tension forces caused by the movement in the y-direction.

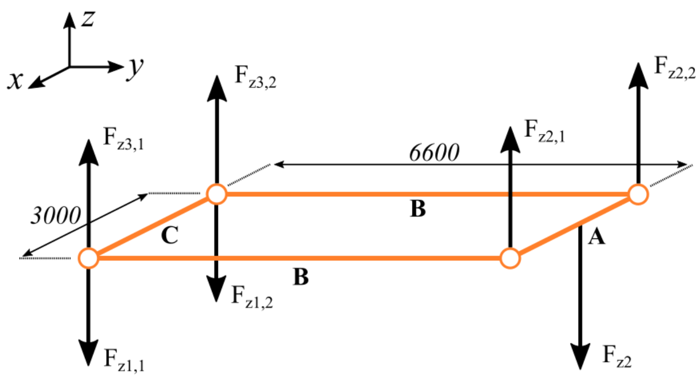

Figure 41: Overview of the forces acting on the nacelle carrier

The forces pointing downwards can be calculated with the help of Fig. 34 when the moments are taken about the left connection point. Doing this leads to force F_{z2} being 4444 kN and $F_{z1,1}$ and $F_{z1,2}$ being 1932 kN. Since F_{z2} is equally divided over forces $F_{z3,1}$ and $F_{z3,2}$ they both are 2222 kN. Forces $F_{z1,1}$ and $F_{z1,2}$ are equal thus being 966 kN each. Lastly $F_{z3,2}$ and $F_{z3,2}$ are the same as $F_{z1,1}$ and $F_{z1,2}$ which is 966 kN. With this information the shear force and moment diagram on beam A can be drawn as in Fig. 42.

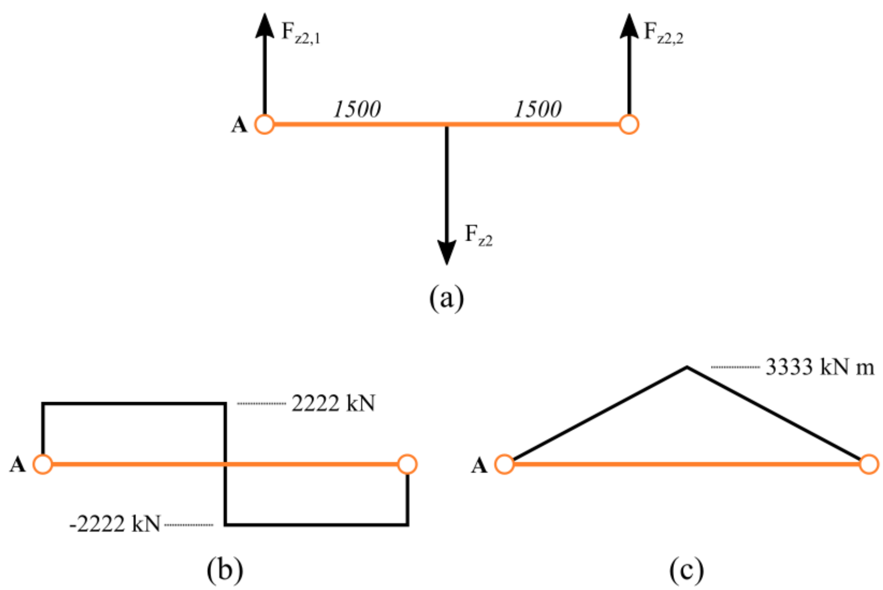

Figure 42: Forces acting on beam A (a), shear force diagram (b), bending moment diagram (c)

According to the DNVGL-ST-N001 standard the allowable yield stress is calculated by multiplying the yield stress of S690 steel with 0.6. For each load case the forces are multiplied by the total amplification factor of 2.24 and an allowable yield strength of 4.14 MPa is used. The von Mises yield criterion is used to design the structural components. The von Mises stress is calculated by the maximum shear, bending and axial stresses acting on a beam. The formula for the von Mises stress is given in Eq. 7.

$$\sigma_{vm} = \sqrt{(\sigma_{ax} + \sigma_b)^2 + 3\tau_{sh}^2} \tag{7}$$

$$\text{With } \sigma_{ax} = \frac{F_{ax}}{A},\ \sigma_b = \frac{Mc}{I_{xx}},\ \tau_{sh} = \frac{F_{sh}}{A}$$

Here is σ_{ax} the axial stress, σ_b the bending stress and τ_{sh} the shear stress. Since there are many possible combinations of the height, width and plate thickness, the width of the beam is always set to $\frac{2}{3}$ of the beam height. For some beams this might lead to less standardized dimensions for the beam, but for the goal of the tool design this is acceptable. The beams are also designed with an uniform plate thickness. The values used for the plate thickness are 10,12,15 or 20 mm which are standard values within Huisman. The height of the beam is selected with a plate thickness of 20 mm and is then increased with increments of 200 mm until the maximum stresses are below the allowable yield stress. The plate thickness is then lowered until the beam fails again.

In most cases the beams of one tool are designed with the same height and width. The reason for this approach is that the basic design focuses on the primary structural steel and not the secondary structural required for a more detailed design. Nevertheless, the plate thickness can be lowered for beams that have a significant lower von Mises stress than their counterparts. The calculations done for the nacelle carrier are presented in Table 9. The other calculation sheets for the lower x-table, counterweight carrier, upper y-table and the main frame are also included in Appendix D.

Table 9: Calculation sheet for the nacelle carrier

Beam A			**Beam B**		
Yield Strength	6.90E+08	Pa	Yield Strength	6.90E+08	Pa
Allowable yield	4.14E+08	Pa	Allowable yield	4.14E+08	Pa
Safety factor	0.6	[-]	Safety factor	0.6	[-]
Load factor	2.24	[-]	Load factor	2.24	[-]
Width	800	mm	Width	400	mm
Height	1200	mm	Height	600	mm
Thickness side	15	mm	Thickness side	10	mm
Thickness top/bottom	15	mm	Thickness top/bottom	10	mm
Inner width	770	mm	Inner width	380	mm
Inner height	1170	mm	Inner height	580	mm
Beam length	3	m	Beam length	6.6	m
Cross sect. Area	0.0591	m^2	Cross sect. Area	0.0196	m^2
Ixx	1.243E-02	m^4	Ixx	1.021E-03	m^4
Maximum shear force	2222	kN	Maximum shear force	0	kN
Maximum bending moment	3333	kNm	Maximum bending moment	0	kNm
Maximum axial force	0	kN	Maximum axial force	330	kN
Maximum shear stress	8.42E+07	Pa	Maximum shear stress	0.00E+00	Pa
Maximum bending stress	3.60E+08	Pa	Maximum bending stress	0.00E+00	Pa
Maximum axial stress	0.00E+00	Pa	Maximum axial stress	3.77E+07	Pa
Von Mises Stress	3.89E+08	Pa	Von Mises Stress	3.77E+07	Pa

When the calculation sheet is executed for each part of the HMC an overview of the specifications of the tool can be given. This overview can be found in Appendix D.

4.3.3 3D-model

The last step in the design of the tool is the creation of a 3D-model. The calculations done for each part will now be used to create a model to for a graphical representation of the tool. This model will also provide information on the size and weight which can be used in the dynamic analysis of the tool. The sizes of each part may differ from what was first predicted during the wireframe design. The main cause for this difference is the fact that the size of the beams and wheel sets were not taken into account when the wireframe was designed. The tool is designed in the educational version of SolidWorks 2019.

Nacelle carrier

The front beam that was labelled beam 'A' in the calculation sheet is the largest beam of the nacelle carrier. The stress caused by the bending moment in the beam was dominant over the maximum shear stress. Since this beam had to be relatively large compared to other beams the design was adjusted so that the height of the beam decreases to the outsides ending at a height of 600 mm. This shape follows the shape of the bending moment diagram, but contrary to the bending moment the shear moment is not explicitly lower at the ends of the beam. For a beam with a height of 600 mm and the same plate thickness the maximum shear stress is still below the allowable yield, so this is acceptable. The other beams were then designed to fit the larger front beam of the nacelle carrier with a height of 600 mm. Since the forces on these beams were significantly lower, the thickness of those beams was decreased from 15 to 10 mm. The 3D-model also includes the wheels that allow the nacelle carrier to roll on the lower x-table. The main reason to include these wheels is to think about their position and to take the space they occupy into account. The wheels are roughly dimensioned by dividing the weight of the nacelle over the four wheels. A third beam which was not included in the wireframe is added in the middle of the carrier to act as the rack for the drive system. The model of the nacelle carrier is given in Fig. 43.

Lower x-table

As said earlier the x-table will function as the rails for the nacelle carrier. Since the width of the beam and the wheels both take up additional space the lower x-table becomes larger than its wireframe. The wheels of the lower x-table are modelled for the same reason as the nacelle carrier and have the same dimensions. A secondary structure is added below the primary to support the electrical motors. On the outside of both shorter beams a rack is added for the drive system which moves the x-table along the x-axis. The model of the lower x-table is given in Fig. 44.

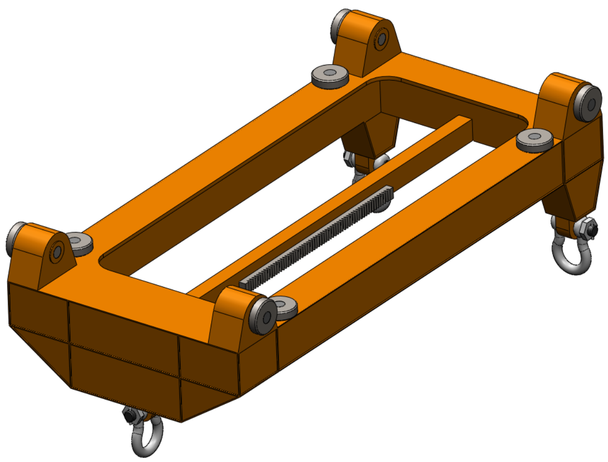

Figure 43: Isometric view of the nacelle carrier

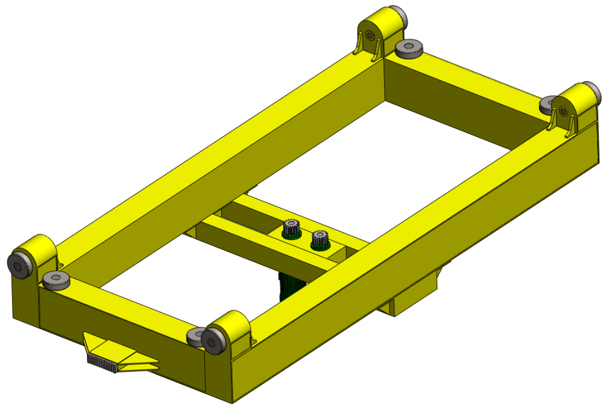

Figure 44: Isometric view of the lower x-table

Counterweight carrier

The counterweight carrier which is shown in Fig. 45 enables the movement of the counterweight along the x-axis. The total mass of the counterweight consists of the counterweight blocks and the weight of the carrier. The required amount of mass is therefore determined by assuming that the carrier is made from solid steel with a density of 8000 kg/m^3. The volume of the carrier can be calculated in SolidWorks and is then multiplied by the density of steel. This mass is then subtracted from the total required mass of the counterweight. The carrier is designed with removable steel blocks so that the total mass of the counterweight can be changed for other nacelles or loads. On the bottom of the carrier a rack is mounted for the drive system so that the carrier can be moved in the x-direction.

Upper y-table

The upper y-table provides the movement of the counterweight in the y-direction as the name suggests. In the same way the lower x-table became larger than first designed, the upper y-table also became larger than its original wireframe. The upper y-table contains the wheel systems for the movement in the y-direction as well as the x-direction. It could have been noticed that the counterweight carrier did not have any wheels, however the carrier was designed with rails for the wheels of the upper table. The upper table also includes secondary structural steel to support a total of 8 electrical motors. The larger motors have a capacity of 145 kW whereas the smaller motors have a capacity of 5.5 kW each. The support structures for these motors are considered secondary structures and are only designed so that the position of the motors are taken into account for the design. Since the upper table uses the main frame as its rails to move in the y-direction, the table is equipped with clamps to ensure that it does not fall of. The model is presented in Fig. 46.

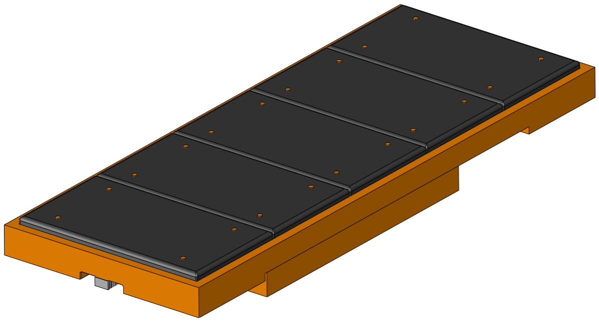

Figure 45: Isometric view of the counterweight carrier

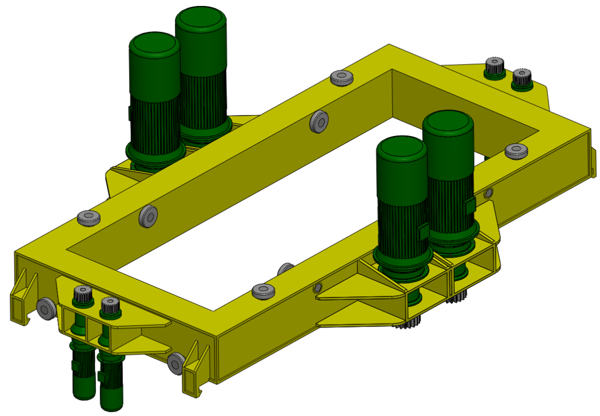

Figure 46: Isometric view of the upper y-table

Main frame

The main frame is the bridge between the tool and the crane and also between the lower and upper section of the tool. The longs beams of the tool act as a rails for the upper y-table to move the counterweight 2.5 meters both ways. The long rack in the middle of main frame enables the upper table to move this distance. Four stopblocks are added onto the long beams to function as redundant stops for the upper y-table. When something might go wrong with the drive system of the upper table the shackles will be protected by these mechanical stopblocks. The main frame is also equipped with two 10 kW motors to move the lower x-table 0.1 meters in both ways along the x-axis. The 3D-model of the main frame is presented in figure Fig. 47.

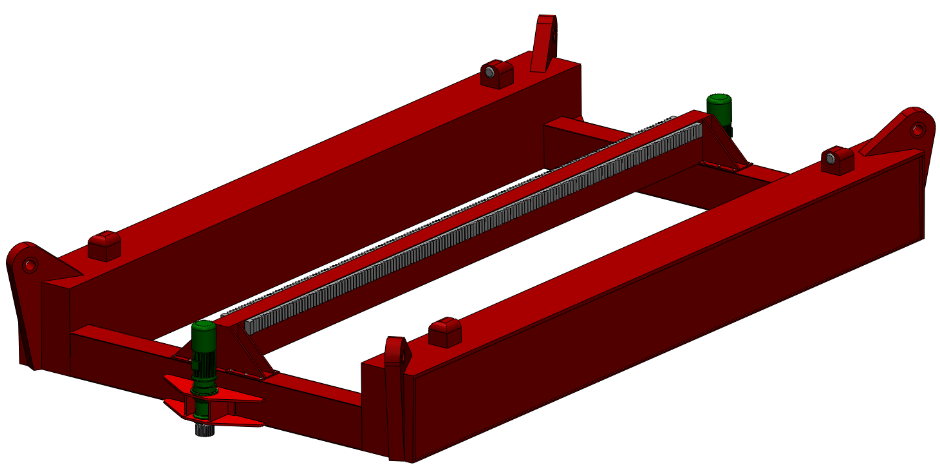

Figure 47: Isometric view of the main frame

Assembly

Up till now each part has been presented separately, however this does not yet provide a clear overview of the tool. In Fig. 48 the parts are therefore assembled and this gives a clear impression of the size of each part compared to the nacelle. The tool without the nacelle has a maximum length of 11.5 meters and height of 5.1 meters. The maximum width of the tool is 7.8 meters and is equal to the length of the counterweight.

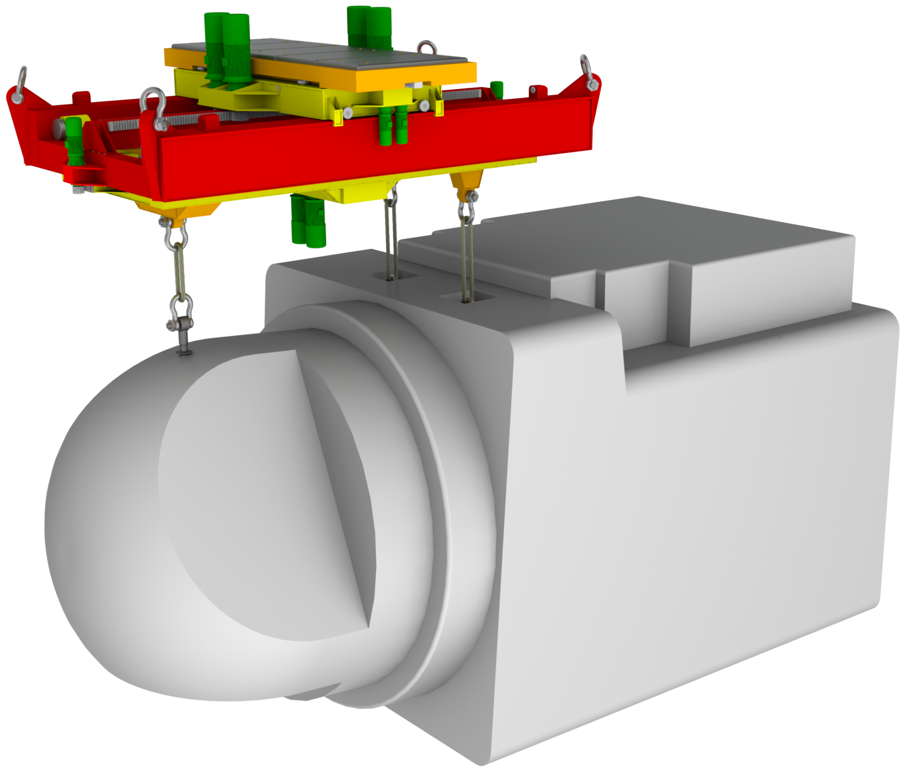

Figure 48: Isometric view of the complete assembly

During the design of the tool the ability to the tool was taken into account. Therefore, the racks and secondary secondary structures are modular so that they can be installed after the parts are places within each other. The steps required for assembling the tool are presented below:

1. The main frame of the tool is placed on a special frame that supports the corner points of the main frame and simultaneously creates enough space below the main frame for the lower x-table and nacelle carrier. This has to be done without the rack for the drive system to enable the installation of the lower parts.
2. Install the lower x-table on the main frame.
3. Install the nacelle carrier on the lower x-table.
4. Install the rack for the drive system on the main frame.
5. Install the upper y-table on the main frame.
6. Install the counterweight on top of the upper y-table.

The total weight of the system can be estimated using the 3D-model, the weight of the electric motors. In addition to these values a factor of 30% is added to take secondary structural steel and other parts into account. The weight of each part and the total weight is given in Table 10.

Table 10: Mass overview of each part

Part	Mass
Nacelle carrier	~6.9 t
Lower x-table	~12.4 t
Main frame	~15.8 t
Upper y-table	~5.8 t
Counterweight	130 t
Total weight	170.9 t

5 Dynamic analysis

The goal of this thesis is to explore the technological feasibility of the designed hook mounted compensator. The second part of the main research question also implied a study on the performance of the tool. Since the developed tool is a new concept it is not yet proven that the principle will function as expected. A dynamic analysis will be performed in this chapter to evaluate the working principle of the tool. If it turns out the tool indeed works as expected its performance can be looked into.

5.1 Mathematical model

The first step in the dynamic analysis is to transform the concept into a mathematical model. A mathematical model represents a system, and especially the behaviour of a system in an abstract way. The mathematical model will include the tip of the crane, lifting hook, tool and nacelle. Since the goal is to evaluate the working principle of the concept, it is not of any significant value to develop a more extensive model.

5.1.1 The double pendulum model

The concept that was designed in the previous chapter is very similar to a common physics problem called the double pendulum. This system is already often studied which makes it an ideal starting point for the mathematical model (26) (27) (28). One version is the so called 'simple' double pendulum. This system consists of two pendulums containing a point mass which is suspended with a cable or rope. The first pendulum is suspended from a fixed pivot point and the second pendulum is attached to the end of the first pendulum. A graphical representation of the 'simple' double pendulum is given in Fig. 50. The dynamics of this system can be described the the equations of motion. These can be determined by various methods, but one proven method is the Newton-Euler approach. In this method the equations for the angular acceleration of angles α_1 and α_2 will function as the equation of motion. The angular acceleration can be determined with Newton's law of motion which has the form $I\ddot{\alpha} = \tau$. Where I represents the moment of inertia, $\ddot{\alpha}$ the angular acceleration and τ the moment sum around the respective pivot point. The system is first split up into two sections: the upper pendulum and the lower pendulum. For the upper pendulum the moment sum has to be taken around point O and for the lower pendulum around point m_1. The resulting equations of motion of a double pendulum are given in Eq. 8 and Eq. 9. In these equations F_t represents the force acting through the respective cable of the pendulum. In Eq. 9 a fictitious force was added which is required to take the moving pivot point into account. When the angular acceleration of α_1 is multiplied with l_1 the net acceleration of the lower pendulum due to the acceleration of the upper pendulum can be calculated. Since this only can have an effect on point mass m_2 this is multiplied with l_2 which results in an additional component in the moment sum. This phenomenon can best be explained with a graphical representation of the dynamic behaviour of a double pendulum given in Fig. 49. In the figure a double pendulum is given with the initial angles set to zero. When a counterclockwise moment is applied to pivot point O the upper pendulum will also rotate counterclockwise. This can be seen in figure b where the system is given after a small time step. The dynamics of a double pendulum show that the lower pendulum will assume the position as given in the figure. It can be seen that the lower pendulum has rotated clockwise contrary to the upper pendulum. This behaviour is correctly represented by the fictitious term added in the equation of motion for the lower pendulum. The negative sign before the term indicates the angular acceleration in the opposite direction.

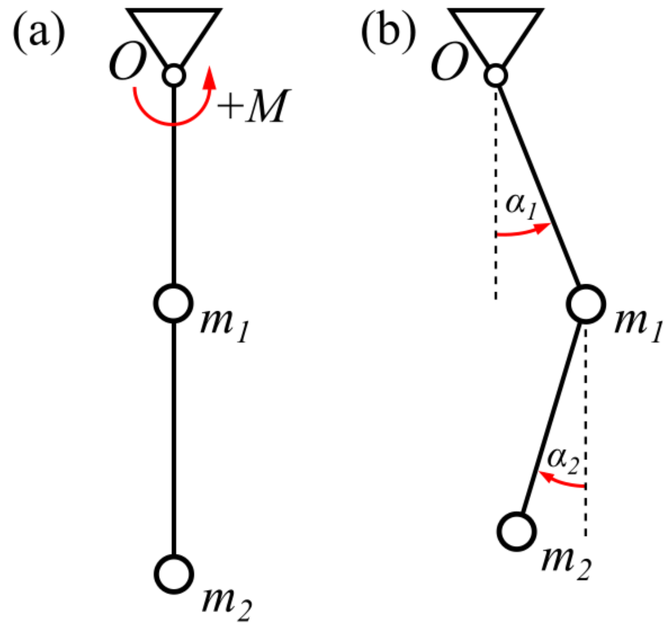

Figure 49: Explanation of the fictitious force

$$m_1 {l_1}^2 \ddot{\alpha}_1 = -m_1 g(l_1 sin(\alpha_1)) + F_{t,2} sin(\alpha_2)(l_1 cos(\alpha_1)) - F_{t,2} cos(\alpha_2)(l_1 sin(\alpha_1)) \tag{8}$$

$$m_2 {l_2}^2 \ddot{\alpha}_2 = -m_2 g(l_2 sin(\alpha_2)) - m_2 l_2 (l_1 \ddot{\alpha}_1) \tag{9}$$

Although the concept for the hook mounted compensator is very similar to the simple double pendulum there is a significant difference that has to be looked into. In the case of the simple double pendulum the assumption can be made that the force always acts along the cable or rope. However, the main frame of the concept is not suspended from one cable, but from four, going from each corner to the lifting hook. The forces in each cable are not necessarily equal which makes the simplification to one cable inaccurate. Therefore, the cable of the lower pendulum is replaced by a rigid body to take the differences between each cable into account. The compound double pendulum is a different version of the previously discussed simple double pendulum and replaces the cables by rigid bodies with a distributed mass. A model of the compound double pendulum is shown in Fig. 51. The major difference that is of interest for this study's concept is the fact that a rigid body is able to transfer forces and moments.

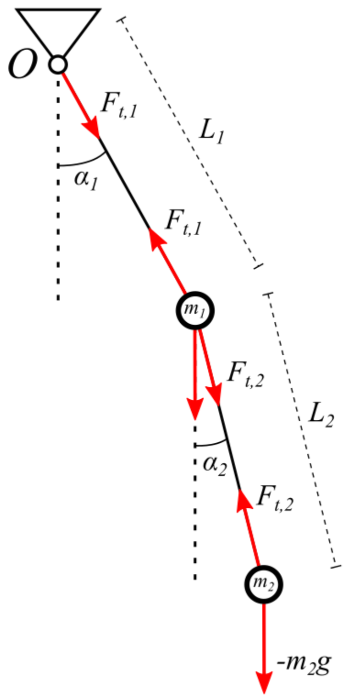

Figure 50: Simple double pendulum

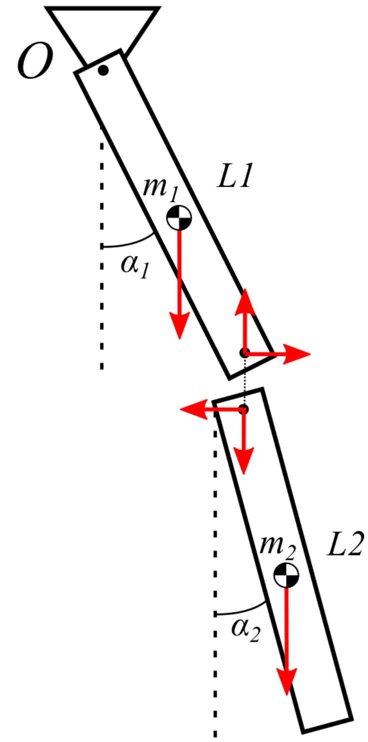

Figure 51: Compound double pendulum

5.1.2 Concept model

The hook mounted compensator will be modelled as a double pendulum where the upper pendulum is suspended by a cable and the lower pendulum by a rigid body. For the sake of clarity, the motion of the crane tip is not taken into account. The crane tip will instead be modelled as a fixed pivot point which results in a more straightforward derivation of the equations of motion. The proposed mathematical model is presented in Fig. 52.

In this model the crane tip is represented by pivot point O and from this point the lifting hook of the crane is suspended by a cable with length l_1. The lifting hook is modelled as the first point mass m_h and also acts as a pivot point for the lower pendulum. The tool is then represented by the lower pendulum which consists of two point masses on a rigid body. The two red links placed perpendicular to the black link represent the XY-tables for the nacelle and counterweight. Both the nacelle and counterweight can move along these links according to the proposed working principle. The two point masses on the lower pendulum are always positioned so that their combined CoG remains at the same position as shown in Fig. 52. The constants l_3 and l_4 are determined by the mass ratio between the nacelle and the counterweight. In this model α_1 and α_2 represent the angles between the vertical axis and the upper pendulum and lower pendulum respectively.

The equations of motion will be approached using the same Newton-Euler method that was used for the simple double pendulum. Since the working principle guarantees that the CoG of the tool always remains at the same position in the rigid frame the two point masses are replaced by one larger point mass called m_{tot}. The mass of this point is then equal to the sum of the nacelle and the counterweight. This assumption

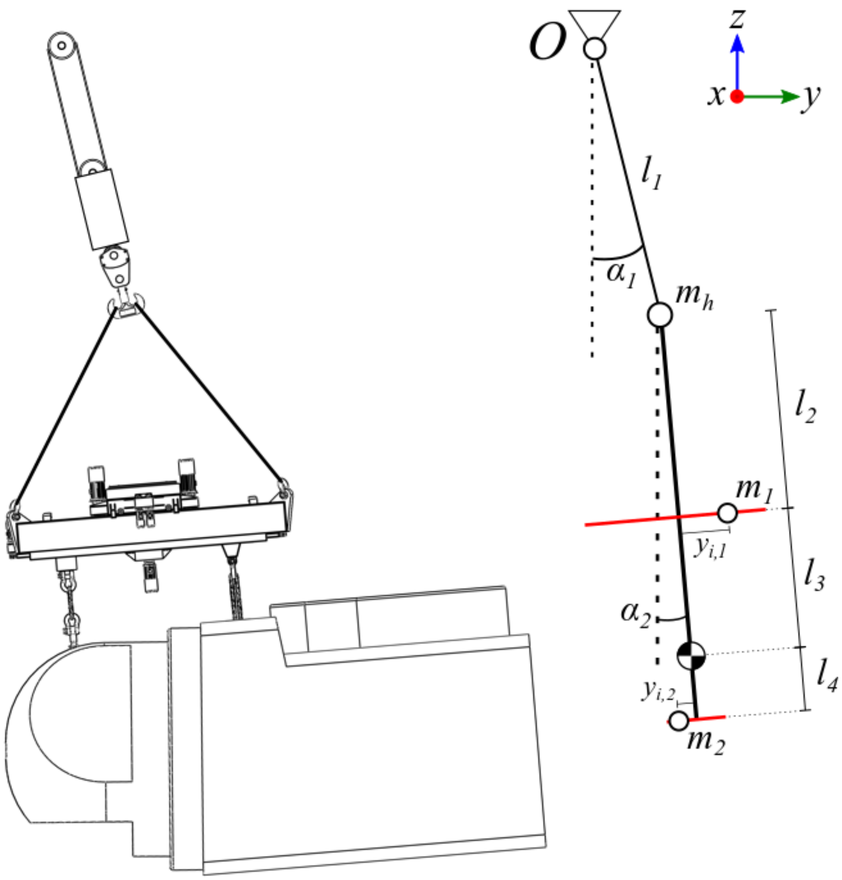

Figure 52: Schematically drawn model of the mathematical model

will lead to a smaller moment of inertia, but for the sake of studying the working principle this difference is negligible. The figure also contains the different forces that act on the upper and lower pendulum. Here the forces indicated by the letter 'T' are the interaction forces between the two pendulums and the fixed pivot point. The letter 'G' refers to the gravitational forces. Lastly, the forces F_1 and F_2 represent the forces that are a result of moving m_1 and m_2 along the red links.

The equations for the angular acceleration for both pendulums can be derived by combining the kinematics and the force equations for the system:

Kinematics

The kinematics of both pendulums can be described by the following set of equations. Let $\mathbf{j}$ be the unit vector along the y-axis being positive in the right direction and let $\mathbf{k}$ be the unit vector along the z-axis being positive in the upward direction. The origin is taken as point pivot point O. Then $\mathbf{r}$ will describe the position, $\mathbf{v}$ the velocity and $\mathbf{a}$ the acceleration of masspoints m_h and m_{tot}.

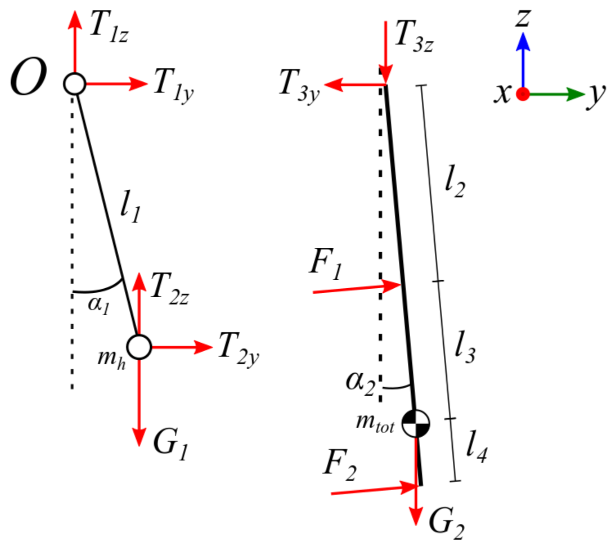

Figure 53: Overview of the forces acting on the system

For the upper pendulum:

$$\mathbf{r} = l_1 sin(\alpha_1)\mathbf{j} - l_1 cos(\alpha_1)\mathbf{k}$$

$$\dot{\mathbf{r}} = \mathbf{v} = l_1\dot{\alpha}_1 cos(\alpha_1)\mathbf{j} + l_1\dot{\alpha}_1 cos(\alpha_1)\mathbf{k}$$

$$\dot{\mathbf{v}} = \mathbf{a}$$

$$a_y = l_1\ddot{\alpha}_1 cos(\alpha_1) - l_1\dot{\alpha}_1^2 sin(\alpha_1) \tag{10}$$

$$a_z = l_1\ddot{\alpha}_1 sin(\alpha_1) + l_1\dot{\alpha}_1^2 cos(\alpha_1) \tag{11}$$

For the lower pendulum:

Let L be $l_2 + l_3$.

$$\mathbf{r} = (l_1 sin(\alpha_1) + L sin(\alpha_2))\mathbf{j} - (l_1 cos(\alpha_1) - L cos(\alpha_2))\mathbf{k}$$

$$\mathbf{v} = (l_1\dot{\alpha}_1 cos(\alpha_1) + L\dot{\alpha}_2 cos(\alpha_2))\mathbf{j} + (l_1\dot{\alpha}_1 cos(\alpha_1) + L\dot{\alpha}_2 cos(\alpha_2))\mathbf{k}$$

$$a_y = l_1\ddot{\alpha}_1 cos(\alpha_1) - l_1\dot{\alpha}_1^2 sin(\alpha_1) + L\ddot{\alpha}_2 cos(\alpha_2) - L\dot{\alpha}_2^2 sin(\alpha_2) \tag{12}$$

$$a_z = l_1\ddot{\alpha}_1 sin(\alpha_1) + l_1\dot{\alpha}_1^2 cos(\alpha_1) + L\ddot{\alpha}_2 sin(\alpha_2) + L\dot{\alpha}_2^2 cos(\alpha_2) \quad (13)$$

Forces
Let T_{1z} and T_{1y} be the forces that act on the upper pendulum at pivot point O.
Let T_{2z} and T_{2y} be the interaction forces that act on the upper pendulum at m_h.
Let G_1 be the gravitational force $m_1 g$ acting on mass m_h.
Let T_{3z} and T_{3z} be the interaction forces that act on the top of the lower pendulum. Where $T_{3z} = -T_{2z}$ and $T_{3y} = -T_{2y}$ due to Newton's law of equal and opposite reaction.
Let G_2 be the gravitational force $m_2 g$ acting on mass m_{tot}.
Let F_1 be the acceleration force of the counterweight.
Let F_2 be the acceleration force for the nacelle.

Using Newton's laws of motion, the following equations can be derived:

$$m_h a_y = T_{1y} + T_{2y} \quad (14)$$

$$m_h a_z = T_{1z} + T_{2z} - G_1 \quad (15)$$

$$I_1\ddot{\alpha}_1 = l_1 sin(\alpha_1)(T_{2z} - G_1) + l_1 cos(\alpha_1)T_{2y} \quad (16)$$

$$m_{tot} a_y = T_{3y} = -T_{2y} \quad (17)$$

$$m_{tot} a_z = T_{3z} - G_2 = -T_{2z} - G_2 \quad (18)$$

$$I_{tot}\ddot{\alpha}_2 = L sin(\alpha_2)G_2 + l_2 F_1 + (l_2 + l_3 + l_4)F_2 - l_1 L m_{tot}\ddot{\alpha}_1 = L sin(\alpha_2)G_2 + (l_3 + l_4)F_2 - l_1 L m_{tot}\ddot{\alpha}_1 \quad (19)$$

The last term in Eq. 20 cannot be found in the force diagram from Fig. 53, because this is the fictitious force, explained for the double pendulum. F_1 and F_2 are not present in Eq. 17 and Eq. 18, because they cancel each other out. This can be proven by the following set of equations:

Let $y_{i,1}$ and $y_{i,2}$ be the positions on the tool of the counterweight and nacelle respectively.

$$y_{i,2} = -r y_{i,1} \text{ where } r = \frac{m_2}{m_1}$$

When this equation is differentiated two times it results in the next equation:

$$\ddot{y}_{i,2} = -r\ddot{y}_{i,1}$$

These accelerations can then be used in the equations for F_1 and F_2.

$$F_1 = m_1\ddot{y}_{i,1} \text{ and } F_2 = m_2\ddot{y}_{i,2}$$

Substituting r in the previous equation proves that $F_1 = -F_2$.

Equations of motion

The equations of motion for the tool can be determined by combining the kinematic and force equations. Eq. 12 and Eq. 13 can be substituted in Eq. 17 and Eq. 18 to solve for T_{2y} and T_{2z}. Then Eq. 16 and Eq. 20 can be solved for $\ddot{\alpha}_1$ and $\ddot{\alpha}_2$ to receive the equation of motions. Substituting the equations and solving the equations for α_1 and α_2 is done with the help of MATLAB version R2021b and the associated script is included in section E.1. The solutions for $\ddot{\alpha}_1$ and $\ddot{\alpha}_2$ are given in the equations below:

$$I_{tot}\ddot{\alpha}_2 = Lsin(\alpha_2)G_2 + l_2F_1 + (l_2 + l_3 + l_4)F_2 - l_1Lm_{tot}\ddot{\alpha}_1 = Lsin(\alpha_2)G_2 + (l_3 + l_4)F_2 - l_1Lm_{tot}\ddot{\alpha}_1 \quad (20)$$

$$\ddot{\alpha}_1 = -\frac{2(l_3+l_4)F_2cos(\alpha_1-\alpha_2)+2L^2\dot{\alpha_2}^2m_{tot}sin(\alpha_1-\alpha_2)+Lgm_{tot}sin(\alpha_1-2\alpha_2)+Lgsin(\alpha_1)(m_{tot}+2m_h)}{2l_1Lm_{tot}+2l_1Lm_h-2l_1Lm_{tot}cos(\alpha_1-\alpha_2)} \quad (21)$$

$$\ddot{\alpha}_2 = -\frac{Lgm_{tot}sin(\alpha_2) - (l_3 + l_4)F_2 + l_1Lm_{tot}\ddot{\alpha}_1}{L^2m_{tot}} \quad (22)$$

5.2 Simulations

The mathematical model now has to be implemented in programming software to simulate the system and analyze its dynamic behaviour. The model is coded in MATLAB's Simulink environment where the equations of motion can be solved with respect to time. For this MATLAB version R2021b is used.

In addition to the equations of motion the model requires a control system which changes the position of the nacelle and counterweight during the simulation. A proportional-integral-derivative (PID) controller will be used to control the force F_2. This controller uses a control error to calculate the required action for the system. The control error can be given by the generic equation Eq. 23. Here r is the reference signal and y the measured output signal of the system. The software provides a built-in PID tuner that estimates the correct coefficients for the controller. MATLAB enables the user to adjust the response time and robustness of the system, but for most simulations the coefficients estimated by MATLAB will be used. If other parameters are selected it will be mentioned during the respective simulation. An overview of the Simulink model is presented in Fig. 54, the equations of motion are put into a subsystem due to its large size.

$$e = r - y \quad (23)$$

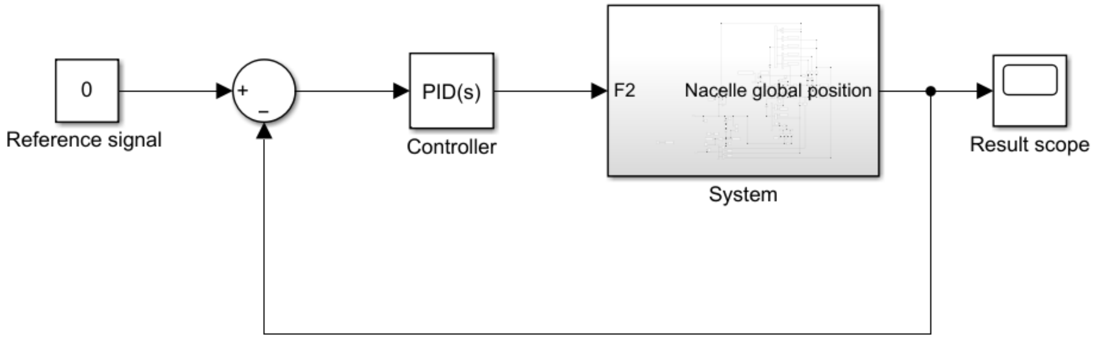

Figure 54: The controlled model

5.2.1 Model verification

Verification of the model is required to check if the model behaves as was written in the mathematical model. This way possible errors in the Simulink model can be identified and solved. There are a few basic checks that can be done to see if the equations are implemented accordingly. For the first check the masses are located in the center of their XY-table resembling a simple double pendulum. The double pendulum should remain at rest when the initial angle, angular velocity and acceleration are set to zero .

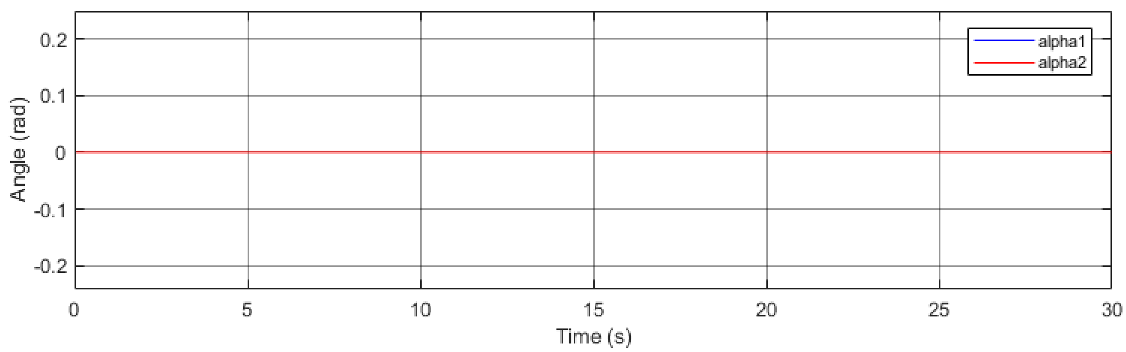

Figure 55: Model check with initial conditions equal to zero

In Fig. 55 it can be seen that both angles remain zero which is in line with the expectations. A second check can be done to see if the dynamic behaviour of the system is also the same as that of the double pendulum without the tool's feature of moving the nacelle and counterweight. If this check passes it can be confirmed that the model behaves as was described by the mathematical model. The results of this check can be seen in Fig. 56 and Fig. 57. It is clear that both models are exactly the same when simulated with equal parameters and equal initial conditions.

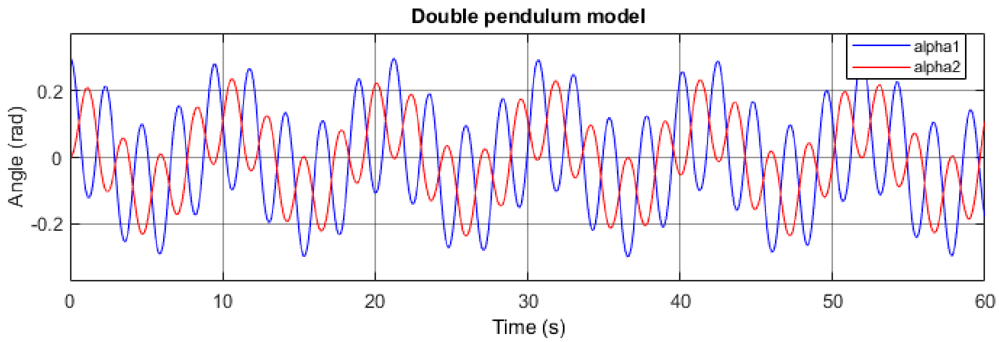

Figure 56: Double pendulum model with initial conditions α_1 = 0,3 rad and α_2 = 0 rad

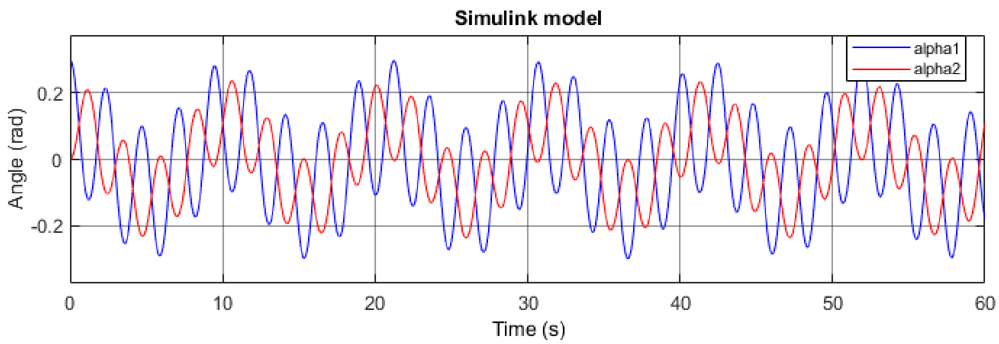

Figure 57: Simulink model with initial conditions α_1 = 0,3 rad and α_2 = 0 rad

5.2.2 Model validation

Validation of the model is required to check if the model accurately presents the physical system in reality. But because this model is a representation of a tool that currently does not yet exist its validation is more difficult. However, checks can be executed to validate that the model indeed behaves as it is expected to behave in the real world. The first check done in the verification step is also relevant for the validation of the model. Because if the model is hanging in a vertical position with $\alpha_1 = 0$ and $\alpha_2 = 0$ the model will gain no angular acceleration when no external forces are exerted on the system. The second check can be described as follows, if the initial conditions of the system are $\alpha_1 = 0$ and $\alpha_2 = 0$ and the nacelle is accelerated in the positive y-direction the tool should initially move in the opposite direction. This check can be performed by applying a horizontal force for a short duration. For this test a force of -650 kN will be applied for 3 seconds. If the model works accordingly α_2 should first become negative before starting to show common double pendulum behaviour. It can be seen that it is indeed the case for the experiment shown in Fig. 58.

5.2.3 Results

Now the Simulink model is verified and validated it can be used to study the dynamic behaviour of the tool. The first important step is to study the working principle to see if it actually works as expected. To do this a reference set-up will be used where the dimensions are based on the 3D SolidWorks model and the specifications of the installation vessel and the turbine. The mathematical model uses four constants for the length of the cables and the distances between the masses and the CoG of the tool. The values taken for each constant of the reference set-up are presented in Table 11.

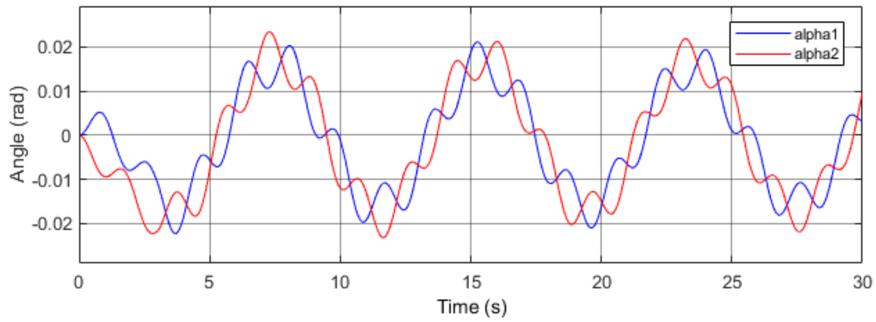

Figure 58: Simulink model with initial conditions $\alpha_1 = 0$ rad and $\alpha_2 = 0$ rad

Table 11: Parameter values of the reference set-up

Parameter	Value
l_1	7.74 m
l_2	7.74 m
l_3	1.18 m
l_4	0.24 m
m_h	170 t
m_1	130 t
m_2	650 t
g	9.81 m/s^2

The reference set-up only considers the last phase of the installation phase where the nacelle is already lifted up above the turbine tower. The constants l_3 and l_4 are derived from the locations where the rack and pinon drives transfer the forces to the main frame. Then l_1 and l_2 can be calculated by subtracting the values for l_3, l_4 and the distance to the bottom of the nacelle from the available vertical space of 30 meters. For the reference set-up l_1 and l_2 are assumed to be equal, if the controlled model proves to be functional the influence of these variables will also be explored.

The first simulation has the goal to evaluate the concept's proposed working principle. This test is done by setting the initial angles of the system to 0.017 radians. With a maximum displacement of 0.5 meters and a total length of 30 meters this leads to an angle of 0.017 radians which roughly equals one degree. The PID controller uses the global x-coordinate of the nacelle as the measured signal and the reference signal is set to be 0. This is the most direct control error where the PID controller will try to move the nacelle to the 0 x-coordinate. In Fig. 59 the global position of the nacelle is given for the controlled model and is then compared to a model with no control which is an exact copy of the model without the PID controller. This means that in the uncontrolled model the nacelle and counterweight will always remain in the center of their XY-table. If the concept works as expected it should show that the x-coordinate converges faster to zero.
For this test the PID Tuner App in MATLAB Simulink indicates that it is not able to find a stable configuration for the controller. When the controller is then tuned with parameters that show stable behaviour in the first period it results in Fig. 59. It can be seen that for the first minute the model has a smaller amplitude than the uncontrolled model. However, the instability of the controller then causes the amplitude to increase further and further beyond the amplitude of the uncontrolled model.

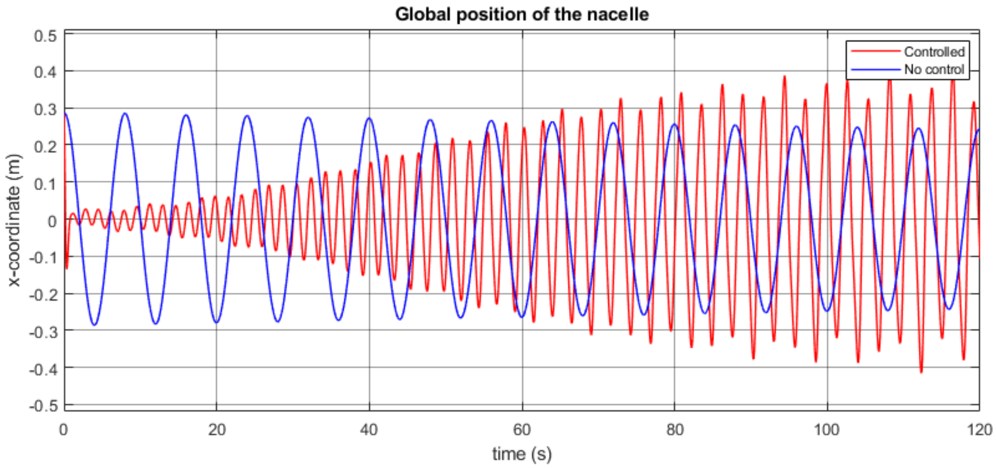

Figure 59: The global position of the nacelle for a controlled and uncontrolled model

Since the parameters of the controller are automatically tuned in MATLAB Simulink it is not clear if the proposed principle does not work as expected or that the automatic tuner causes problems for this particular model. To find out what causes the unexpected results a set of tests will be performed. The corresponding approach is given in the flowchart in Fig. 60.

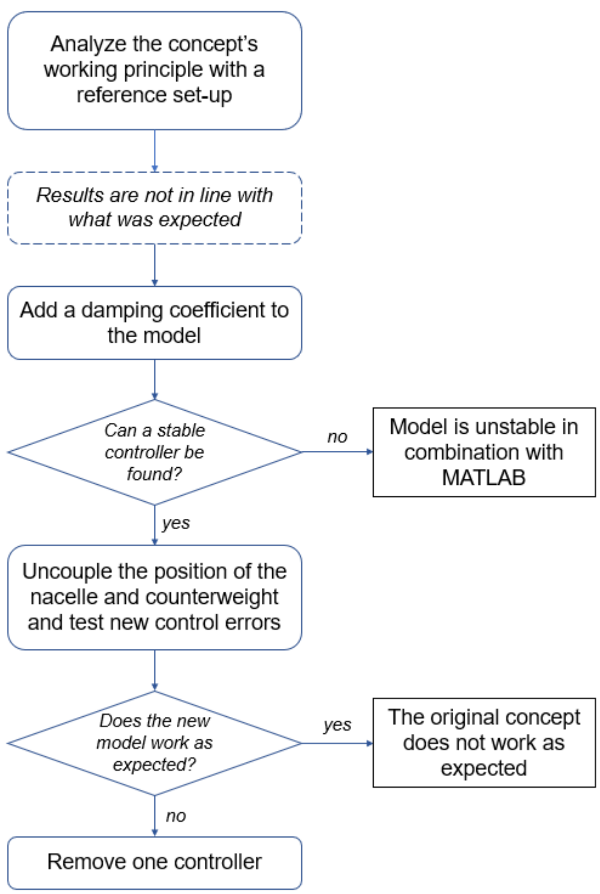

Figure 60: Flowchart for studying the cause of the unexpected results

Damping coefficient

The first test consists of a small change to the equations of motion. This test is done to get a better understanding of the compatibility of the MATLAB PID tuner. Depending on the damping factor the system should always be able to become stable, since a very large damping coefficient would quickly bring the system to rest. If this is not the case it indicates that the PID tuner is not suitable for this model. A damping factor is added to the equations of motions that subtracts a fraction of the angular velocity from the acceleration. This factor could represent the damping effects caused by air resistance and secondary cables running from the crane to the tool. Initially, a relatively small value of 0.005 was selected as the damping coefficient so that it has not much impact on the model, but a comparison with the uncontrolled model is now possible. The results are presented in Fig. 61.

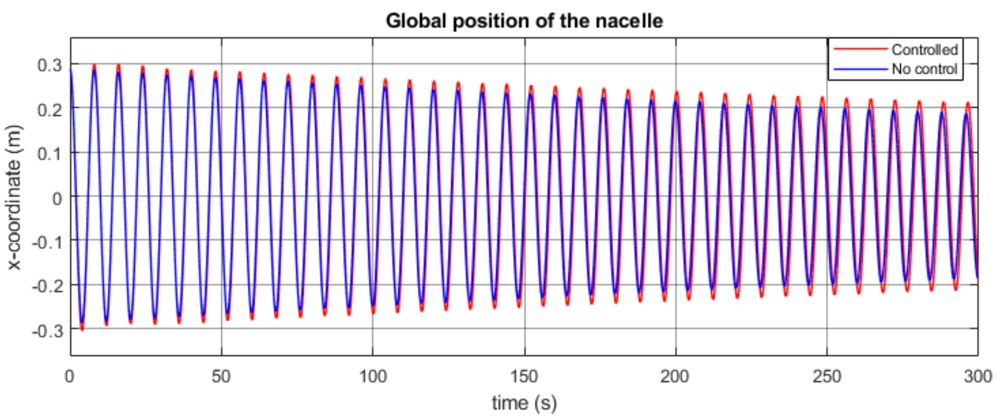

Figure 61: The global position of the nacelle for a controlled and uncontrolled model

The models are simulated for 300 seconds and it can be seen that in both cases the nacelle starts at the same x-coordinate which is logical since the initial conditions are equal. However, after the first swing the controlled version of the model has a slightly larger amplitude than the uncontrolled model. To understand why the system is not able to decrease the oscillation faster than the uncontrolled model a closer look has to be taken at the controlled variable F_2. In Fig. 62 two plots are given with angle α_2 and force F_2. Here it can be seen that when α_2 is positive, force F_2 is also always positive. What then happens within the tool can be compared to the 'pumping' of a children's swing, where you start swinging higher without any external forces. In the first seconds of the simulation the force F_2 causes a small increase in the amplitude, before it starts decreasing similarly to the uncontrolled model due to the damping factor. This result shows that the PID controller does work for the model with a damping factor. Although it can only create a stable controller by selecting very low parameters, it proves that the automatic tuner is compatible. A second test is required to identify the cause of the unstable results from the first simulation.

Uncoupled model

The previous test with the damped model showed that the PID tuner is able to find a stable configuration. However, it is still not clear if the initial principle does not work as expected or that the controller is not suitable for this system. This test will be done to understand why the controlled model does not show a better result than the uncontrolled model. The previous simulations were performed with a model where the position of the nacelle and counterweight were coupled. For this test the positions of the nacelle and

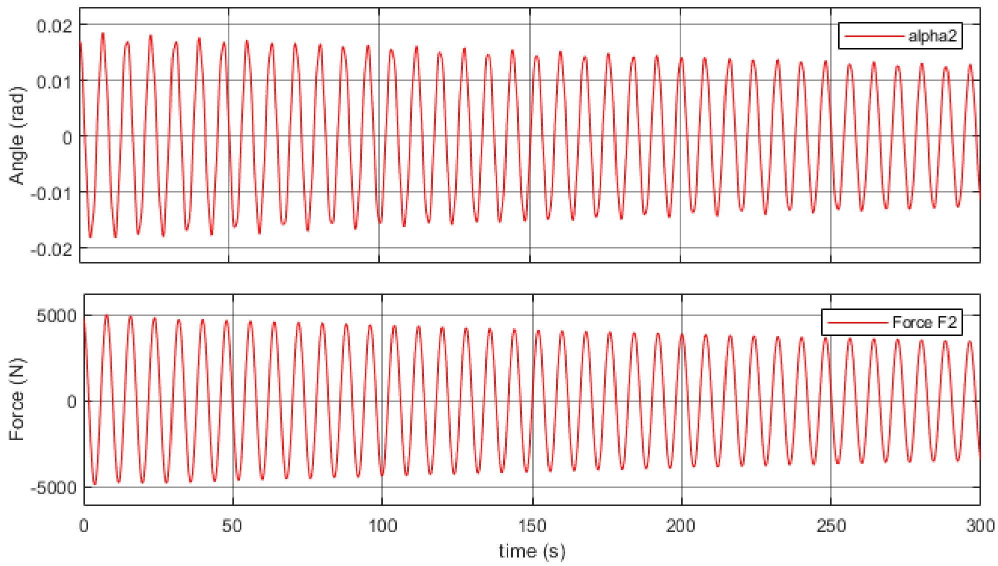

Figure 62: The force F_2 and angle α_2 compared during the simulation

counterweight will be uncoupled so that they can be independently actuated. Secondly, different control errors will be evaluated to study if a better control rule can be established. These tests will give a better view on the performance of the control system in combination with the Simulink model.
In the new model, the force F_1 is no longer directly linked to F_2, but the counterweight will be actuated independently. This also means that the CoG of the tool will no longer remain at the same position, but is dynamic. The exact position of the CoG is a result of the position of the nacelle and counterweight. The damping factor from the previous experiment is also used to guarantee that a stable control model can be found. These changes require a recalculation of the equations of motion which result in the new set of EoM given in Eq. 24 and Eq. 25. A new MATLAB script can also be found in section E.2.

$$\ddot{\alpha}_1 = -\frac{A_1 Lcos(\alpha_1-\alpha_2)-A_2L_c^2sin(\alpha_1)-A_3L_c^2cos(\alpha_1)+L_c^2gm_{tot}sin(\alpha_1)+L_c^2gm_hsin(\alpha_1)-r_{G2}Lgm_{tot}cos(\alpha_1-\alpha_2)}{l1L_c^2(m_{tot}+m_h)-Ll_1m_{tot}L_ccos(\alpha_1-\alpha_2)} \tag{24}$$

$$\ddot{\alpha}_2 = -\frac{r_{G2}gm_{tot} - A_1 + l_1L_cm_{tot}\ddot{\alpha}_1}{L_c^2m_{tot}} \tag{25}$$

Where, A_1 is equal to $l_2F_1 + (l_2 + l_3 + l_4)F_2$, A_2 to $(F_1 + F_2)cos(\alpha_2)$ and A_3 to $(F_1 + F_2)sin(\alpha_2)$. Since the CoG is no longer fixed, r_{G2} is added which indicates the arm for the moment caused by the tools gravitational force. The variable L_c is shortest distance from point m_h to the CoG of the tool.

For this model a second PID controller was required that controls force F_1 which is no longer depending on force F_2. The hypothesis is that this model has more freedom to find a solution so that the controlled model can bring the system to rest faster than the uncontrolled model. The test is first done with the initial control error which leads to the graph in Fig. 63.

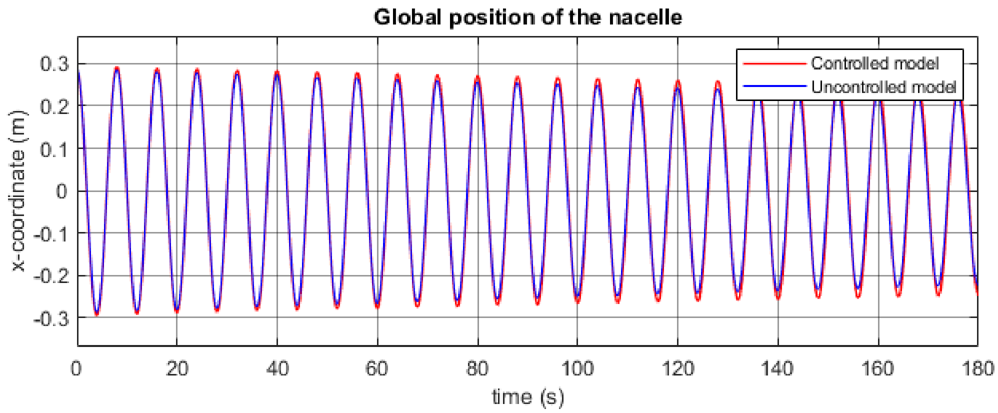

Figure 63: The global position of the nacelle for the new controlled and uncontrolled model

It is immediately clear that the controlled model shows the same behaviour as the coupled model. The result is very similar to that of the previous simulation because MATLAB tunes the controller to the point where it almost has no additional input. Simply uncoupling the forces does not result in a system which is able to decrease the swinging faster than the uncontrolled model. It is possible that the initial control error is not the best option for this model. This is why three other control errors will also be studied. If a control error is found that shows the ability to dampen out the oscillation faster it will also be tested with the original model.

Control error variation 1: 0 - $(\alpha_1 + \alpha_2)$

In Fig. 64 the results can be seen when $\alpha_1 + \alpha_2$ is selected as the measured signal and 0 as the reference signal. The goal of the PID controller is then to bring the sum of both angles to zero which could decrease the time it takes to bring the tool closer to zero, however this control error does not explicitly cause the controller to bring the nacelle to the vertical axis. Since the sum of both angles does not explicitly mean that both angles are going to zero, because when one is negative and the other positive it also leads to a total sum of zero. The new control error causes the controlled model to be almost equal to the uncontrolled model. For this case the controller decides to minimally actuate the nacelle and counterweight.

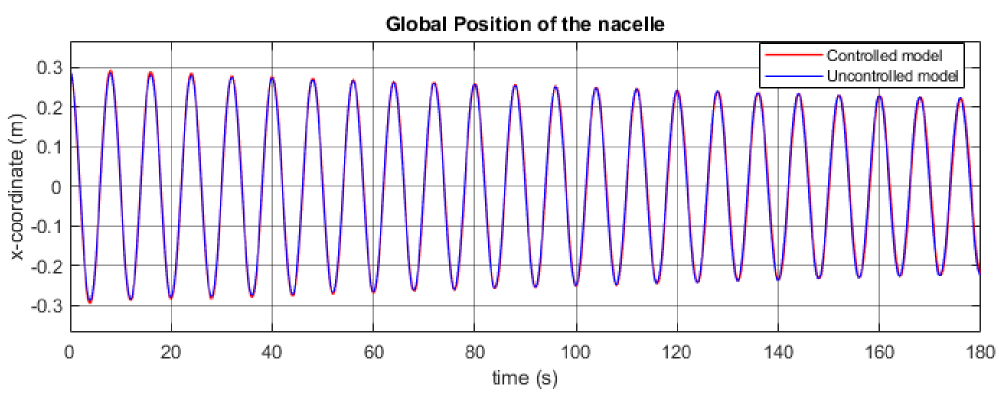

Figure 64: Control error variation 1: 0 - $(\alpha_1 + \alpha_2)$

Control error variation 2: 0 - ($\ddot{\alpha}_1 + \ddot{\alpha}_2$)

The results of choosing $\ddot{\alpha}_1 + \ddot{\alpha}_2$ as the measured signal while keeping the reference signal equal to zero are shown in Fig. 65. This control error leads to an interesting result, a clear damping effect can be seen that decreases the amplitude of the swinging faster than that of the uncontrolled model. However, this graph also shows that the center line of the oscillation starts to deviate from the zero line further into the simulation. This is a side-effect of the control error which does not explicitly say that both angles should converge to zero.

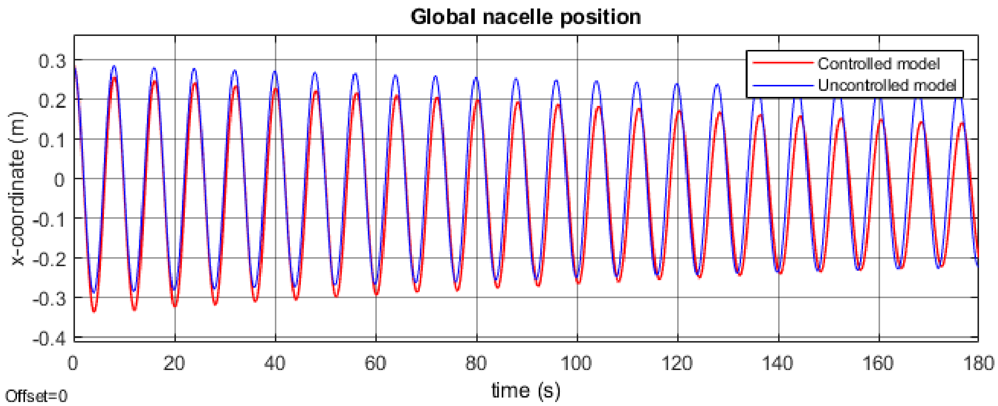

Figure 65: Control error variation 2: 0 - ($\ddot{\alpha}_1 + \ddot{\alpha}_2$)

Control error variation 3: global x-coordinate hook - global x-coordinate CoG tool

The third control error that is evaluated uses the global x-coordinate of the hook and the tool's CoG as the reference and measured signal respectively. The goal of this control error is to keep the CoG below the hook of the crane thus decreasing the moment caused by the weight of the tool. The results of this control error are given in Fig. 66. The results are similar to that of control error variation 1. The difference between the controlled and uncontrolled model is very small due to a small input of the controller.

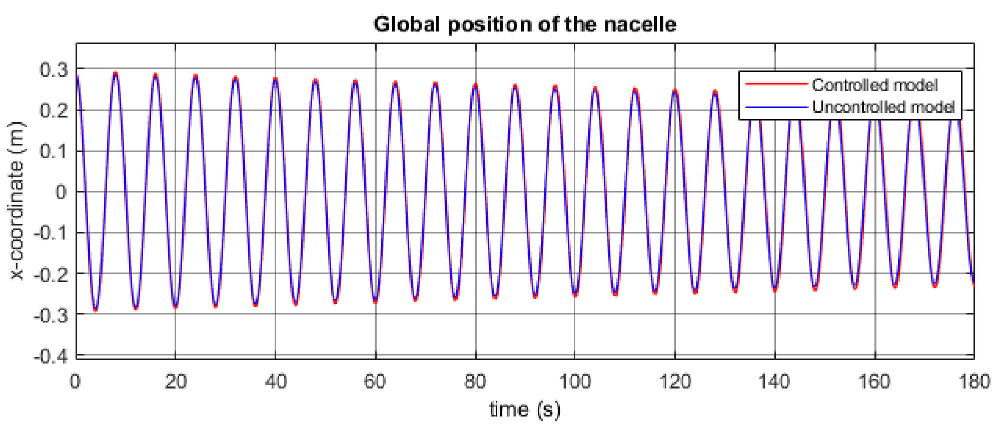

Figure 66: Control error variation 3: global x-coordinate hook - global x-coordinate CoG tool

Up to this point the dynamic analysis has not been successful in providing concrete information on the dynamic behaviour of the developed concept. The mathematical model, in combination with MATLAB Simulink and its integrated control system has proven to be a complex task. The previous tests showed that the uncoupling of the counterweight from the nacelle does not result in a system that dampens out oscillation faster than an uncontrolled system. The variations on the initial control error with the goal of damping the oscillation of the model did also not show the expected results. However, the results from controller error variation 2 do strongly suggest that a damping effect can be achieved with this concept.

Although a new working principle and several new control errors were studied, a simulation that shows successful damping of the system has not been achieved. But because the previous model showed that damping is possible it is interesting to evaluate one more model. With the implementation of the second controller, it became clear that tuning both controllers is very complex. The complexity comes from the fact that the controllers directly affect each other through the model. Due to this fact MATLAB did not come to the exact same solution for every simulation. A third and last test might provide useful information with the use of only one PID controller.

This third test will consider a system where only one mass will be actuated. For this reason, only one PID controller is needed and the complexity of tuning two conflicting PID controllers is avoided. The choice between the counterweight and the nacelle is fairly easy, since moving the nacelle is a lot more difficult than moving the counterweight on top of the tool. So, for this model a new Simulink model is created that uses the same equations of motion. Contrary to that model, F_2 is now set to zero since the nacelle is no longer actuated. The previously used control errors did not lead to any results with the preferred outcome, however due to trial and error a new control error was found that has a significant damping effect on the system. This control error uses the sum of α_1 and α_2 as the measured signal and the global x-coordinate of the lifting hook as the reference signal. The results of this simulation are given in Fig. 67.

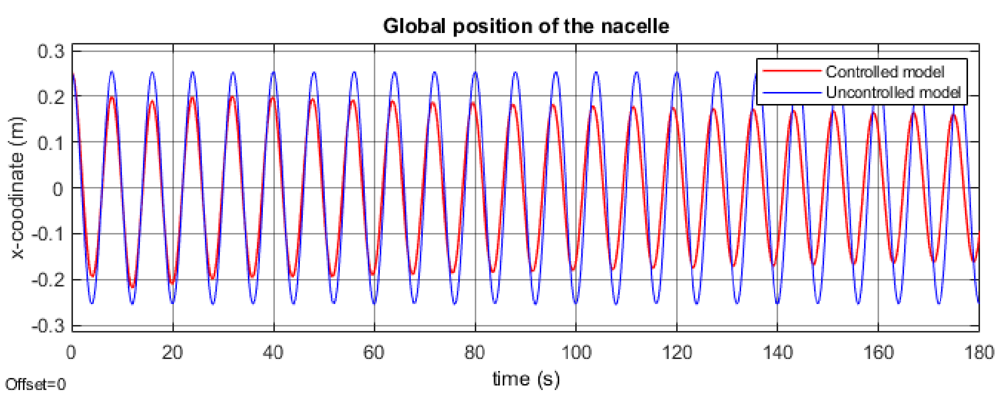

Figure 67: New model with control error: global x-coordinate hook - $(\alpha_1 + \alpha_2)$

In this simulation the artificial damping coefficient was removed so that it can be proved that the model also works without it. It can be seen that the nacelle starts at an amplitude of approximately 0.25 meters and it is reduced to approximately 0.16 meters after 180 seconds. This is a decrease of 36% in a span of 3 minutes.

6 Conclusions

This master thesis aimed to develop a design for a hook mounted compensator to improve the installation of the nacelle. This section will summarize the findings of this research in relation to the sub-questions and finally, the main research question.

Q1. How is the current installation process for offshore wind turbines defined and how can the relevant installation steps be described?

From the literature it has become evident that the installation process of an offshore wind farm highly depends on the location, weather conditions and available materials. Thus, the exact installation procedure cannot be described by a standard process. However, the order in which the parts of a single wind turbine are installed is always the same: foundation, transition piece, tower, nacelle and turbine blades.

Q2. What are common problems that arise during the installation of an offshore wind turbine as a result of unwanted motion and how do these problems affect the installation process?

It can be concluded that unwanted motion due to bad weather conditions results in true challenges during the installation of an offshore wind turbine. The procedure requires a lot of precision and the additional motions threaten the ability to achieve this. The issues are not solely for one component, but are present for the installation of each one.

Q3. The installation of which turbine component is the most innovative and has the most potential to improve the installation of an offshore wind turbine?

The selection for a turbine component was done using the process of elimination. For the installation of a monopile an effective solution already exists which successfully compensates for motion and keeps the inclination of the monopile within the boundaries. The installation of the transition piece and tower are very similar to the installation of the monopile due to their shape. For this reason, a similar solution could be utilized. The installation of the nacelle also requires a significant amount of precision and is not often studied in the literature. The installation of the blades is also very interesting since this part is very susceptible to the wind. However, improvements for this part of the installation are already heavily studied. Taking existing research and solutions into account the nacelle was selected for the design of the hook mounted compensator.

Q4. What methods can be adopted to generate and evaluate different concepts for hook mounted compensators?

To develop concepts for a hook mounted compensator a design methodology was adopted that consists of the following three distinct phases: analysis, synthesis and evaluation. This methodology resulted in seven concepts for the hook mounted compensator. Since it is very difficult to evaluate non-existing concepts on a qualitative basis the analytic hierarchy method was adopted. The adopted methods proved to be suitable for the goal of this thesis.

Q5. What is the technological feasibility of the developed concept?

The technological feasibility of the concept was explored with a concept design and a dynamics analysis. From the design phase it can be concluded that the concept can be built from five main parts: the lower x-table, the nacelle carrier, the main frame, the upper y-table and the counterweight. The concept has an approximated weight of 170.9 tonnes and a maximum length of 11.5 meters, a width of 7.8 meters and a height of 5.1 meters which all is in accordance with the design requirements. The concept was then translated into a mathematical model for a dynamic analysis. The results of the dynamic analysis suggest that the concept has the ability to compensate for motion. However, the PID tuner in MATLAB Simulink proved not to be suitable for this research.

Upon analyzing the answers to all of the sub-question the main research question can be answered which was defined as follows:

What hook mounted motion compensation tool can be developed for turbine installation from a floating vessel, and how does its performance compare to the conventional installation process?

All in all, it can be concluded that a hook mounted motion compensation tool can be developed for the installation of the nacelle. This tool consists of two table which allow the nacelle and a counterweight to move in the opposite direction with the goal to compensate for unwanted motion. The dynamic analysis was inconclusive on the performance of the developed concept, but the results showed that ability to dampen out a given oscillation to the system. A render of the design of the developed hook mounted compensator is given in Fig. 68.

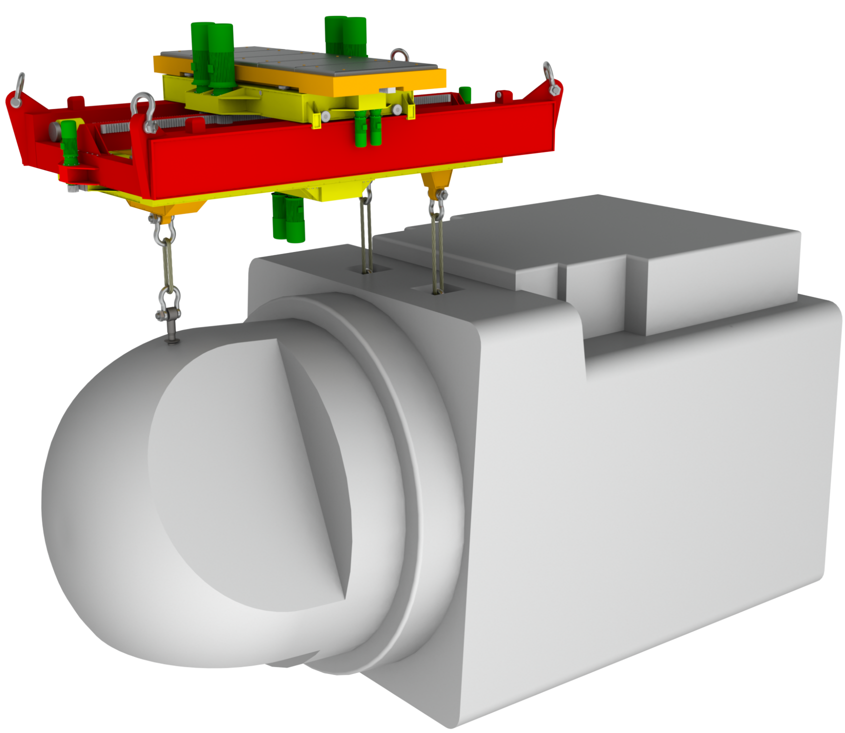

Figure 68: A render of the final concept design

7 Recommendations

During the course of this study assumptions were made and methods were adopted with the goal to design a hook mounted compensator. This chapter will discuss if these were appropriate and will give recommendations for future research.

- The approximation for the maximum amplitude of the nacelle during installation was based on data from the lifting hook during the installation of the nacelle with a 3D motion compensated crane. It is important for future research to investigate the exact level of motion that can occur during the installation. This can lead to more accurate design requirements for the design phase and the dynamical analysis.
- In this research a first design is given for the hook mounted compensator. This was done with beams with a rectangular hollow steel section. Additionally, the weight and size of secondary steel structures were estimated during the design. Although this was acceptable for this master thesis, it is expected that more iterations in the design will result in a lighter and more compact tool.
- For the dynamic analysis several forces were neglected that could make the analysis more accurate. The effects of the wind and secondary cables connected to the tool or nacelle could be taken into account. The concept was only modelled in 2D, whereas in a 3D model the rotation about the vertical axis could be taken into consideration. The rotation about the horizontal axes could also lead to challenges in relation to the mating of the nacelle to the tower. All these factors would help in better understanding the dynamic behaviour of the concept.
- The developed mathematical model was implemented in MATLAB Simulink and for the actuation of the nacelle and counterweight a PID controller was used. The controller was automatically tuned by MATLAB which led to an inconclusive result on the working principle of the tool. Although the results indicated that the tool is able to compensate for motion it is worth to perform a more extensive control study for a better understanding.

References

[1] Tabassum-Abbasi, Premalatha, M., Abbasi, T., Abbasi, S. (2014). Wind energy: Increasing deployment, rising environmental concerns. Renewable and Sustainable Energy Reviews, 31, 270–288. https://doi.org/10.1016/j.rser.2013.11.019

[2] WindEurope. (2019, February). Offshore Wind in Europe - Key trends and statistics 2019. https://windeurope.org/about-wind/statistics/offshore/european-offshore-wind-industry-key-trends-statistics-2019/

[3] Woodacre, J., Bauer, R., & Irani, R. (2015). A review of vertical motion heave compensation systems. Ocean Engineering, 104, 140–154. https://doi.org/10.1016/j.oceaneng.2015.05.004

[4] Rules for Classification and Construction - Ship Technology. (2013). Germanischer Lloyd SE, Hamburg. https://rules.dnv.com/docs/pdf/gl/maritimerules/gl_i-1-15_e.pdf

[5] Active Heave Compensator - Telesto AHC. (2019, June 24). Screaton & Associates. Retrieved on 9-12-2021, from https://screaton.co.uk/products/hook-ahc/

[6] Arvind Keprate. (2015). Impact of Passive Heave Compensator on Offshore Lifting. Journal of Shipping and Ocean Engineering, 5(4). https://doi.org/10.17265/2159-5879/2015.04.003

[7] Tong, W. (2010). Wind Power Generation and Wind Turbine Design. Amsterdam University Press.

[8] WindEurope. (2020, February). Offshore Wind in Europe - Key trends and statistics 2020. https://windeurope.org/about-wind/statistics/offshore/european-offshore-wind-industry-key-trends-statistics-2020/

[9] Kallehave, D., Byrne, B. W., LeBlanc Thilsted, C., & Mikkelsen, K. K. (2015). Optimization of monopiles for offshore wind turbines. Philosophical Transactions of the Royal Society A: Mathematical, Physical and Engineering Sciences, 373(2035), 20140100. https://doi.org/10.1098/rsta.2014.0100

[10] Quandt, M., Beinke, T., Ait Alla, A., and Freitag, M. (2017). Simulation based investigation of the impact of information sharing on the offshore wind farm installation process. Journal of Renewable Energy, (1), 11 pp

[11] Li, L., Guachamin Acero, W., Gao, Z., & Moan, T. (2016). Assessment of Allowable Sea States During Installation of Offshore Wind Turbine Monopiles With Shallow Penetration in the Seabed. Journal of Offshore Mechanics and Arctic Engineering, 138(4). https://doi.org/10.1115/1.4033562

[12] Acero, W. G., Gao, Z., & Moan, T. (2017). Methodology for Assessment of the Allowable Sea States During Installation of an Offshore Wind Turbine Transition Piece Structure Onto a Monopile Foundation. Journal of Offshore Mechanics and Arctic Engineering, 139(6). https://doi.org/10.1115/1.4037174

[13] Jiang, Z. (2021). Installation of offshore wind turbines: A technical review. Renewable and Sustainable Energy Reviews, 139, 110576. https://doi.org/10.1016/j.rser.2020.110576

[14] Jiang, Z., Gao, Z., Ren, Z., Li, Y., & Duan, L. (2018). A parametric study on the final blade installation process for monopile wind turbines under rough environmental conditions. Engineering Structures, 172, 1042–1056. https://doi.org/10.1016/j.engstruct.2018.04.078

[15] J. (2020, August 25). Offshore jack-up installatieschepen. Jan De Nul. Retrieved on 9-12-2021, from https://www.jandenul.com/nl/vloot/navires-dinstallation-autoelevateurs

[16] Pieffers, T. (2019, November 27). Heerema develops floating wind turbine installation method. Project Cargo Journal. Retrieved on 9-12-2021, from https://www.projectcargojournal.com/offshore/2019/11/27/heerema-develops-floating-wind-turbine-installation-method/

[17] J. (2020). Kraanschepen. Jan De Nul. Retrieved on 10-12-2021, from https://www.jandenul.com/nl/vloot/kraanschepen

[18] Wenau, S., Bihler, V., Oguro, A., Haberkern, J., Frielinghaus, G., & Preu, B. (2020, October 17). Challenges in offshore wind farm installation. PES - Power Energy Solution. Retrieved on 3-6-2022, from https://pes.eu.com/wind/challenges-in-offshore-wind-farm-installation/

[19] Vis, I. F., Ursavas, E. (2016). Assessment approaches to logistics for offshore wind energy installation. Sustainable Energy Technologies and Assessments, 14, 80–91. https://doi.org/10.1016/j.seta.2016.02.001

[20] Stableonboard. (2021). Entertainment. Retrieved on 10-12-2021, from https://www.stableonboard.com/entertainment/

[21] Jiang, Z. (2018). The impact of a passive tuned mass damper on offshore single-blade installation. Journal of Wind Engineering and Industrial Aerodynamics, 176, 65–77. https://doi.org/10.1016/j.jweia.2018.03.008

[22] Haliade-X offshore wind turbine. (2021). GE Renewable Energy. Retrieved on 10-12-2021, from https://www.ge.com/renewableenergy/wind-energy/offshore-wind/haliade-x-offshore-turbine

[23] Jones, J. Christopher, "A Method of Systematic Design", Conference on Design Methods, Pergamon, Oxford, 1963.

[24] Vaidya, O. S., Kumar, S. (2006). Analytic hierarchy process: An overview of applications. European Journal of Operational Research, 169(1), 1–29. https://doi.org/10.1016/j.ejor.2004.04.028

[25] Motion Compensated Platform. (2021). Huisman Equipment. Retrieved on 7-2-2022, from https://www.huismanequipment.com/en/products/renewables

[26] Levien, R. B., & Tan, S. M. (1993). Double pendulum: An experiment in chaos. American Journal of Physics, 61(11), 1038–1044. https://doi.org/10.1119/1.17335

[27] Stachowiak, T., & Okada, T. (2006). A numerical analysis of chaos in the double pendulum. Chaos, Solitons Fractals, 29(2), 417–422. https://doi.org/10.1016/j.chaos.2005.08.032

[28] Cross, R. (2005). A double pendulum swing experiment: In search of a better bat. American Journal of Physics, 73(4), 330–339. https://doi.org/10.1119/1.1842729

[29] Wikinger Offshore Wind Farm Installation - Full Length. (2017, December 7). [Video]. YouTube. https://www.youtube.com/watch?v=rwOBl5AeKWQt=274sab_channel=Fred.OlsenWindcarrier

[30] How it all comes together at sea: installing an offshore wind farm. (10-6-2020). [Video]. YouTube. https://www.youtube.com/watch?v=mDvS7tizetgt=143sab_channel=SiemensGamesa

[31] Turbine installation at offshore wind farm: DanTysk. (6-2-2015). [Video]. YouTube. https://www.youtube.com/watch?v=aTQePX9i2pkab_channel=Vattenfall

[32] Standard DNVGL-ST-N001 Marine operations and marine warranty, Det Norske Veritas (2018).

[33] Hilkert, J. M. (2008). Inertially stabilized platform technology Concepts and principles. IEEE Control Systems, 28(1), 26–46. https://doi.org/10.1109/mcs.2007.910256

[34] TRADEINN RETAIL SERVICES, S.L. (z.d.). Feiyutech. Retrieved on 16-3-2022, from https://www.techinn.com/en/feiyutech-ak2000c-3-axis-gimbal-stabilizer/137904878/p

[35] Kljuno, E., & Williams, R. L. (2008). Vehicle Simulation System: Controls and Virtual-reality-based Dynamics Simulation. Journal of Intelligent and Robotic Systems, 52(1), 79–99. https://doi.org/10.1007/s10846-008-9204-y

[36] MPI CableRobot Simulator. (2015, September 23). [Video]. YouTube. https://www.youtube.com/watch?v=W7nGL-_5SDwt=2s

[37] LT975 - Blade Dragon. (n.d.). Liftra. Retrieved on 17-6-2022, from https://liftra.com/products/lt975-blade-dragon.html

[38] Boom Lock allows offshore installation at higher wind speeds. (2015, June 12). Offshore Wind Industry. Retrieved on 17-6-2022, from https://www.offshorewindindustry.com/news/boom-lock-allows-offshore-installation-higher

[39] Huisman to deliver cutting-edge monopile gripper for Jan De Nul Group. (2018). Huisman Equipment. Retrieved on 17-6-2022, from https://www.huismanequipment.com/nl/media_centre/press_releases/163-127_Huisman-to-deliver-cutting-edge-monopile-gripper-for-Jan-De-Nul-Group

A Scientific research paper

Design of a motion compensating tool to improve the installation of offshore wind turbines

D. Burggraaf, H. Polinder, J. Jovana
Department of Maritime and Transport Technology
Delft University of Technology
Delft, The Netherlands
dburggraaf@student.tudelft.nl

O. van der Meij
Huisman Equipment
Schiedam, The Netherlands

***Abstract*—New trends in the offshore wind industry show that wind farms are being built further onto sea. This also means that turbines have to be installed in deeper waters resulting in new challenges for the offshore wind industry. The commonly used jack-up vessels have a limited operating depth and therefore floating installation vessels become an interesting alternative. The downside of using floating installation vessels is that they encounter more unwanted motions. A motion compensating tool can help to decrease the negative effects of the unwanted motions. The designing steps for a motion compensating tool are presented resulting in a final concept design. The concept is eventually worked out in a mathematical model to evaluate the dynamic behaviour.**

***Index Terms*—Motion compensation, Offshore wind industry, Offshore wind turbines, Floating installation vessel**

I. INTRODUCTION

The increasing energy demand, the fact we are running out of fossil fuels and the acceptance of global warming has led to an increase in the demand for renewable energy sources. Wind energy is one of the most promising renewable energy sources currently available [1]. The first offshore wind farms (OWF) were built relatively close to the shore, but recent trends show that new farms are being built further off the coast and in deeper waters. The increasing depth and distance to shore introduce new challenges in the offshore wind industry. A jack-up vessel is a common installation vessel for offshore wind turbines, this vessel can lift itself out of the water with the help of long support legs. However, a jack-up vessel has a maximum operating depth resulting in challenges due to these trends. An alternative is a floating installation vessel, this vessel is not limited by a maximum operating depth. A floating vessel is more susceptible to wind and waves, resulting in more unwanted motions which decrease the workability of the floating installation vessel [2]. And since the installation of a wind farm can be heavily delayed when a vessel is not able to operate Huisman Equipment wants to investigate options for a tool that can compensate for the additional unwanted motions. Therefore, the following research question is proposed: **What hook mounted motion compensation tool can be developed for offshore wind turbine installation from a floating vessel, and how does its performance compare to the conventional installation process?**

II. BACKGROUND INFORMATION

There is no standard process when it comes to installing an OWF [3], but the installation order of an offshore wind turbine (OWT) is always the same: foundation - transition piece - tower - nacelle - blades. The installation of an OWT is a complex process and it is unavoidable that challenges will be present. This study focuses on the problems caused by unwanted motions during the installation. In [4] and [5] it becomes clear that for the installation of an OWT a lot of precision is required and that bad weather conditions can easily lead to downtime. Unwanted motions are a well-known problem in the offshore industry and a lot of motion compensating solutions are already on the market. Motion compensating technologies can be divided into three distinct categories: passive, active and hybrid compensation. Passive compensation uses an open-loop system without any feedback. Contrary to the passive system, an active system uses feedback to effectively compensate for motion. The third category combines both types of compensation and is called a hybrid system. It is used to reduce the total power consumption and cost of expensive sensors and controllers. The offshore industry is not the only industry where unwanted motions form a problem. Motion compensating solutions can be found in many other industries and even in daily appliances. A good example are the stabilizers used for cameras to keep them levelled while the user is moving. The existing technologies in- and outside the offshore industry will be used as inspiration for the design stage.

A case study is defined to set the study's scope. In this case study a turbine component is selected for which the tool will be designed. For the installation of the foundation well functioning tools are already developed. The installation of the transition piece and the tower is very similar to the installation of the foundation, so it could be assisted with similar solutions. The installation of the blades is an interesting subject, but is already heavily studied [6]. For these reasons the nacelle was selected as the component for the design. Tools for the installation of the nacelle are not yet explored and this makes it an interesting and innovative choice. Secondly, an offshore wind turbine is selected that is representative for the current and future turbines. This resulted in the Haliade X 12MW turbine from GE Renewable Energy which can be seen in Fig. 1. Lastly, a floating installation vessel is selected to enable the use of data about the installation vessel. The Les Alizés was selected since it is capable of installing the Haliade X.

Fig. 1. The Haliade X by GE Renewable Energy

III. DESIGN METHODOLOGY

To derive design solutions for a motion compensating tool, a design methodology is adopted which consists of the following three main stages: analysis, synthesis and evaluation, shown in Fig. 2.

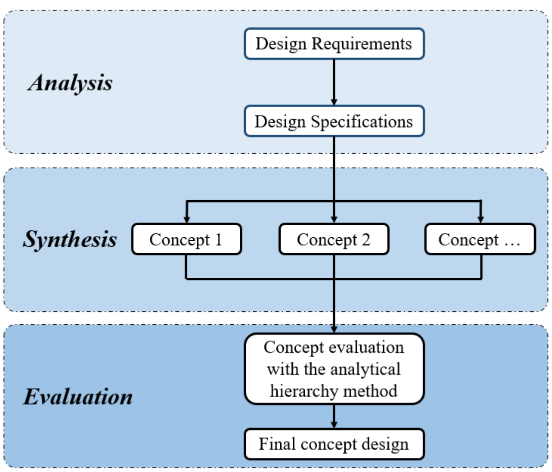

Fig. 2. A flowchart of the process of the design methodology

A. Design Analysis

The first step in the design analysis is to determine the design requirements. The design requirements describe the aspects of the tool which are necessary to achieve its goal. An overview of the design requirements considered relevant for this design is given in Table I. The performance specifications are a result of the listed design requirements and describe the tasks the design must fulfil. The performance specifications are listed in Table II.

TABLE I
DESIGN REQUIREMENTS

R1	Motion compensating technology
R2	Position and orientation measurements
R3	Connection between the crane and the load
R4	Minimize impact on lifting capacity
R5	Minimize impact on lifting height
R6	Maintain or improve safety
R7	Technological feasibility
R8	Economic feasibility

TABLE II
PERFORMANCE SPECIFICATIONS

S1	Compensate for unwanted motion of the nacelle relative to the tower
S2	Measure position and orientation of the nacelle

B. Design Synthesis

The main goal of the concept is to compensate motion during the installation of a nacelle this function is the most important. A technology to measure the required inputs for a system is also necessary, but this is the case for every concept that is generated. Which measuring system can be applied and what needs to be measured depends on the exact concept, but will be relatively similar for each solution. So for this thesis solutions will be explored for the core problem, the compensation of unwanted motions. Seven concepts are created and the core principle of each concept is briefly explained below.

Concept 1: Inverted quadropod; This concept aims to counter the movement of the crane tip by keeping the nacelle in the same position using its moment of inertia. It can be compared to a child on a swing which does the opposite of 'pumping' the swing.

Concept 2: Tower gripper; A gripper that makes a direct connection to the tower. The motion of the nacelle can then be reduced using the tower as an anchor point.

Concept 3: Guiding line; A large guiding cable starting from the crane passing through the nacelle and is then anchored inside the tower. The nacelle can then slowly be lowered onto the tower.

Concept 4: Inverted hexapod; A system comprised of six hydraulic actuators which can position the nacelle relative from the crane.

Concept 5: XY-tables with a counterweight; A system that contains two x-y tables to move the nacelle and a counterweight in the horizontal plane.

Concept 6: Intelligent tugger system; This concept is comprised of several intelligent cables that can pull the nacelle towards the crane.

Concept 7: Propulsion system; The last concept uses thrust to control the dynamic behaviour of the nacelle.

C. Design Evaluation

It is often difficult to evaluate non-existing concepts on a quantitative base. Therefore the analytic hierarchy process is selected for the concept evaluation. This process compares each concept against the other concepts for each criterion. A set of six criteria is defined which are deemed important for a motion compensator. Since not all criteria are equally important, weighting factors are determined which is also done with the analytic hierarchy method. This results in the overview presented in Table III.

TABLE III
OVERVIEW OF CRITERIA AND WEIGHTING FACTORS

Criterion	Weighting factor
Motion compensating capability	0,22
Impact on lifting height	0,09
Impact on lifting capacity	0,06
Technical feasibility	0,39
Economic feasibility	0,04
Impact on equipment	0,20

The analytic hierarchy process results in the evaluation shown in Fig. IV. The guiding line, propulsion system and tower gripper have a low score due to their low expected technical feasibility. The guiding line and tower gripper require a physical connection to the turbine tower which is a time consuming and complex interaction. The propulsion system requires an incredible amount of power which is deemed not feasible. The inverted hexapod is very expensive, large and requires additional connections to the mast of the crane. The tugger system has a relative low mass and size, but a system that is solely comprised of tuggers is very limited in the degrees of freedom it can control. The second best concept is the inverted quadropod, but whether it will work is difficult to predict. This is why this concept scored slightly lower than the X-Y table which has the best score. The X-Y table is expected to have good motion compensating capabilities since it aims to position the nacelle at the desired location. Secondly, this concept could also compensate for relative motion between the nacelle and turbine tower. In the table it can be seen that X-Y table has a score of 23,16 which is the highest score in the list. The X-Y table concept is chosen for the final concept design.

IV. FINAL CONCEPT DESIGN

In this chapter the concept will be further developed to get a deeper understanding of the working principle and design of the tool. A 3D-model of the tool will be made to estimate the size and weight.

Working principle

The core idea of the tool was briefly explained before, but for the final concept design an improved description of the

TABLE IV
RESULTS OF THE ANALYTIC HIERARCHY PROCESS

Concept	Score	Rank
Inverted Quadropod	18,64	3
Tower Gripper	9,76	5
Guiding Line	7,31	7
Inverted Hexapod	12,86	4
X-Y Table	**23,16**	**1**
Intelligent tugger system	20,33	2
Propulsion system	7,94	6

tool is essential. The core working principle can be explained from a simplified static perspective. The goal of the tool is to position the nacelle above the tower at any given time. Normally the nacelle is swinging beneath the crane which makes the installation more difficult. If the nacelle could be independently moved from the nacelle carrier to keep it above the tower it could improve the installation. Two XY-tables will be designed, a system that can move an object in two dimensions, to achieve this. A counterweight is added that will move in the opposite direction of the nacelle to keep the center of gravity of the whole system in the same position and maintain the moment equilibrium. This principle is presented in Fig. 3.

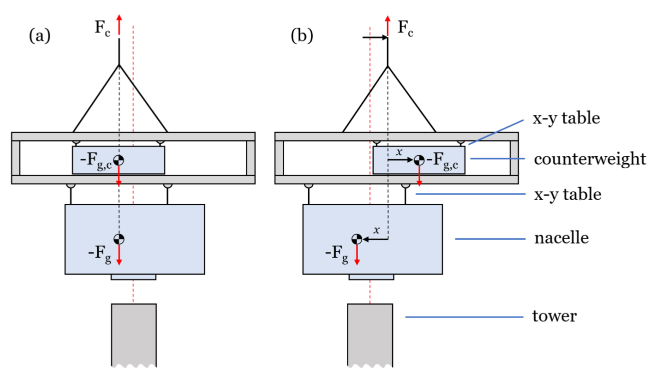

Fig. 3. An overview of the working principle

Since the nacelle is very heavy a ratio will be implemented between the counterweight and the nacelle. A ratio where the mass of the counterweight is five times smaller than that of the nacelle is selected resulting in a counterweight with a mass of 130 tonnes. If a larger ratio would be applied the displacement rapidly increases as the mass approaches zero. The concept also requires a few quantities to be known for it to function. The position of the nacelle has to be known so that its relative distance to the reference point can be determined. This includes the position in the global coordinate system as well as the local coordinates within the XY-table. The same is true for the counterweight, only the global position of the counterweight is not needed.

Concept configuration

Since the dimensions of the nacelle are specified by GE its dimensions are used as a starting point for the design. The complex shape of the nacelle is reduced to a rectangular box with an approximate length of 22 meters, and a width and height of 10 meters. The nacelle also has special connection points to connect to the nacelle carrier. The design will utilize these points so that it fully compatible with the Haliade X. The tool can be divided into three main parts: lower x-y table, main frame, upper x-y table. These parts will allow the nacelle and counterweight to be moved in two directions so that the nacelle and counterweight can be moved relative to the main frame which is connected to the crane. The tool is first approached as a wireframe. To estimate the size of each part, data about the dynamics of the lifting hook during the installation of the nacelle. This data was provided by Huisman Equipment. If the displacement of the nacelle is assumed to be on a similar level as that of the lifting hook it results in a maximum displacement of ±0.1 meters in the x-direction and ±0.5 meters in the y-direction. The movement in the x-direction is lower due to this direction being in the direction of the crane, so it can be controlled better. With a mass ratio of five this means that the counterweight has to move ±0.5 and ±2.5 meters in the respective direction. These values resulted in the wireframe presented in Fig 4. The nacelle and counterweight will be actuated by a rack and pinion drive which will be driven by electric motors. This option is most suitable for the required range and power.

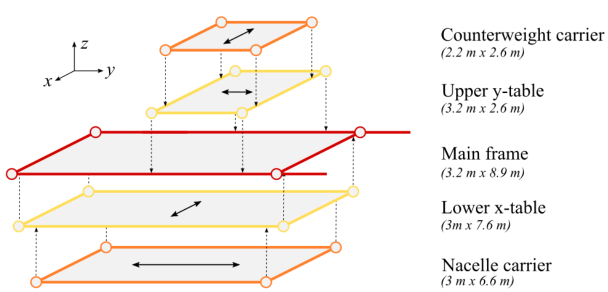

Fig. 4. An overview of the wireframes with dimensions

Tool Design

The structural design of the tool will be used to estimate the dimensions and weight of the tool. This is required to answer the question if the tool is technological feasible. Each link of the wireframe is designed from a rectangular hollow shape and made from S690 steel. Each beam is subjected to the worst load case since physical tests are not possible. The offshore standard (DNVGL-ST-N001) for marine operations and warranty is used to determine the load amplification factor. The von Mises stress is used to evaluate the maximum stress in the beams due to the bending and shear stress. The estimated weight of the tool is 171 tonnes including the counterweight. The tool also has a maximum length of 11.5 meters, a width of 7.8 meters and a height of 5.1 meters. The parts are then modelled and assembled in SolidWorks resulting in the 3D-model shown in Fig 5.

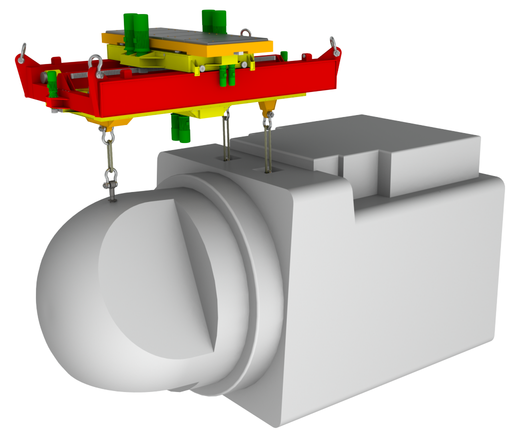

Fig. 5. An overview of the 3D-model

V. DYNAMIC ANALYSIS

A dynamic analysis is performed to develop a mathematical model of the concept. This model will be verified and validated to confirm that it behaves as it is modelled.

Mathematical model

A mathematical model represents a system, and especially the behaviour of a system in an abstract way. The model is bounded to the nacelle, tool, lifting hook and crane tip. A larger model would not add any significant value in this stage of the development. The concept is similar to the simple double pendulum. However, the main frame is not supported by one cable, but suspended from each corner point. Therefore it is more accurate to model the lower pendulum as a rigid body since the assumption that the interaction force with the upper pendulum acts along the cable is not valid. The proposed mathematical model is given in Fig 6. In this model the crane tip is represented by pivot point O and from this point the lifting hook is suspended via a cable with length l_1. The lifting hook is modelled as the first mass point m_h and also acts as a pivot point. The tool is then suspended from the lifting hook by a rigid massless link. Since the center of gravity (CoG) of the lower pendulum remains at the same position the nacelle and the counterweight are reduced to one mass point (m_{tot}). The movements of the nacelle and counterweight are implemented as forces F_1 and F_2 and are equal to the forces required for moving the masses. The equations of motion for the model can be derived with the Newton-Euler method and combining the kinematic and force equations. The equations of motion are given in Eq 1. and Eq 2. These equations are then programmed in MATLAB Simulink. The model is then verified and validated for a model without the control aspect of the concept.

$$\ddot{\alpha}_1 = -\frac{2(l_3+l_4)F_2cos(\alpha_1-\alpha_2)+2L^2\dot{\alpha_2}^2m_{tot}sin(\alpha_1-\alpha_2)+Lgm_{tot}sin(\alpha_1-2\alpha_2)+Lgsin(\alpha_1)(m_{tot}+2m_h)}{2l_1Lm_{tot}+2l_1Lm_h-2l_1Lm_{tot}cos(\alpha_1-\alpha_2)} \quad (1)$$

$$\ddot{\alpha}_2 = -\frac{Lgm_{tot}sin(\alpha_2)-(l_3+l_4)F_2+l_1Lm_{tot}\ddot{\alpha}_1}{L^2m_{tot}} \quad (2)$$

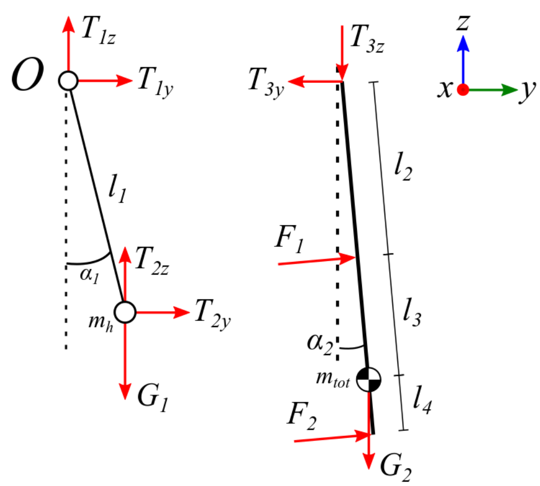

Fig. 6. The mathematical model

VI. CONCLUSIONS & FUTURE RESEARCH

This study aimed to develop and design a concept that could improve the installation of the nacelle by decreasing the unwanted motion due to the use of a floating installation vessel. It can be concluded that unwanted motions due to bad weather conditions result in true challenges during the installation of an offshore wind turbine. The installation of the nacelle of the turbine was selected as the most innovative and improvable part to develop a concept for. In total seven concept were created from which one was selected for a final concept design. This resulted in a tool with two XY-tables that can be used to move the nacelle and a counterweight relative to the main frame of the tool. The dynamical analysis resulted in a mathematical model of the tool which was based on a double pendulum. The mathematical model was verified and validated to confirm that it behaves as expected without a control system. To explore the performance of the tool a control system needs to be developed. It can then be compared to the conventional installation of the nacelle.

REFERENCES

[1] Tabassum-Abbasi, Premalatha, M., Abbasi, T., Abbasi, S. (2014). Wind energy: Increasing deployment, rising environmental concerns. Renewable and Sustainable Energy Reviews, 31, 270–288. *https://doi.org/10.1016/j.rser.2013.11.019*

[2] Woodacre, J., Bauer, R., & Irani, R. (2015). A review of vertical motion heave compensation systems. Ocean Engineering, 104, 140–154. *https://doi.org/10.1016/j.oceaneng.2015.05.004*

[3] Quandt, M., Beinke, T., Ait Alla, A., and Freitag, M. (2017). Simulation based investigation of the impact of information sharing on the offshore wind farm installation process. Journal of Renewable Energy, (1), 11 pp

[4] Li, L., Guachamin Acero, W., Gao, Z., & Moan, T. (2016). Assessment of Allowable Sea States During Installation of Offshore Wind Turbine Monopiles With Shallow Penetration in the Seabed. Journal of Offshore Mechanics and Arctic Engineering, 138(4). *https://doi.org/10.1115/1.4033562*

[5] Acero, W. G., Gao, Z., & Moan, T. (2017). Methodology for Assessment of the Allowable Sea States During Installation of an Offshore Wind Turbine Transition Piece Structure Onto a Monopile Foundation. Journal of Offshore Mechanics and Arctic Engineering, 139(6). *https://doi.org/10.1115/1.4037174*

[6] Jiang, Z. (2018). The impact of a passive tuned mass damper on offshore single-blade installation. Journal of Wind Engineering and Industrial Aerodynamics, 176, 65–77. *https://doi.org/10.1016/j.jweia.2018.03.008*

B Initial concept calculations

Inverted quadropod

One way to estimate the technical feasibility of the inverted quadropod concept is to do a simple calculation for a worst-case scenario. The system is sketched in Fig. 69 If the amplitude A is known we can determine the maximum angular acceleration of the nacelle, resulting in a torque created by the moment of inertia. Because this feasibility of this concept depends on the moment of inertia it is good the check if the moment caused by the resultant forces in the cable are of the same order as the torque caused by the moment of inertia. This leads to the following calculations:

$$L = 15m, A = 0.5m, T = 8s$$
$$\theta = asin(\tfrac{0.5}{15}) = 1.91° = 0.033rad$$
$$\alpha_{max} = \theta(\tfrac{4pi^2}{8^2}) = 0.021\tfrac{rad}{s^2}$$

The generator in the nacelle is the dominating weight and has the shape of a cylinder with a radius of approximately 4m.

$$M = 650000kg, R = 4m$$
$$I = 0.5MR2 = 5,200,000kgm^2$$
$$\tau = \alpha_{max}I = 107kNm$$
$$F_{c,y} = -F_g, F_{c,y}0.5 = 3188.25kNm$$
$$F_{c,x} = sin(\theta) * -F_g * cos(\theta)L = 3188.25kNm$$

So, in this situation the torque caused by the moment of inertia is 60 times smaller than the sum of the torques caused by the resulting force in the cable. Even if we ignore the torque caused by $F_{c,x}$ when the tip of the beam follows the movement of the crane exactly, the torque caused by the moment of inertia is 30 times too small.

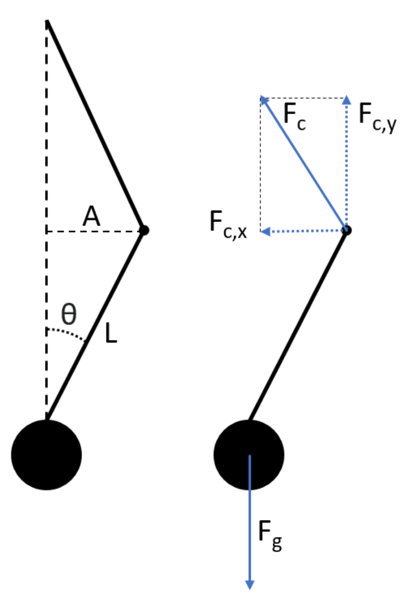

Figure 69: Calculation sketch

Intelligent tugger system
This system has quite a lot of advantages over other concepts, but is highly depended on the cable speeds and accelerations that can be achieved. Secondly since the tugger system is only capable of pulling the load towards the crane it depends on the gravity of the load to move it away from the crane. To get a better insight into this problem, a simplified pendulum in Fig. 70 is used to calculate the maximum acceleration that can be achieved by gravity if the load had to move away from the crane.

$$M = 650000kg, g = 9.81\frac{m}{s^2}, A = 0.5m, L = 20m$$
$$\theta = asin(\frac{0.5}{20}) = 1.43°$$
$$F_g = Mg = 6376.5kN$$
$$F_s = sin(\theta)F_g = 159,4kN$$
$$\alpha_{max} = \frac{F_s}{M} = 0.245\frac{m}{s^2}$$

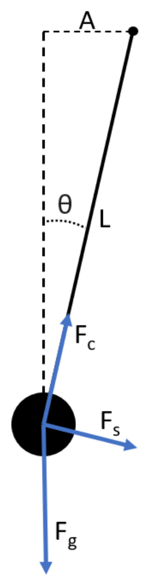

Figure 70: Calculation sketch

Propulsion system
The concept containing a propulsion system work on the principle of generated force by thrusters. The force that had to be countered is a result of the moving crane tip. As the angle is relatively small it is safe to say that the thrusters have to overcome the same F_s as in the calculations for the tugger system. The sketch that is used for the calculations is given in Fig. 71. Let's assume that air is used as medium and the diameter of the thruster is 3 meters. The diameter of the in- and outlet of the thruster is also assumed to be equal If the generalized equation for thrust is used it results in the following calculation:

$$\rho_{air} = 1.225\frac{kg}{m3}, A = 7.06m2, V1 = 8.6\frac{m}{s}, F = 159.4kN$$
$$F = (\rho_1 A_1 V_1)V_1 - (\rho_2 A_2 V_2)V_2$$
$$F = (V_2^2 - V_1^2)$$
$$V_2 = \sqrt{((F + \rho A V_1^2)/)} = 136\frac{m}{s}$$

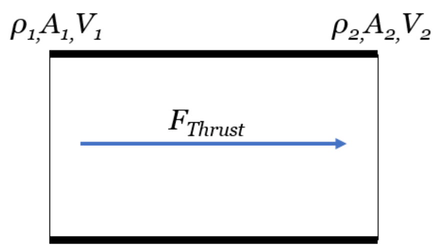

Figure 71: Calculation sketch

C Analytic Hierarchy Process

C1: Motion compensation capability	A	B	C	D	E	F	G	EV	PV
A	1	3	5	1/3	1/2	1/3	5	1.23	0.155847
B	1/3	1	3	1/2	1/3	1/3	3	0.77	0.098399
C	1/5	1/3	1	1/4	1/5	1/5	1/2	0.32	0.040497
D	3	2	4	1	1/2	2	1/3	1.35	0.171069
E	2	3	5	2	1	3	5	2.64	0.335886
F	3	3	5	1/2	1/3	1	3	1.56	0.198302
G	1/3	1/3	2	3	1/5	1/3	1	0.64	0.081468
								7.87	**1.00**

C2: Impact on lifting height	A	B	C	D	E	F	G	EV	PV
A	1	1/3	1/2	1	1	1/5	1/2	0.56	0.081106
B	3	1	1	2	1	1/3	1	1.10	0.160722
C	2	1	1	1/2	1/3	1/5	1/3	0.58	0.084508
D	1	1/2	2	1	1/2	1/5	1/3	0.62	0.089548
E	1	1	3	2	1	1/2	1	1.17	0.170307
F	5	3	5	5	2	1	2	2.84	0.413809
G	2	1	3	3	1	1/2	1	1.37	0.199247
								6.87	**1.00**

C3: Impact on lifting capacity	A	B	C	D	E	F	G	EV	PV
A	1	2	1/5	3	5	1/3	1	1.10	0.13028
B	1/2	1	1/3	3	5	1/5	1	0.91	0.106874
C	5	3	1	5	6	2	3	3.09	0.364812
D	1/3	1/3	1/5	1	1	1/5	1/3	0.39	0.046525
E	1/5	1/5	1/6	1	1	1/6	3	0.44	0.05224
F	3	5	1/2	5	6	1	3	2.54	0.299269
G	1	1	1/3	3	1/3	1/3	1	0.73	0.086209
								8.47	**1.00**

C4: Technical feasibility	A	B	C	D	E	F	G	EV	PV
A	1	3	4	2	2	2	3	2.25	0.276609
B	1/3	1	5	1/3	1/3	1/2	3	0.83	0.102577
C	1/4	1/5	1	1/5	1/5	1/3	1/3	0.30	0.037037
D	1/2	3	5	1	1/2	1/2	3	1.28	0.157646
E	1/2	3	5	2	1	3	5	2.17	0.267024
F	1/2	2	3	2	1/3	1	3	1.29	0.159107
G	1/3	1/3	3	1/3	1/5	1/3	1	0.50	0.061121
								8.12	**1.00**

C5: Economic feasibility	A	B	C	D	E	F	G	EV	PV
A	1	2	1/3	3	1/2	1/3	2	0.94	0.112402
B	1/2	1	1/4	2	1/3	1/6	1/2	0.49	0.058559
C	3	4	1	5	3	1/2	3	2.23	0.265014
D	1/3	1/2	1/5	1	1/3	1/7	1/5	0.32	0.037685
E	2	3	1/3	3	1	1/5	1/2	0.93	0.110723
F	3	6	2	7	5	1	5	3.49	0.415617
G	1/2	2	1/3	5	2	1/5	1	0.94	0.112402
								8.40	**1.00**

C6: Impact on equipment	A	B	C	D	E	F	G	EV	PV
A	1	3	4	5	1	5	1	2.26	0.32996
B	1/3	1	2	3	1	5	1	1.39	0.202976
C	1/4	1/2	1	2	1/3	2	1/3	0.66	0.096663
D	1/5	1/3	1/2	1	1/5	2	1/3	0.46	0.067385
E	1	1	3	5	1	3	1	1.72	0.251629
F	1/5	1/5	1/2	1/2	1/3	1	1/5	0.35	0.051388
G	1	1	3	3	1	5	1	1.72	0.251629
								6.85	**1.00**

Weights	C1	C2	C3	C4	C5	C6	EV	PV
C1	1	5	4	1/3	5	2	2.01	0.222796
C2	1/5	1	2	1/5	3	1	0.79	0.087222
C3	1/4	1/2	1	1/6	3	1/2	0.56	0.062096
C4	3	5	6	1	7	3	3.52	0.389045
C5	1/5	1/3	1/2	1/7	1	1/3	0.34	0.037789
C6	2	1	2	3	3	1	1.82	0.201051
							9.04	**1**

D Initial HMC calculations

D.1 Lower x-table

The lower x-table will enable movement of the nacelle in the x-direction. In combination with the nacelle carrier the nacelle will now be able to move in both the x- and y-direction. Beam A is once again the beam that carries the loads of the nacelle carrier and the bogies to the main frame of the tool. An overview of the forces acting on the lower x-table can be seen in Fig. 72.

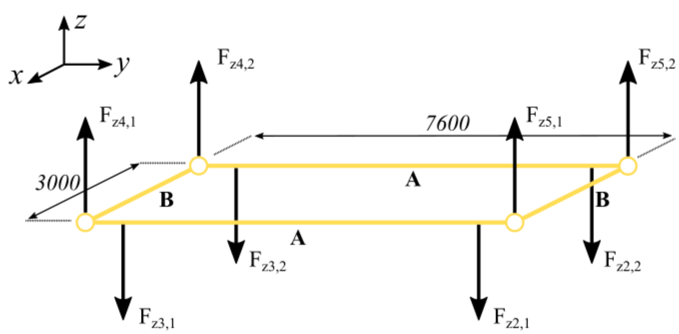

Figure 72: Overview of the forces acting on the lower x-table

To determine the shear and bending moment diagram from Fig. 73, the forces acting on beam A have to be calculated. Forces $F_{3,1}$ and $F_{2,1}$ were already determined in the calculations for the nacelle carrier and were 966 kN and 2222 kN respectively. When the moment is taken about the left end of beam A it can be calculated that $F_{z5,1}$ is 2139 kN. When the sum of the vertical forces is set to zero it results that $F_{z4,1}$ will be 1049 kN. The complete calculation sheet for the beams of the lower x-table can be seen in Table 12.

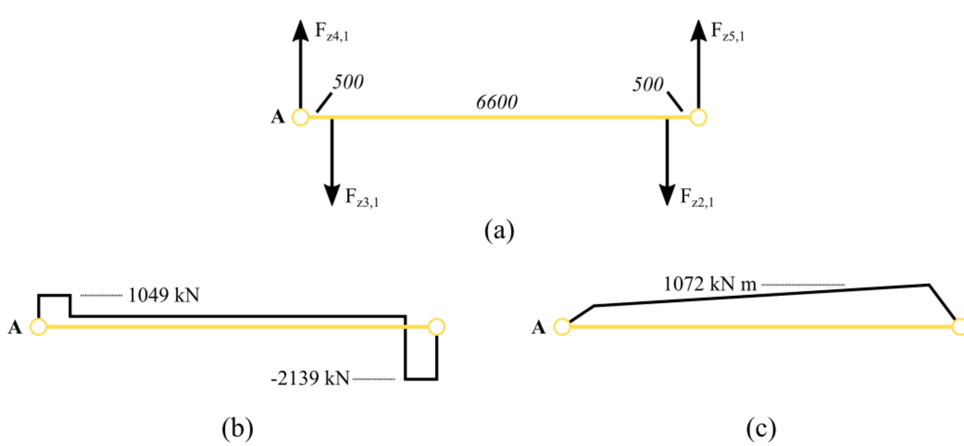

Figure 73: Forces acting on beam A (a), shear force diagram (b), bending moment diagram (c)

Table 12: Calculation sheet for the lower x-table

Beam A		
Yield Strength	6.90E+08	Pa
Allowable yield	4.14E+08	Pa
Safety factor	0.6	[-]
Load factor	2.24	[-]
Width	533.3333	mm
Height	800	mm
Thickness side	15	mm
Thickness top/bottom	15	mm
Inner width	503.3333	mm
Inner height	770	mm
Beam length	7.6	m
Cross sect. Area	0.0391	m^2
Ixx	3.607E-03	m^4
Maximum shear force	2139	kN
Maximum bending moment	1072	kNm
Maximum axial force	0	
Maximum shear stress	1.23E+08	Pa
Maximum bending stress	2.66E+08	Pa
Maximum axial stress	0.00E+00	Pa
Von Mises Stress	3.41E+08	Pa

Beam B		
Yield Strength	6.90E+08	Pa
Allowable yield	4.14E+08	Pa
Safety factor	0.6	[-]
Load factor	2.24	[-]
Width	533.3333	mm
Height	800	mm
Thickness side	10	mm
Thickness top/bottom	10	mm
Inner width	513.3333	mm
Inner height	780	mm
Beam length	3	m
Cross sect. Area	0.026267	m^2
Ixx	2.455E-03	m^4
Maximum shear force	0	kN
Maximum bending moment	0	kN m
Maximum axial force	80	kN
Maximum shear stress	0.00E+00	Pa
Maximum bending stress	0.00E+00	Pa
Maximum axial stress	6.82E+06	Pa
Von Mises Stress	6.82E+06	Pa

D.2 Upper y-table

The upper y-table lets the counterweight move in the y-direction. The table contains the wheels for the counterweight carrier as well as for the table itself. When the dimensions of the wireframes are used it results in the force diagrams shown in Fig. 74.

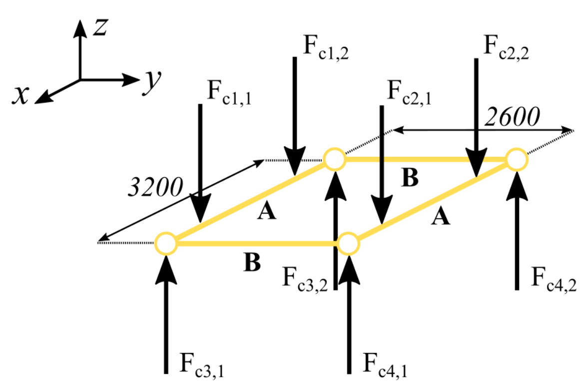

Figure 74: Overview of the forces acting on the upper y-table

To determine the shear and bending moment diagram from Fig. 75, the forces acting on beam A have to be calculated. Forces $F_{c1,1}$ and $F_{c2,1}$ were already determined in the calculations of the counterweight carrier and are both 319 kN. When the moment is taken about the left end of beam A it can be calculated that $F_{c4,1}$ is also 319 kN. When the sum of the vertical forces is set to zero it results that $F_{c3,1}$ will be equal to

$F_{c4,1}$. The complete calculation sheet for the beams of the upper y-table can be seen in Table 13.

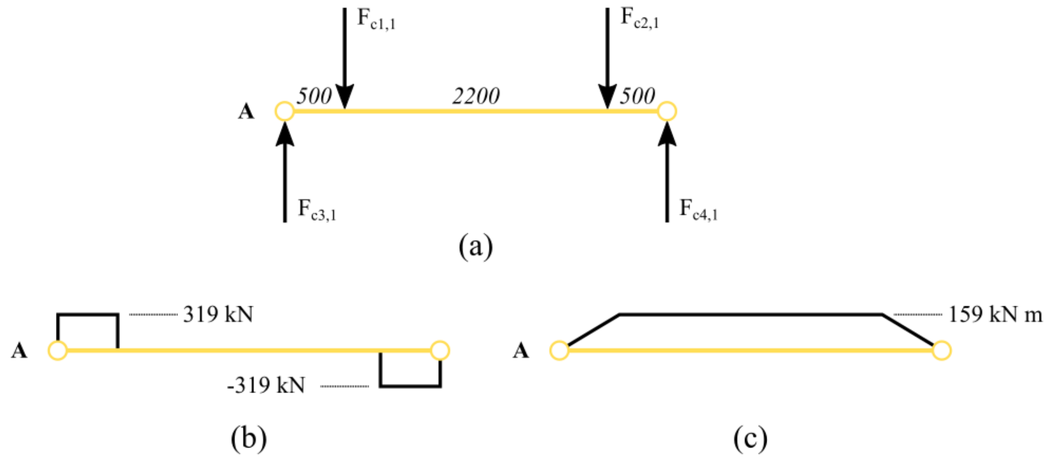

Figure 75: Forces acting on beam A (a), shear force diagram (b), bending moment diagram (c)

Table 13: Calculation sheet for the upper y-table

Beam A			**Beam B**		
Yield Strength	6.90E+08	Pa	Yield Strength	6.90E+08	Pa
Allowable yield	4.14E+08	Pa	Allowable yield	4.14E+08	Pa
Safety factor	0.6	[-]	Safety factor	0.6	[-]
Load factor	2.24	[-]	Load factor	2.24	[-]
Width	266.6667	mm	Width	266.6667	mm
Height	400	mm	Height	400	mm
Thickness side	10	mm	Thickness side	10	mm
Thickness top/bottom	10	mm	Thickness top/bottom	10	mm
Inner width	246.6667	mm	Inner width	246.6667	mm
Inner height	380	mm	Inner height	380	mm
Beam length	3.2	m	Beam length	2.6	m
Cross sect. Area	0.012933	m^2	Cross sect. Area	0.012933	m^2
Ixx	2.943E-04	m^4	Ixx	2.943E-04	m^4
Maximum shear force	319	kN	Maximum shear force	0	kN
Maximum bending moment	159	kNm	Maximum bending moment	0	kNm
Maximum axial force		kN	Maximum axial force	315	kN
Maximum shear stress	5.52E+07	Pa	Maximum shear stress	0.00E+00	Pa
Maximum bending stress	2.42E+08	Pa	Maximum bending stress	0.00E+00	Pa
Maximum axial stress	0.00E+00		Maximum axial stress	5.46E+01	
Von Mises Stress	2.60E+08	Pa	Von Mises Stress	5.46E+01	Pa

D.3 Counterweight carrier

In the design configuration section of this report the wireframe of the counterweight carrier only indicates the interface points with the upper y-table. The counterweight carrier is mostly integrated in the carrier and can be adjusted to the rest of the design. Since the counterweight is made from steel no structural calculations are used for the design of the counterweight carrier including the counterweight.

D.4 Main frame

The main frame brings the lower section and the upper section of the tool together and is simultaneously the connection with the installation crane. The main frame provides rails for the lower x-table and for the upper y-table. The force diagram of the main frame is shown in Fig. 76.

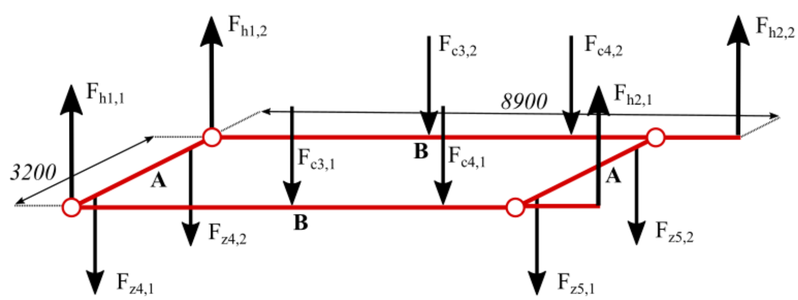

Figure 76: Overview of the forces acting on the main frame

In the figure it can be seen that the main frame is not symmetric. This is a result of the asymmetric location of the CoG of the nacelle within the nacelle carrier. The center of the rails of the counterweight has to be positioned in such a way that it is located above the center line of the CoG of the nacelle.

The main frame consists of four beams, two beams labelled A and two beams labelled B. The beams indicated with the letter 'A' are supporting the lower x-table. The beams indicated with the letter 'B' are supporting the upper y-table, beams A and the cables leading to the lifting hook. The shear and bending moment diagram from Fig. 77 can be created by calculating the forces on beam A. Forces $F_{z5,1}$ and $F_{z5,2}$ were used in the calculation since these are the largest and because the main frame is designed as symmetric as possible the left A beam will also be designed using these forces. $F_{z5,1}$ and $F_{z5,2}$ were already calculated in section about the lower x-table and are both 2139 kN. In contrast with most previous beam calculations the shear stress on this beam is dominant instead of the bending moment stress. Therefore, the position of the lower x-table is changed to be on the outside providing the scenario with the maximum shear force. When the moment sum is then taken about the right end of the beam and set to zero force $F_{i1,1}$ can be calculated to be 2273 kN. To calculate the maximum bending moment the lower x-table is once again positions in the center to calculate the maximum bending moment. This then leads to a maximum bending moment of 214 kNm.

The calculation for beam B is slightly more difficult since there more forces acting on this beam. $F_{z5,1}$ is already determined, but the maximum shear force $F_{z4,1}$ still has to be calculated. This can be done in the

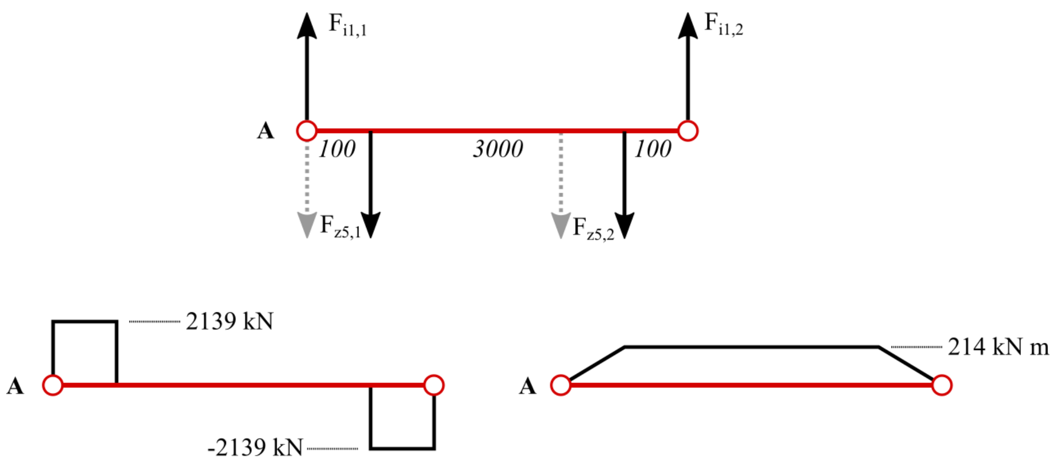

Figure 77: Forces acting on beam A (a), shear force diagram (b), bending moment diagram (c)

same was as it was done for $F_{z5,1}$, leading to a maximum shear force of 1115 kN. The same approach is taken to calculate the maximum shear forces $F_{c3,1}$ and $F_{c4,1}$ resulting in 418 kN. When the moment sum is then taken about the left end of the beam and set to zero force $F_{h2,1}$ can be calculated to be 2419 kN. Using the sum of the vertical forces $F_{h1,1}$ can be calculated and is 1804 kN. When every maximum shear force is put into the calculation for beam B the maximum shear force and moment diagram for beam B shown in figure Fig. 78 can be drawn. The resulting calculation sheet for the beams of the main frame can be seen in Table 14.

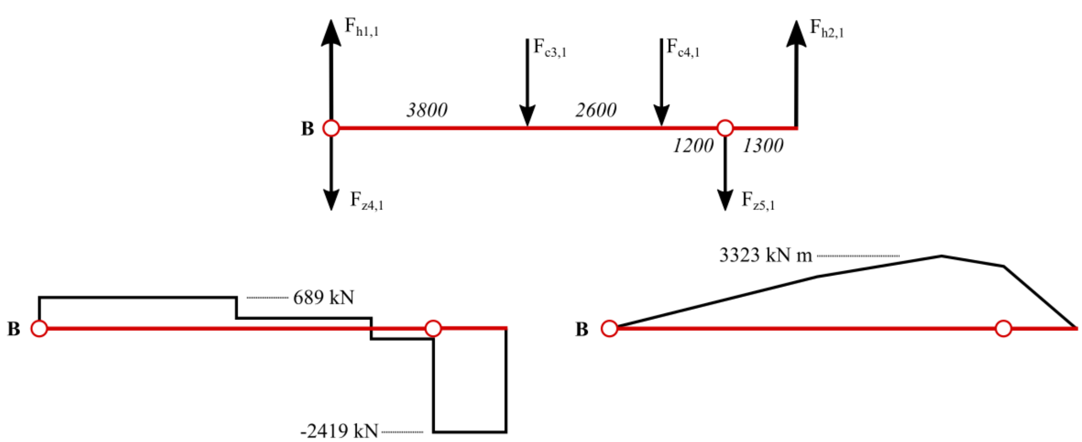

Figure 78: Forces acting on beam B (a), shear force diagram (b), bending moment diagram (c)

Table 14: Calculation sheet for the main frame

Beam A		
Yield Strength	6.90E+08	Pa
Allowable yield	4.14E+08	Pa
Safety factor	0.6	[-]
Load factor	2.24	[-]
Width	400	mm
Height	600	mm
Thickness side	15	mm
Thickness top/bottom	15	mm
Inner width	370	mm
Inner height	570	mm
Beam length	3.2	m
Cross sect. Area	0.0291	m^2
Ixx	1.49E-03	m^4
Maximum shear force	2272	kN
Maximum bending moment	214	kNm
Maximum axial force	0	kN
Maximum shear stress	1.75E+08	Pa
Maximum bending stress	9.65E+07	Pa
Maximum axial stress	0.00E+00	Pa
Von Mises Stress	3.18E+08	Pa

Beam B		
Yield Strength	6.90E+08	Pa
Allowable yield	4.14E+08	Pa
Safety factor	0.6	[-]
Load factor	2.24	[-]
Width	800	mm
Height	1200	mm
Thickness side	20	mm
Thickness top/bottom	20	mm
Inner width	760	mm
Inner height	1160	mm
Beam length	8.9	m
Cross sect. Area	0.0784	m^2
Ixx	1.63E-02	m^4
Maximum normal force	2419	kN
Maximum bending moment	3323	kNm
Maximum axial force	0	kN
Maximum normal stress	6.91E+07	Pa
Maximum bending stress	2.73E+08	Pa
Maximum axial stress	0.00E+00	Pa
Von Mises Stress	2.98E+08	Pa

E MATLAB Code

E.1 Coupled model

```
clc, clear

syms l1 l2 l3 l4 L mh m1 m2 m_tot a1(t) a2(t)
syms A1 A2 A3 T1y T1z T2y T2z g a1_d a2_d a1_dd a2_dd rG2 Lc

%constants
Io = mh*l1^2;
It = m_tot*L^2;

%% Kinematics

%Upper pendulum
r1y = l1*sin(a1);
r1z = -l1*cos(a1);

v1y = diff(r1y);
v1z = diff(r1z);

a1y = diff(v1y);
a1z = diff(v1z);
a1y = subs(a1y, {diff(a1(t),t),diff(a1(t),t,t)},{'a1_d','a1_dd'});
a1z = subs(a1z, {diff(a1(t),t),diff(a1(t),t,t)},{'a1_d','a1_dd'});

% A1 = [v1y;v1z;a1y;a1z];
% A1 = subs(A1, {diff(a1(t),t),diff(a1(t),t,t)},{'a1_d','a1_dd'});

%Lower pendulum
r2y = l1*sin(a1)+L*sin(a2);
r2z = -l1*cos(a1)-L*cos(a2);

v2y = diff(r2y);
v2z = diff(r2z);

a2y = diff(v2y);
a2z = diff(v2z);
a2y = subs(a2y, {diff(a1(t),t),diff(a1(t),t,t),diff(a2(t),t), ...
    diff(a2(t),t,t)},{'a1_d','a1_dd','a2_d','a2_dd'});
a2z = subs(a2z, {diff(a1(t),t),diff(a1(t),t,t),diff(a2(t),t), ...
    diff(a2(t),t,t)},{'a1_d','a1_dd','a2_d','a2_dd'});

```

```
%%Forces

eq5 = mh*a1z == T1y + T2y;

eq6 = mh*a1y == T1z + T2z - mh*g;

eq7 = Io*a1_dd == l1*sin(a1)*(T2z-mh*g)+l1*cos(a1)*T2y;

eq8 = m_tot*a2y == -T2y;

eq9 = m_tot*a2z == -T2z-m_tot*g;

eq10 = It*a2_dd == -L*sin(a2)*m_tot*g-l1*L*m_tot*a1_dd+A1;

sol.T2y = solve(eq8, T2y);
sol.T2z = solve(eq9,T2z);

sol2 = solve(eq10, a2_dd);
sol1 = solve(eq7,a1_dd);
sol1 = subs(sol1, [T2z,T2y], [sol.T2z,sol.T2y]);
sol1 = subs(sol1,a2_dd,sol2);

eq11 = a1_dd == sol1;

Solution1 = solve(eq11, a1_dd);
Solution1 = simplify(Solution1,'Steps',5);
pretty(Solution1)
pretty(sol2)
```

E.2 Uncoupled model

```
clc, clear

syms l1 l2 l3 l4 L mh m1 m2 m_tot a1(t) a2(t)
syms A1 A2 A3 T1y T1z T2y T2z g a1_d a2_d a1_dd a2_dd Lc rG2

%constants
Io = mh*l1^2;
It = m_tot*Lc^2;

%% Kinematics

%Upper pendulum
r1y = l1*sin(a1);
r1z = -l1*cos(a1);

v1y = diff(r1y);
v1z = diff(r1z);

a1y = diff(v1y);
a1z = diff(v1z);
a1y = subs(a1y, {diff(a1(t),t),diff(a1(t),t,t)},{'a1_d','a1_dd'});
a1z = subs(a1z, {diff(a1(t),t),diff(a1(t),t,t)},{'a1_d','a1_dd'});

% A1 = [v1y;v1z;a1y;a1z];
% A1 = subs(A1, {diff(a1(t),t),diff(a1(t),t,t)},{'a1_d','a1_dd'});

%Lower pendulum
r2y = l1*sin(a1)+L*sin(a2);
r2z = -l1*cos(a1)-L*cos(a2);

v2y = diff(r2y);
v2z = diff(r2z);

a2y = diff(v2y);
a2z = diff(v2z);
a2y = subs(a2y, {diff(a1(t),t),diff(a1(t),t,t),diff(a2(t),t), ...
    diff(a2(t),t,t)},{'a1_d','a1_dd','a2_d','a2_dd'});
a2z = subs(a2z, {diff(a1(t),t),diff(a1(t),t,t),diff(a2(t),t), ...
    diff(a2(t),t,t)},{'a1_d','a1_dd','a2_d','a2_dd'});

%%Forces
```

```
eq5 = mh*a1z == T1y + T2y;

eq6 = mh*a1y == T1z + T2z - mh*g;

eq7 = Io*a1_dd == l1*sin(a1)*(T2z-mh*g)+l1*cos(a1)*T2y;

eq8 = m_tot*a2y == -T2y+A3;

eq9 = m_tot*a2z == -T2z-m_tot*g+A2;

eq10 = It*a2_dd == -rG2*sin(a2)*m_tot*g-l1*Lc*m_tot*a1_dd+A1;

sol.T2y = solve(eq8, T2y);
sol.T2z = solve(eq9,T2z);

sol2 = solve(eq10, a2_dd);
sol1 = solve(eq7,a1_dd);
sol1 = subs(sol1, [T2z,T2y], [sol.T2z,sol.T2y]);
sol1 = subs(sol1,a2_dd,sol2);

eq11 = a1_dd == sol1;

Solution1 = solve(eq11, a1_dd);
Solution1 = simplify(Solution1,'Steps',5);
pretty(Solution1)
pretty(sol2)
```